



SAPIENZA
UNIVERSITÀ DI ROMA

PhD COURSE IN PHARMACEUTICAL SCIENCES

XXXII CYCLE

Author
Roberta Franzini

Final Dissertation

*Stereodynamics of chiral and
conformationally flexible molecules
studied by chromatography and chiro-
optical methods*

A.A. 2018/2019

Supervisor
Prof. Claudio Villani

Table of Contents

Abstract	2
General Introduction	6
PART A - Investigation of the stereodynamics and optical properties of helically distorted and axially chiral compounds	16
• PART A1 - Stereostable and stereolabile helicenes investigated by enantioselective HPLC and chiro-optical methods	18
• PART A2 - Stereodynamics and optical properties of axially chiral benzodithiophenes and porphyrazine derivatives.....	77
PART B - Chiral bioactive tricyclic compounds with a seven-membered ring: variable temperature HPLC and NMR	108
PART C - Investigation on the isomerization <i>cis/trans</i> in conformationally flexible proline-rich-peptides and small molecules	152

- PART C1 - *Cis/Trans* isomerization by amidic bond rotation in proline-rich small molecules studied by dynamic-HPLC and stochastic model computations.....154
- PART C2 - *Anti/Syn* isomerization in polyfunctionalized indole with a stereolabile centre studied by HPLC with assignment of the absolute configuration.....188

Conclusions and future perspectives.....205

List of publications.....208

Congress communications.....211

Abstract

PART A

Conformational chirality arises from the presence of stereogenic elements different than the stereogenic centre, as axis, plane and helix. Compounds that exhibit such elements have peculiar characteristics profitably exploited in material chemistry, supramolecular chemistry and asymmetric catalysis. In this work is reported the study of the stereodynamics of helicenes, in the first part, and axially chiral compounds, in the second part, that allowed to determine the energetic barriers of the stereomutation events. Enantioselective HPLC coupled to electronic circular dichroism and optical rotation dispersion has been employed to separate and characterize the enantiomers of the studied compounds gathering valuable information about their outstanding chiroptical properties and interconversion rates.

PART B

Compounds with a non-planar seven-membered ring in their molecular backbone are known to be chiral. The absence of planarity allows the existence of two enantiomeric species

that can interconvert due to a ring-flip mechanism. Many bioactive compounds like benzodiazepines or dibenzoazepinones, widely prescribed for different therapeutic applications, present this structural feature. In this study, is reported the investigation of the stereodynamic behaviour of three different bioactive compounds: the anti-HIV drug Nevirapine and the anti-epileptic Oxcarbazepine, both showing a seven membered ring fused in a tricyclic system, and Estazolam, a triazole-benzodiazepine without a stereogenic centre. Low temperature dynamic-HPLC with chiral stationary phase coupled to computer simulations and NMR studies were employed to demonstrate the presence of two enantiomers in rapid interconversion and to measure the kinetic parameters of the process for all the three investigated compounds.

PART C

In the first section are reported the results from the period of my academic program at the Ludwig-Maximilians University (LMU) of Munich (GE) under the supervision of Prof. Dr. Oliver Trapp, during the second year of my PhD course. Xaa-Pro bond is a common structural element that can give rise to

trans and *cis* isomers thanks to rotation around the amidic bond. *Trans/cis* isomerization influences the structure of peptides and proteins resulting as an important feature in controlling signal transduction, aggregation, enzymatic catalysis. This pattern is common in catalytically active small peptides and the *trans/cis* isomerization can influence the performance of catalysis and the outcome of the reaction. Here is reported the optimization of an analytical method to chromatographically resolve mixtures of conformers *trans* and *cis* of proline rich small molecules. The kinetic parameters of the isomerization processes have been measured by variable temperature HPLC experiments coupled to stochastic model-based computations. In the second part it will be discussed the assignment of a chemical correlation and the absolute configuration of four stereoisomers of a conformationally flexible indole derivative featuring a β -ketoester fragment and two stereogenic centres. The two diastereoisomeric pairs have *syn*- and *anti-periplanar* conformations and can be easily converted into each other by treatment with a base. In this study a combination of different techniques is employed: HPLC, X-ray, ECD, NMR and computational methods.

HPLC with ECD detection allowed to chemically correlate the four stereoisomers and the AC is assigned for two of the stereoisomers (one in *anti*-periplanar conformation and one in *syn*-periplanar) by X-ray.

General Introduction

Stereoisomers are defined as compounds that only differ by the spatial orientation of the atoms. Stereomutation happens when a bond between two atoms breaks and reforms with a different three-dimensional arrangement or by rotation, switching in this case between different conformations. A chiral molecule exists as a couple of non-superimposable mirror images and the relative stereoisomers are called enantiomers, while all the other kinds of stereoisomers are called diastereoisomers including the geometric (*cis/trans*) isomers [1]. An interesting kind of stereoisomerism is the one exhibited by atropisomers, conformational isomers in which the rotation around a single bond is restricted. It is not uncommon, also in natural products, the coexistence in a single compound of different stereogenic elements as the centre, the axis or the plane [2]. Nowadays, stereochemistry is a multidisciplinary science and the study of the stereomutation phenomena and the chemical-physical properties of stereoisomers is a key topic in organic chemistry, medicinal chemistry and nanomaterials. The

different spatial arrangement of atoms is responsible for the different properties of stereoisomers. The implications of the different biological activity of enantiomers are well known and thus, the design of stereoisomeric drugs requires additional procedures to assure the precise stereoisomeric composition of a product with respect to identity, strength, quality and purity [3]. The stereochemical stability is then considered as a fundamental parameters when developing a new drug or an asymmetric synthetic pathway and even in nanomaterials for sensing devices and optoelectronics. Control over the stereochemistry, and in particular over stereodynamic behaviour is of major interest in developing gear-like compounds [4] applicable in remote stereocontrol by stereochemical relay, or in the design of molecular switches, molecular motors and propellers [5]. The interconversion between two stable stereoisomers may be induced by various factors as temperature, pH, redox reactions. The strong interest for molecular bistability in chiral compounds is testified also by the assignment of the Nobel Prize in Chemistry in 2016 [6]. Many techniques can be used to study the stereomutation events and to selectively isolate stereoisomers and unravel their properties. In this

dissertation the results derived by HPLC with chiral and achiral stationary phases, nuclear magnetic resonance and chiro-optical measurements will be discussed. In recent years the flourish of novel chiral stationary phases (CSP) for liquid chromatography [7] and the technological innovations [8] have made HPLC a favoured choice for the separation of both enantiomers and diastereoisomers and a valid method to study the stereomutation processes by on-column or off-column approaches. A chiral stationary phase forms reversible non-covalent diastereoisomeric interactions with a chiral analyte. The two diastereomeric complexes may have very different energies that translates in high selectivity. The equation (1) allows a mathematical correlation between the chromatographic selectivity (α) and the energy difference of the transient diastereoisomers.

$$\Delta\Delta G^{\circ}_{2,1} = \Delta G^{\circ}_2 - \Delta G^{\circ}_1 = -RT \ln(k'_2/k'_1) = -RT \ln \alpha \quad (1)$$

where $\Delta\Delta G^{\circ}_{2,1}$ is the difference between the Gibbs free energies of interaction of the two enantiomers with the selector, R is the gas constant, T is the absolute temperature and α is the ratio of the retention factors k'_2 and k'_1 of the two

enantiomers. The reversible interaction between analyte and stationary phase is referred to as primary equilibrium while the interconversion processes between two stereoisomers, in the mobile phase and in the stationary phase are referred to as secondary equilibria (fig. 1).

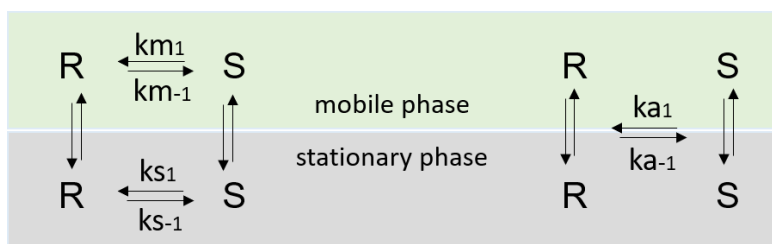


Fig.1 - Primary and secondary equilibria of the enantiomers R and S taking place in the chromatographic column. ($k_{m1} = k_{m-1}$ = kinetic rate constant of the R/S interconversion in mobile phase; k_{s1} = kinetic rate constant of the S to R conversion in the stationary phase; k_{s-1} = kinetic rate constant of the R to S conversion in the stationary phase; k_{a1} = apparent kinetic rate constant for S to R conversion; k_{a-1} = apparent kinetic rate constant for R to S conversion).

The apparent rate constants k_{a1} and k_{a-1} are considered as the averaged values for the interconversion taking place in the mobile phase and in the stationary phase. These values can be measured by computer simulations of the experimental

chromatograms and can be assimilated to the constant measurable in solution. Dynamic chromatography is an important and well-established technique in the study of those stereodynamic processes that take place in the same the time scale of the chromatographic separation [9]. A successful chromatographic separation of stereoisomers affords two distinct peaks and the lack of separation must be explored in two directions: on one side the optimization of the analytical method and on the other the investigation of an eventual on-column stereomutation process. Stereoisomers may undergo interconversion during the chromatographic process even at or near room temperature. In this kind of scenario, the competition between resolution and isomerization may results in an elution profile characterised by a typical shape showing a plateau between the peaks. A temperature dependent coalescence or decoalescence of peaks can be observed (fig. 2) as the isomerization becomes faster or slower than the elution process. Computer simulation of exchange-deformed elution profiles gives the apparent rate constants for the on-column interconversion that are fitted into the Eyring equation (2) and (3) to obtain the enthalpic

and entropic contributes to the energetic barrier of isomerization (ΔG^\ddagger).

$$\ln(k/T) = -\Delta H^\ddagger/R * 1/T + \ln \kappa k_b/h + \Delta S^\ddagger/R \quad (2)$$

$$k = (\kappa k_b T/h) e^{-\Delta G^\ddagger/RT} \quad (3)$$

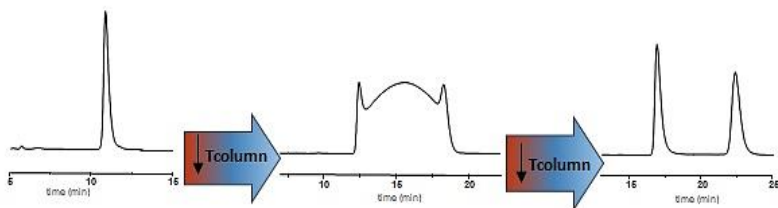


Fig.2 - Different elution profiles of a stereolabile compound. The on-column interconversion process can be slowed down by decreasing the temperature of the chromatographic column (from left to right), observing the decoalescence of the two peaks relative to the two enantiomers.

Low temperature dynamic chromatography results particularly handful to study those stereodynamic processes that happen with an energetic barrier lower than 21 kcal/mol, down to 14 kcal/mol. To bring these rapid interconversion phenomena in the same time-scale as the chromatographic

separation, the column must be cooled down at below zero temperatures. Drastically low temperature-chromatography (temperatures down to -78°C) presents practical and instrumental difficulties related to the increased viscosity of the mobile phases [8]. Fast stereoisomers interconversion can be studied by dynamic-NMR spectroscopy, a technique that has been applied extensively in kinetic studies of stereodynamic processes within a wide range of energetic barriers (from 5 kcal/mol up to over 30kcal/mol), with limitations due to the operational temperatures, boiling points of the deuterated solvents and NMR time-scale. The NMR time-scale is different from HPLC time-scale, with the former one being the faster of the two techniques, thus, making it particularly suitable in the study of rapid interconversions as those generated by single bond rotations. However, dynamic HPLC and dynamic NMR are complementary methods and when possible it is of great value to investigate the same stereodynamic behaviour using both approaches [11] [12]. HPLC and NMR can be coupled to chiroptical techniques such as optical rotary dispersion (ORD), circular dichroism (CD), vibrational ORD and CD, and circular polarization of emission (CPE), to afford structural information about chiral

compounds. Circular dichroism in particular plays a fundamental role in the study of conformational stereoisomers and is an invaluable tool for the elucidation of the absolute configuration of chiral compounds, helped by the continuous development of optimised quantum mechanical models [13]. In addition to structural analysis, chiroptical methods have found widespread use in kinetic studies of racemization and diastereomerization reactions.

References

- [1] Christian Wolf, *Dynamic Stereochemistry of Chiral Compounds*, RSC Publishing, Cambridge, 2008.
- [2] Jamie E. Smyth, Nicholas M. Butler and Paul A. Keller, *Nat. Prod. Rep.*, 2015, 32, 1562-1583.
- [3] Department of Health and Human Services, Food and Drug Administration 1992. *FDA's Policy Statement for the Development of New Stereoisomeric Drugs*.
- [4] Jonathan Clayden, *Chem. Commun.*, 2004, 2, 127-135.
- [5] Jochen R. Brandt, Francesco Salerno and Matthew J. Fuchter, *Nat. Rev. Chem.*, 2017, 1(0045), 1-12.
- [6] Ben L. Feringa, *Angew. Chem. Int. Ed.* 2017, 56, 11060 – 11078.
- [7] Michael Lämmerhofer, *J. of Chromat. A*, 2010, 1217, 814–856.
- [8] Darshan C. Patel, M. Farooq Wahab, Daniel W. Armstrong, Zachary S. Breitbach, *J. of Chromat. A*, 2016, 1467, 2–18.
- [9] Christian Wolf, *Chem. Soc. Rev.*, 2005, 34, 595–608.
- [10] Ilaria D'Acquarica, Francesco Gasparrini, Marco Pierini, Claudio Villani, Giovanni Zappia, *J. Sep. Sci.* 2006, 29, 1508-1516.

- [11] Daniele Casarini and Lodovico Lunazzi, Francesco Gasparrini, Claudio Villani, Maurizio Cirilli, Enrico Gavuzzo, *J. Org. Chem.* 1995, 60, 97-102.
- [12] Francesco Gasparrini, Ludovico Lunazzi, Andrea Mazzanti, Marco Pierini, K. Michal. Pietrusiewicz, and Claudio Villani, *J. Am. Chem. Soc.* 2000, 122, 4776-4780.
- [13] Gennaro Pescitelli, Lorenzo Di Bari and Nina Berova, *Chem. Soc. Rev.*, 2011, 40, 4603–4625.

PART A

*Investigation of the stereodynamics
and optical properties of compounds
presenting helical and axial chirality*

PART A-1

*Stereostable and stereolabile helicenes
investigated by enantioselective HPLC and
chiro-optical methods*

1. Introduction

Helicenes are non-planar PAH compounds, in which several ortho-fused aromatic rings constitute a helically distorted structural backbone (fig 1.1). This intriguing class of compounds adopts a helical chiral topology that contributes to the numerous outstanding properties of helicenes. High optical rotation values, inherent chirality, dynamic behaviour, circularly polarized light absorption and emission and many peculiar physical and chemical characteristics justify the increasing interest in helically distorted PAHs.

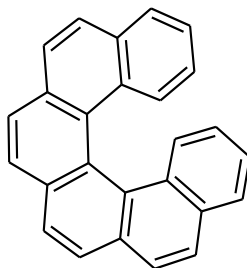


Fig. 1.1 - [6]carbohelicenes structure

While the first synthesis of a carbo[4]helicene was reported by Weitzenböck and Lieb in 1912, it was not until later in the

50's that the interest for helicenes started to grow in the scientific community [1] [2], to reach his peak in the last two decades [3][4][5]. Various synthetic methodologies have been investigated [6], allowing to obtain a wide range of inherently chiral helical compounds. Compounds with the chiral helical structure are nowadays involved in research about supramolecular chemistry, asymmetric catalysis, innovative materials for opto-electronical applications, nanoscience and chiral recognition. Distortion in the ortho-fused aromatic core derives from a balance of forces, on one side the torsional strain in the aromatic backbone and on the other side the steric hindrance in the fjord region (fig 1.2).

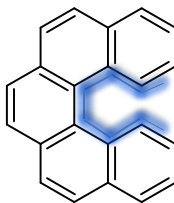


Fig.1.2 - The fjord-region of a [5]helicene is evidenced in blue.

The conformation that results by minimizing the steric hindrance is in distress and exists as a persistent chiral helix. The enantiomers are represented by the right-handed helix

indicated with the configuration P and the left-handed helix indicate by M. The interconversion rate between the two enantiomers of a helicene, and consequently the stability of the helical conformation, depends primarily on intramolecular steric effects and, on a minor scale, on electronic effects. As the number of ortho-fuse aromatic rings grows, the hydrogen atoms of the terminal rings start to overlap increasing the steric tension of the system (fig 1.3). The value n in [n]helicenes represents the number of rings and is an important factor in controlling the rate of interconversion between two differently oriented helices. When n is 4 the overlapping of the terminal aromatic rings is only partial while the torsional angle of the conjugated skeleton increases when n is 5 or more [7]. Therefore, overcrowding in the fjord region forces ortho-fused polyaromatic systems to adopt a non-planar conformation to decrease the Van der Waals interactions [8] [9]. The racemization pathway goes through a conformational change into a non-chiral TS with a C_s symmetry that can originate both the (P) and the (M) configuration [10].

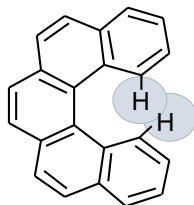


Fig 1.3 - Overcrowding in the fjord region and consequent overlaying of the hydrogen atoms of the terminal rings in a [5]helicenes.

Most of the synthetic methodologies reported in literature follow photochemical pathways or Diels-Alder strategies. In 2015 Mori et al. [11] described a one-step synthesis of a [16]helicene while recently Schulte et al. reported the synthesis of helicene-based coordination cages [12]. In 2016 a synthetic strategy involving photocyclization allowed Upadhyay et al. to synthesize a series of Aza[n]helicenes [13]. Along with the more classic carbo[n]helicenes and hetero[n]helicenes, many efforts have been devoted in the synthesis and characterization of helicene-like compounds as chiral nanographene, peropyrenes and benzotetracenes [14] [15] [16] [17]. The high grade of π conjugation contributes to the high values of optical rotation and circular dichroism of helical chiral compounds which show also a strong and typical Cotton Effect [18]. The unique chiro-optical properties

of this class of compounds are exploited in the design of innovative materials as circularly polarized light emitters [19] to be used in organo-electronics for the production of 3D displays or in cryptography. Helicenes can be used as chiroptical switches [20], this functional molecular devices based on bistability are studied for their application in data storage, molecular machines and asymmetric catalysis. As an example of the wide applicability of this class of compounds, recently it has been reported the synthesis and the application of a thiahelicene-based chiral film [21] in enantioselective electroanalysis. The intense chiro-optical responses of helicenes and related helical chiral compounds are helpful in the assignation of the Absolute Configuration by computational studies of the ECD and ORD spectra.

Resolution of the enantiomeric couples of helicenes and helicene-like compounds is a key step in the science of this category of interesting compounds. HPLC with chiral stationary phase is reported as an efficient and versatile method to resolve racemic mixtures of compounds with helical chirality. Particularly successful in separating the enantiomers of carbo[n]helicenes and hetero[n]helicenes are polysaccharide-based chiral stationary phase, in which a

functionalized polymer of cellulose or amylose is immobilized or coated on silica gel. The selective diastereomeric interactions between analyte and stationary phase allow obtaining good resolutions and high selectivity. Numerous separation methods for the chiral resolution are reported in literature and both normal- phase and reverse-phase HPLC are effective depending on the chemical modifications of the helical molecular backbone [22] [23] [24]. By scaling up the analytical method to a preparative level, it is possible to collect milligrams of optically pure helicenes. This is essential to perform chiro-optical characterization (ECD, VCD, CLP) and to have sufficient data to assign the absolute configuration. The rate of racemization of [n]helicenes is variable and can be measured performing a thermal racemization starting from a single enantiomer. During this kind of experiments, the reaction is monitored over time to determine the kinetic parameters from the decay of the enantiomeric excess. The racemization can be monitored by CSP-HPLC, integrating the area of peaks at different times, or by measuring the decay of the CD or OR signal when the optically pure sample is heated up to a desired temperature for a certain amount of time. For

[n]helicenes in which n is lower or equal than 4, or if n is 5 but the TS of the racemization is stabilized by electronic effects, the ΔG^\ddagger values of stereomutation are usually lower than 24 kcal/mol and the half-lives of the single enantiomers make it difficult to isolate them at or near room temperature. Aza[5]helicenes for example, are reported to have lower values of ΔG^\ddagger [25] of racemization compared to [5]carbohelicenes [26]. Dynamic-HPLC with chiral stationary phase in these cases is an efficient method to study the enantiomerization rate of stereochemically labile helicenes and other helical compounds. D-HPLC is coupled to computer simulations of the dynamic experimental chromatograms to calculate barriers of enantiomerization for [n]helicenes down to 14 kcal/mol.

2.Results and Discussion

2.1 *Hetero[6]helicenes*

Enantiomers of hexahelicenes are normally stereochemically stable and can be successfully resolved by HPLC. Polysaccharide-based chiral stationary phase Chiralpak IA was used to achieve the separation of one aza[6]helicene and two azaoxa[6]helicenes (figure 2.1) in normal phase HPLC.

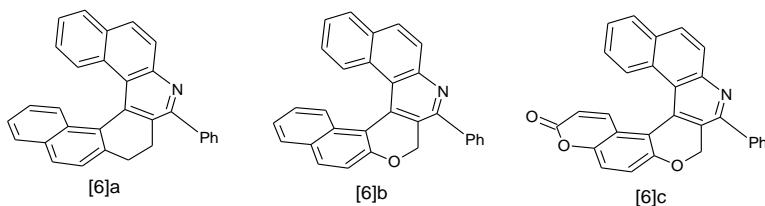


Fig. 2.1 - [6]heterohelicenes obtained by Povarov reaction and resolved by CSP-HPLC.

The three hetero[6]helicenes studied are obtained by Povarov reaction [27] and present one non-aromatic ring that can give partially more flexibility to the ortho-fused system compared to a fully conjugated one. The racemic mixtures of the three compounds were resolved by HPLC in two peaks well separated at the baseline (fig. 2.2-2.4). The ECD detector

shows two opposite signals corresponding to the two enantiomers.

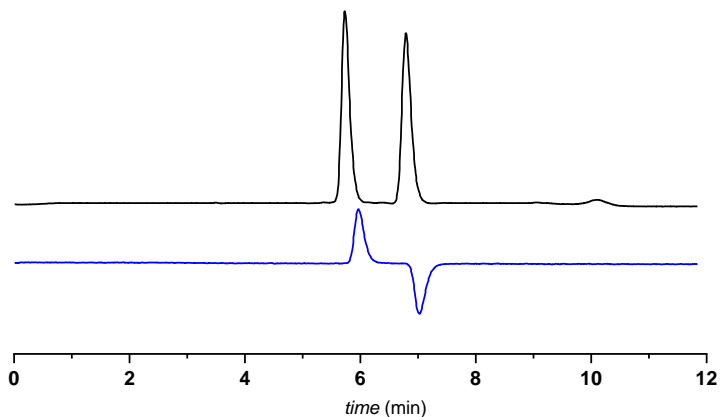


Fig. 2.2 - Elution profile of compound [6]a. Column: Chiralpak IA; Mobile phase: hexane/dichloromethane/methanol (90/10/1 v/v/v); flow rate: 1 ml/min; Detector: UV-VIS 280 nm (black trace) CD 280 nm (blue trace).

tr1 (min)	tr2 (min)	k'1	k'2	α	A% 1
5,73	6,77	0,64	0,93	1,45	50

Tab. 2.1 - Chromatographic parameters of [6]a for the experimental conditions reported in fig. 2.2. Capacity factors and selectivity are calculated starting from the retention time and dead time.

Compound **[6]a** was resolved in two peaks clearly separated at the baseline and in enantiomeric relation as deduced by the relative area and by the CD signal. A higher value of selectivity (see Table 2.2) has been found for compound **[6]b** in the same experimental conditions.

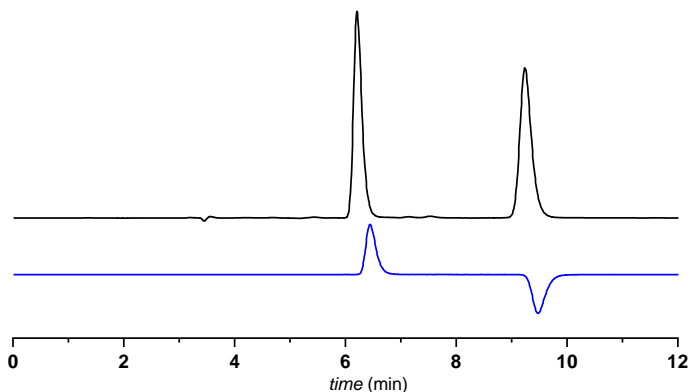


Fig 2.3 - Elution profile of compound **[6]b**. Column: Chiralpak IA; Mobile phase: hexane/dichloromethane/methanol (90/10/1 v/v/v); flow rate: 1 ml/min; Detector: UV-VIS 280 nm (black trace) CD 280 nm (blue trace).

tr1 (min)	tr2 (min)	k'1	k'2	α	A% 1
6,20	9,23	0,77	1,64	2,13	50

Tab. 2.2 - Chromatographic parameters of **[6]b** for the experimental conditions reported in fig 2.3. Capacity factors and selectivity are calculated starting from the retention time and dead time.

Among the three studied compounds [6]c is the more retained one. Therefore, to shorten the analysis time the experimental conditions were adjusted differently increasing the polarity of the mobile phase.

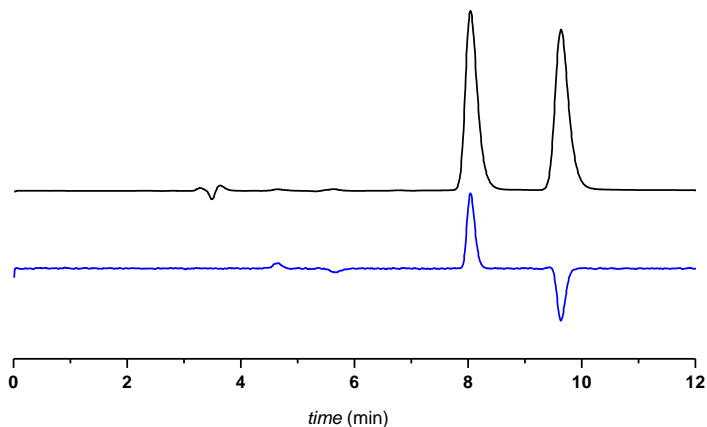


Fig. 2.4. - Elution profile of compound [6]c. Column: Chiralpak IA; Mobile phase: hexane/dichloromethane/methanol (75/25/1 v/v/v); flow rate: 1 ml/min; Detector: UV-VIS 280 nm (black trace) CD 280 nm (blue trace).

tr1 (min)	tr2 (min)	k'1	k'2	α	A% 1
8,04	9,63	1,29	1,75	1,36	50

Tab. 2.3. - Chromatographic parameters of [6]c for the experimental conditions reported in fig 2.4. Capacity factors and selectivity are calculated starting from the retention time and dead time.

The optimized HPLC analytical conditions have been scaled up to semipreparative level and thanks to the stereochemical stability of [6]helicenes it was possible to collect milligrams of optically pure enantiomers. Incubating samples of the single enantiomers of each compounds at different temperatures and in an appropriate solvent it has been possible to monitor the racemization reaction by CSP-HPLC (see figure 2.5).

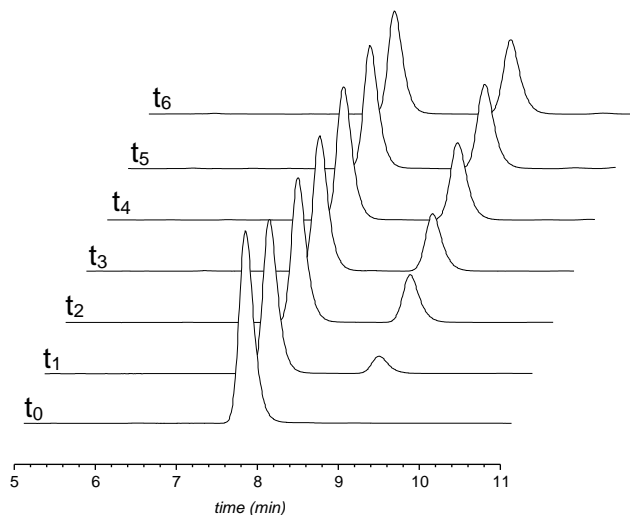


Fig. 2.5 - Racemization of [6]c in decalin at 90°C monitored over time by CSP-HPLC, starting from the first eluted enantiomer, optically pure. ($t_0=0$ min, $t_1=15$ min, $t_2=30$ min, $t_3=60$ min, $t_4=90$ min, $t_5=120$ min, $t_6=140$ min).

The experiment has been repeated for all the three compounds in a range of temperatures between 70 °C and 100 °C for [6]b and [6]c and between 130 °C and 150 °C for [6]a, starting from the single enantiomers dissolved in decalin. The decay of the enantiomeric excess was monitored over time and calculated by integration of the peaks in the elution profile. The kinetic rate constants of the racemization process are obtained as the slope of the line resulting from the correlation between the logarithm of the enantiomeric excess and the reaction time (figure 2.6).

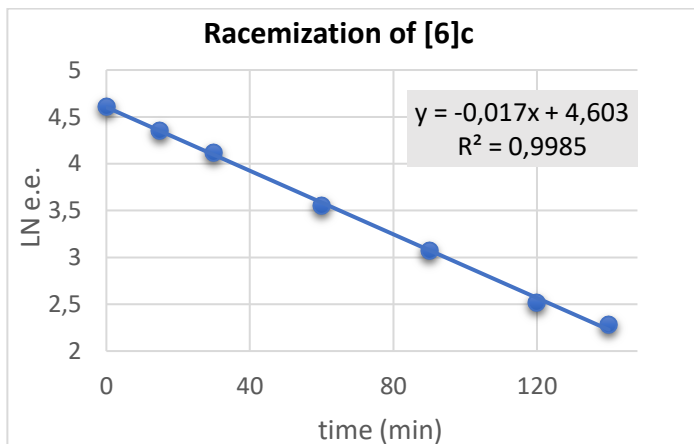


Fig. 2.6 - Variation over time of the enantiomeric excess starting from a single enantiomer of [6]c incubated in Decalin at 90°C and monitored by HPLC.

In table 2.4 are reported the data obtained from the racemization reactions, performed in decalin, of all the three compounds at three different temperatures.

[6]a

T (°C)	k_{rac} (min⁻¹)	R²
130	0,00061	0,9951
140	0,0016	0,9988
150	0,0046	0,9997

[6]b

T (°C)	k_{rac} (min⁻¹)	R²
70	0,0015	0,9997
90	0,0191	0,9958
100	0,0395	0,9991

[6]c

T (°C)	k_{rac} (min⁻¹)	R²
70	0,0018	0,9989
90	0,0169	0,9985
100	0,0449	0,9969

Tab. 2.4. - Kinetic parameters of the racemization for [6]a, [6]b, [6]c, measured at three temperatures.

The Eyring equation allows the linear correlation between the free energy of activation and the temperature of the reaction. From this correlation it is possible to extrapolate the values of the enthalpic and entropic contributes to the activation energy of the racemization process. The slope of the line represents the value of $-(\Delta H^\ddagger/R)$ while the intercept is equal to $\Delta S^\ddagger/R + \ln(k_B/h)$ where R , k_B and h are the gas, the Boltzmann, and the Plank constant respectively (figures 2.7-2.9). From the extracted data it is evident that for this kind of stereomutation process the enthalpy is the driven force, while the entropic contribute is almost null.

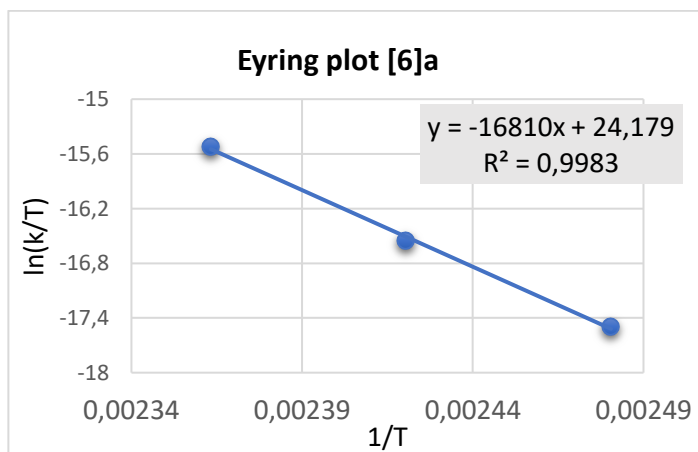


Fig. 2.7 - Eyring plot of compound [6]a. $\Delta H^\ddagger = 33,40$ kcal/mol, $\Delta S^\ddagger = 0,75$ cal/mol*K.

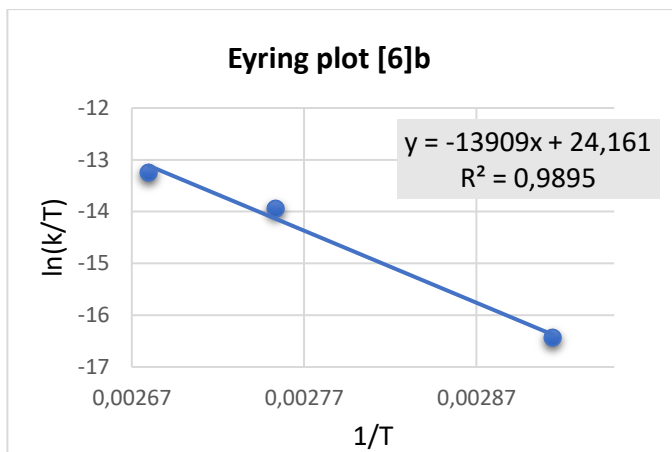


Fig. 2.8 - Eyring plot of compound [6]b. $\Delta H^\ddagger = 27,64$ kcal/mol, $\Delta S^\ddagger = 0,72$ cal/mol*K.

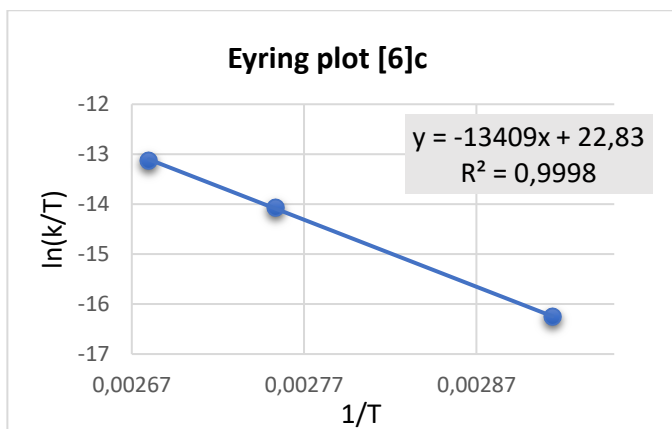


Fig. 2.9 - Eyring plot of compound [6]c. $\Delta H^\ddagger = 26,65$ kcal/mol, $\Delta S^\ddagger = -1,93$ cal/mol*K.

T°C	$\Delta G^{\ddagger}_{\text{rac}}$ (kcal/mol) [6]a
130	33,10
140	33,09
150	33,08
25	33,16

T°C	$\Delta G^{\ddagger}_{\text{rac}}$ (kcal/mol) [6]b	$\Delta G^{\ddagger}_{\text{rac}}$ (kcal/mol) [6]c
70	27,39	27,31
90	27,38	27,35
100	27,37	27,37
25	27,42	27,22

Tab 2.5 - ΔG^{\ddagger} (kcal/mol) of racemization calculated at three temperatures and at 25°C. Errors in $\Delta G^{\ddagger} \pm 0,02$ kcal/mol.

Compounds [6]b and [6]c both present a similar averaged value of $\Delta G^{\ddagger}_{\text{rac}} = 27,30$ kcal/mol. A higher value of approximately 33,05 kcal/mol is calculated for [6]a. This difference may be correlate to the presence of the oxygen atom in the helical backbone of those less stereochemically stable compounds. Additionally, the optical rotation power of the single enantiomers has been studied. The $[\alpha]_D$ resulted ± 633 , ± 790 and ± 730 respectively for [6]a, [6]b and [6]c with

the 1st eluted being the (+) enantiomer and the 2nd eluted the (-) enantiomer. The high values of OR_{sp} are typical of helicenes, being in good agreement with literature data.

2.2 Aza[5]-helicenes

[n]Helicenes with values of $n \leq 5$ and at the same time not hindered in the fjord region, have ΔG^\ddagger of racemization usually lower than 24.5 kcal/mol at 25°C. The two Aza[5]helicenes considered in this study (fig. 2.10) were analysed by CSP-HPLC.

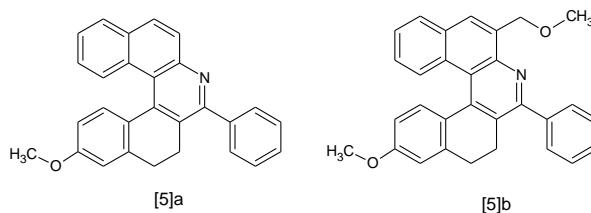


Fig. 2.10 - Structures of the two [5]Aza-helicenes [5]a and [5]b.

Chiral stationary phase Chiralpak IA gave the best results in order of selectivity with a mobile phase composed by hexane, dichloromethane and methanol. The elution profiles of both samples show just one broad peak, as expected for stereolabile helical derivatives (fig. 2.11).

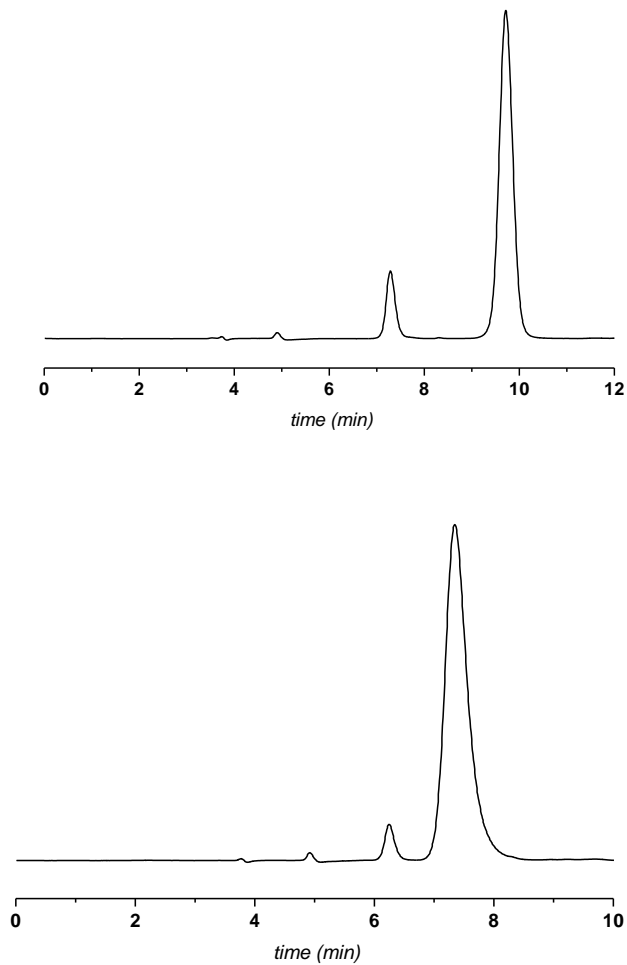


Fig. 2.11 - Elution profile of [5]a (top) and [5]b (bottom). Column: Chiralpak IA; mobile phase: hexane/dichloromethane/methanol (90/10/1 v/v/v); flow rate: 1 ml/min; detector: UV 280 nm; T_{col} : 15 °C.

In the elution profile of both samples are present two peaks: a less retained chemical impurity and one broad peak attributable to the helical derivative. The lack of resolution is due to the fast interconversion between the two enantiomers. Variable temperature HPLC experiments (fig. 2.12 and fig. 2.13) have been performed with the CSP Chiralpak IA, in order to slow down the enantiomerization process and to reach a complete decoalescence of peaks.

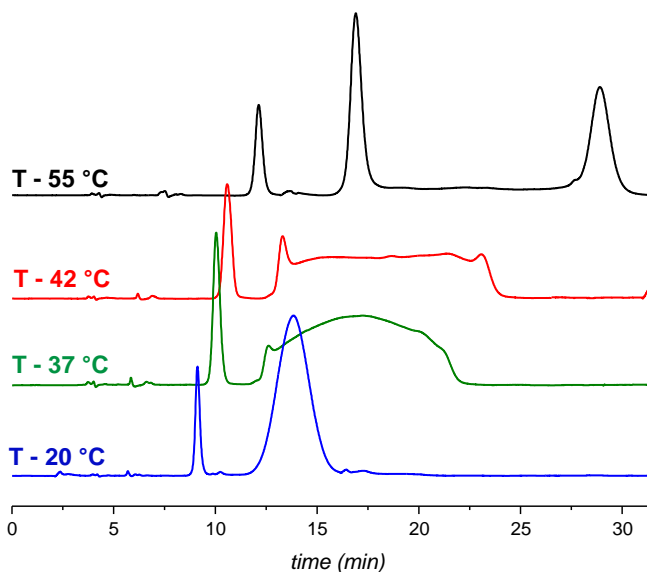


Fig. 2.12 - Dynamic-HPLC experiments performed on compound [5]a. Column: Chiralpak IA; Mobile phase: hexane/dichloromethane/methanol (90/10/1 v/v/v); flow rate: 1 ml/min; Detector: UV 280 nm; T_{col} : variable

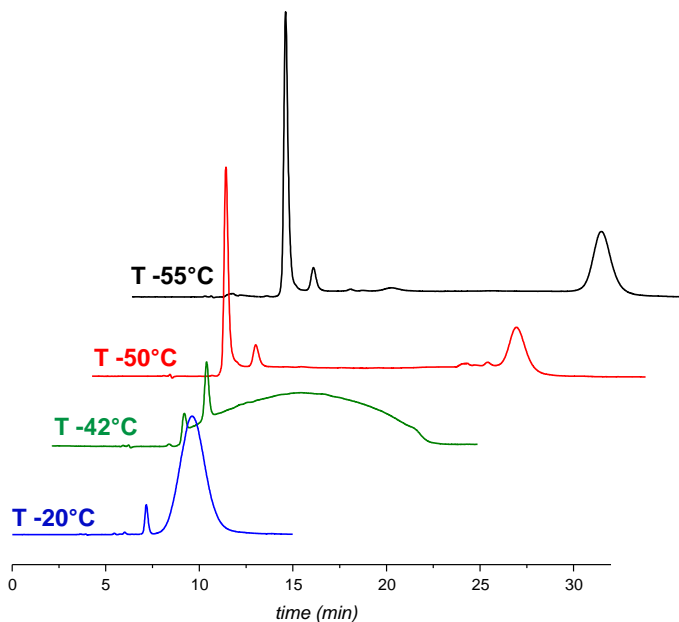


Fig 2.13 - Dynamic-HPLC experiments performed on compound [5]b. Column: Chiralpak IA; Mobile phase: hexane/dichloromethane/methanol (90/10/1 v/v/v); flow rate: 1 ml/min; Detector: UV 280 nm; T_{col} : variable.

Complete decoalescence of peaks, for both compounds, is visible at very low temperature, indicating low energetic barriers of enantiomerization. Elution profile with a plateau between the peaks indicates an interconversion process on column, happening in the same timescale of the chromatographic process. Studying the experimental dynamic chromatograms with a software lab-developed

allow to extract the kinetic parameters of the enantiomerization process. Program *DHPLC y2k* based on the stochastic model elaborate the experimental chromatograms and perform simulation after various iteration cycles to achieve the best fitting result. Simulated chromatograms (red trace), superimposed to the experimental ones (black trace) are reported in figure 2.14.

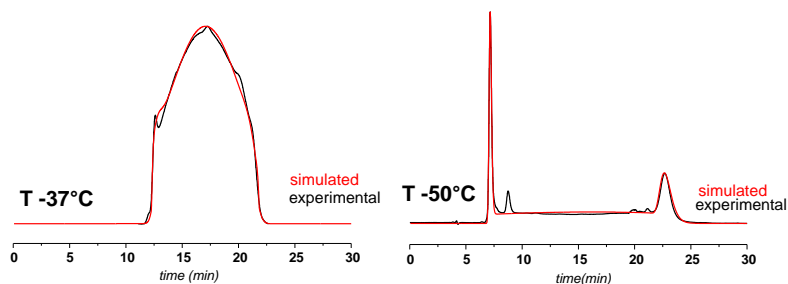


Fig. 2.14 - Experimental and simulated chromatograms of [5]a at -37°C (left) and [5]b at -50°C (right).

Computer simulations gave the apparent rate constants for the on-column interconversion. The calculated activation energies of enantiomerization of [5]a and [5]b (tab. 2.6) are very similar and sensibly lower than those reported in literature for analogues [5]carbohelicenes and [5]azahelicenes. This discrepancy may be caused by the lack

of an unsaturation in one of the five-rings and the incorporation of the nitrogen atom, both contributing to an open geometry. The $\Delta G^{\ddagger}_{1,2}$ are the lowest one and are related to the interconversion of the first eluted enantiomer into the second eluted. This values are more similar to those obtained with other techniques since the influence of the stationary phase is minimized.

[5]a

T_{col} (°C)	k₁ (min⁻¹)	k₋₁ (min⁻¹)	ΔG^{\ddagger}_{12} (kcal/mol)	ΔG^{\ddagger}_{21} (kcal/mol)
-42	0,137	0,077	16,21	16,47
-37	0,211	0,122	16,36	16,62

[5]b

T_{col} (°C)	k₁ (min⁻¹)	k₋₁ (min⁻¹)	ΔG^{\ddagger}_{12} (kcal/mol)	ΔG^{\ddagger}_{21} (kcal/mol)
-50	0,125	0,039	15,67	16,18
-42	0,429	0,149	15,68	16,17

Tab. 2.6. - Kinetic rate constants and energetic barriers of the on-column enantiomerization of [5]a (top) and [5]b (bottom) [6]c. Column temperatures are intended $\pm 0,1$ °C. Errors in $\Delta G^{\ddagger} \pm 0,02$ kcal/mol.

2.3 Hetero[4]helicenes and pyrene-based pseudo-helicenes.

When $n=4$ the interconversion rate of [n]helicenes is usually very high at room temperature since there isn't almost any overlapping of the terminal rings. The presence of substituents in the cove-region is required to stabilize single helical isomers, then, depending on the steric hindrance, the interconversion process can be slowed down ($\Delta G \sim 20$ kcal/mol).

2.3.1 Aza[4]helicenes

Three aza[4]helicenes (fig 2.15) have been studied by enantioselective HPLC in order to achieve a chromatographic resolution of enantiomers and measure the interconversion kinetic parameters.

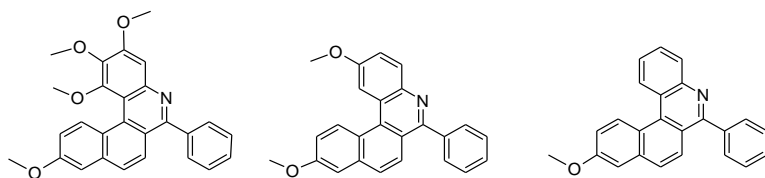


Fig. 2.15 - [4]a, [4]b, [4]c (from left to right) are the aza[4]helicenes investigated.

Amongst them, only [4]a presents a substituent in the cover-region, while [4]b and [4]c show substituents at remote positions of the terminal rings, not relevant for the stereochemical stability. Polysaccharide based CSP like Chiralpak IA or IB are known to be a good choice to obtain the chiral resolution of this kind of compounds. In fact, the chromatographic resolution was attempted using Chiralpak IA as stationary phase and an eluent composed by hexane, dichloromethane and methanol (fig. 2.16-2.18). Unfortunately, all of the three compounds failed to separate, and the elution profiles presented just one peak even decreasing the temperature of the column down to -60°C .

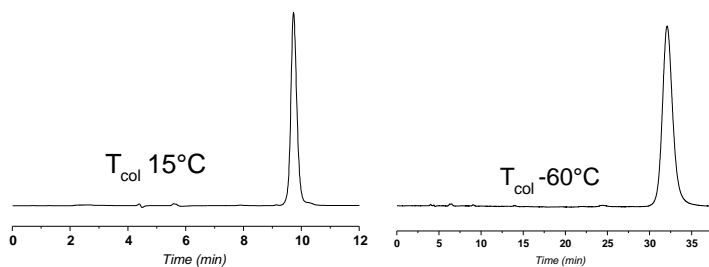


Fig 2.16 - Elution profiles of [4]a obtained performing the experiment at two different temperatures. Column: Chiralpak IA; Mobile phase: hexane/dichloromethane/methanol (90/10/1 v/v/v); 1 ml/min; Detector: UV 280 nm;

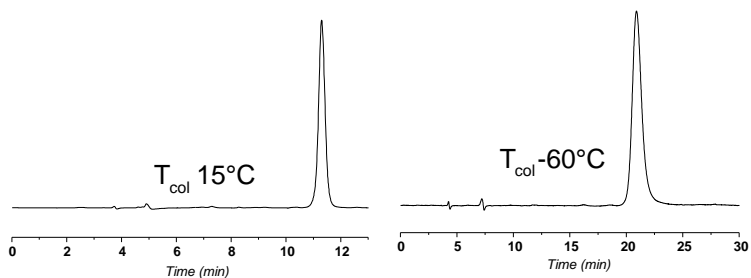


Fig. 2.17 - Elution profiles of [4]b obtained performing the experiment at two different temperatures. Column: Chiralpak IA; Mobile phase: hexane/dichloromethane/methanol (90/10/1 v/v/v); flow rate: 1 ml/min; Detector: UV 280 nm;

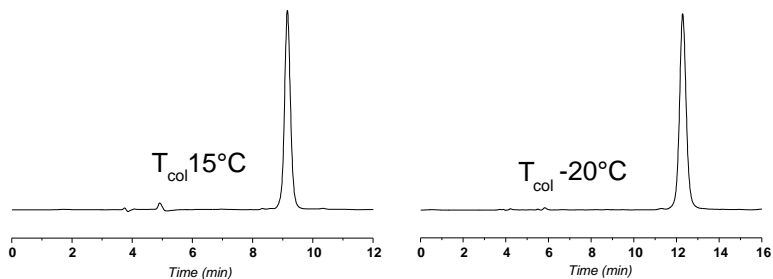


Fig. 2.18 - Elution profiles of [4]b obtained performing the experiment at two different temperatures. Column: Chiralpak IA; Mobile phase: hexane/dichloromethane/methanol (90/10/1 v/v/v); flow rate: 1 ml/min; Detector UV 280 nm;

The presence of just one peak in the experimental chromatograms may be due to a lack in selectivity of the chiral stationary phase, to a fast on-column interconversion

of the enantiomers, or to a combination of both factors. In these cases, dynamic-chromatography resulted insufficient in measuring the kinetic parameters and other techniques as d-NMR can be tried since the ΔG^\ddagger values are expected to be lower than 14 kcal/mol.

2.3.2 Pyrene-fused pseudo-[4]helicenes

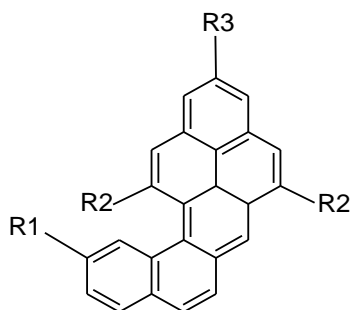
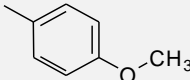
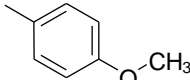
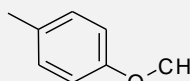
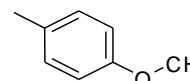
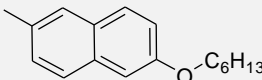


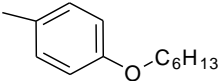
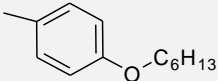
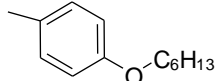
Fig. 2.19 - Polyaromatic helically distorted pseudo[4]helicene core

Figure 2.19 shows the polyaromatic backbone of a series of eight pseudo-[4]helicenes variously derivatized (tab. 2.7). Two of the aromatic rings of the helical core are fused into a pyrene framework. Because of the helical topology, the compounds are chiral and exist as couple of enantiomers. In order to develop an analytical method to chromatographically resolve the M and P stereoisomers of every compound,

different chiral stationary phases and eluents have been tested. The best conditions required the Chiralpak IA CSP and an eluent composed by hexane, dichloromethane and methanol, in accordance with previous experiments on helicenes.

Most of the compounds failed to separate in two distinct peaks at room temperature while in two cases (**7** and **8**) the profiles had a typical shape characteristic of an on-column interconversion: two peaks and a plateau in between (fig. 2.20).

	R1	R2	R3
1	-H		-CH ₃
2	-H		-C(CH ₃) ₃
3	-H		-CF ₃
4	-H		-COOC ₂ H ₅
5	-H		-C(CH ₃) ₃

6	-H		-CF ₃
7	-CF ₃		-C(CH ₃) ₃
8	-OCH ₃		-C(CH ₃) ₃

Tab. 2.7 - Substituents in R1, R2 and R3 of the eight pseudo-[4]helicenes studied. Compounds 7 and 8 are the only one showing a second substituent near the cove region.

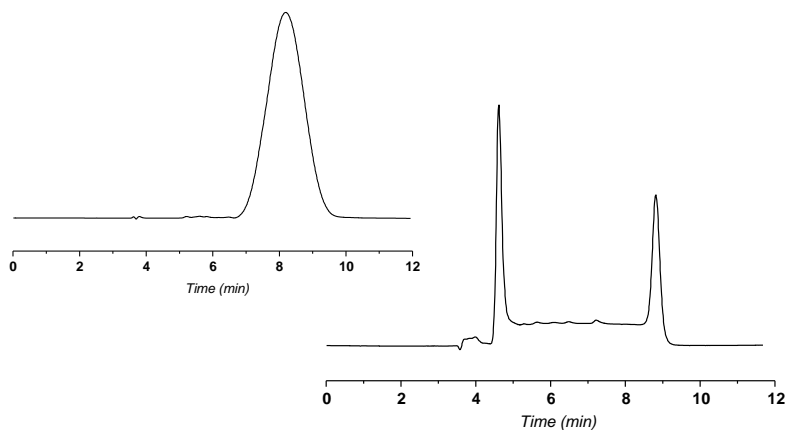


Fig. 2.20 - CSP-HPLC profile of compounds 5 (top) and 8 (bottom) in the same experimental conditions. Column: Chiralpak IA; Mobile phase: hexane/dichloromethane/methanol (90/10/1 v/v/v); flow rate: 1 ml/min; Detector: UV 280 nm; Tcol +20°C.

for compounds **1** to **6**, decreasing the temperature of the chromatographic column resulted in the decoalescence of the broad single peak observed at room temperature into two peaks with a 50/50 area ratio (fig. 2.21-2.26). Therefore, the lack of separation observed in the first screening was attributed not to a weak selectivity of the CSP but to a fast on-column interconversion process. The measurements were performed at 0°C, 10°C, 20°C, 30°C and 40°C. The six compounds with just one substituent in the cove region were almost, but not entirely, baseline separated at 0°C, still presenting some interconversion.

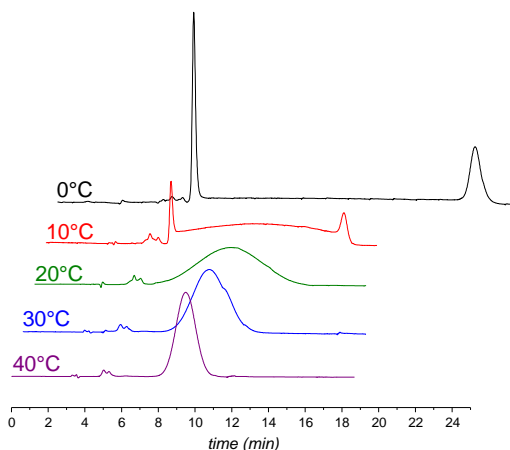


Fig. 2.21 - D-HPLC experiments performed on compound 1. Column: Chiralpak IA; Mobile phase: hexane/dichloromethane/methanol (90/10/1 v/v/v); flow rate: 1 ml/min; Detector: UV 280 nm; T_{col} : variable.

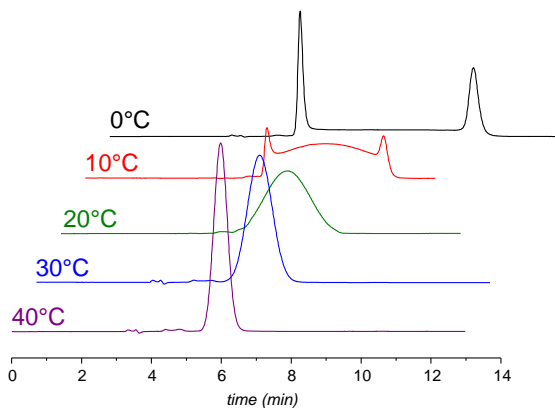


Fig. 2.22 - D-HPLC experiments performed on compound 2. Column: Chiralpak IA; Mobile phase: hexane/dichloromethane/methanol (90/10/1 v/v/v); flow rate: 1 ml/min; Detector: UV 280 nm; T_{col} : variable.

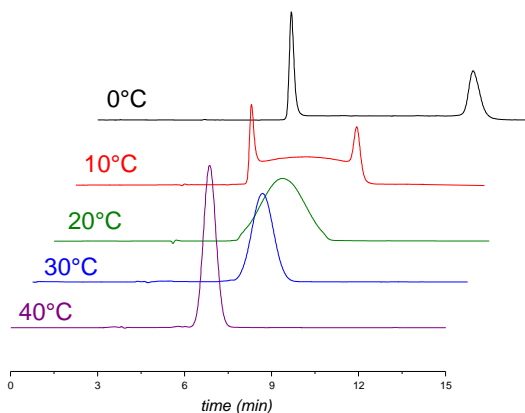


Fig. 2.23 - D-HPLC experiments performed on compound 3. Column: Chiralpak IA; Mobile phase: hexane/dichloromethane/methanol (90/10/1 v/v/v); flow rate: 1 ml/min; Detector: UV 280 nm; T_{col} : variable.

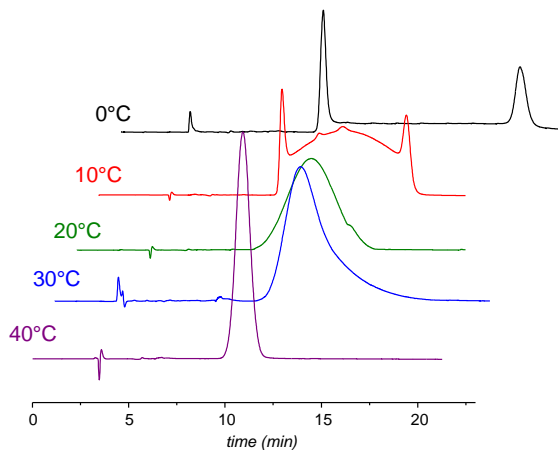


Fig. 2.24 - D-HPLC experiments performed on compound 4. Column: Chiralpak IA; Mobile phase: hexane/dichloromethane/methanol (90/10/1 v/v/v); flow rate: 1 ml/min; Detector: UV 280 nm; T_{col} : variable.

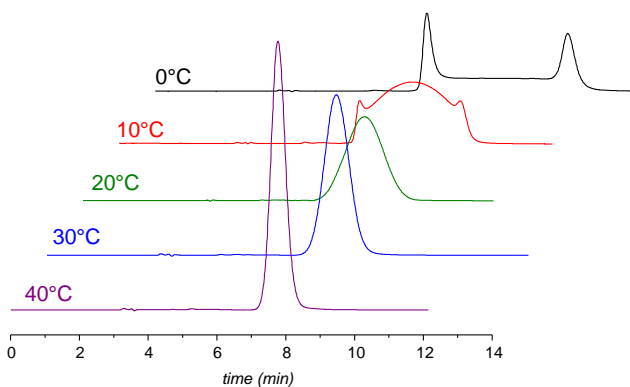


Fig. 2.25 - D-HPLC experiments performed on compound 5. Column: Chiralpak IA; Mobile phase: hexane/dichloromethane/methanol (90/10/1 v/v/v); flow rate: 1 ml/min; Detector: UV 280 nm; T_{col} : variable.

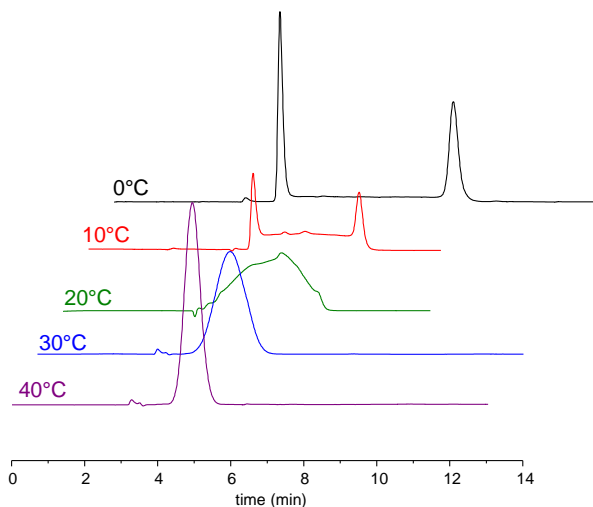


Fig. 2.26 - D-HPLC experiments performed on compound 6. Column: Chiralpak IA; Mobile phase: hexane/dichloromethane/methanol (90/10/1 v/v/v); flow rate: 1 ml/min; Detector: UV 280 nm; T_{col} : variable.

Compounds **7** and **8** were already almost resolved into two peaks at room temperature. The presence of a second substituent, near the cove region increases the steric hindrance and, subsequently, reduces the interconversion rate constant. Accordingly, rising the temperature of the column up to 60°C causes the coalescence of peaks into one broad single peak. Variable temperature HPLC experiments were

performed to study the on-column interconversion process (fig. 2.27 – 2.28).

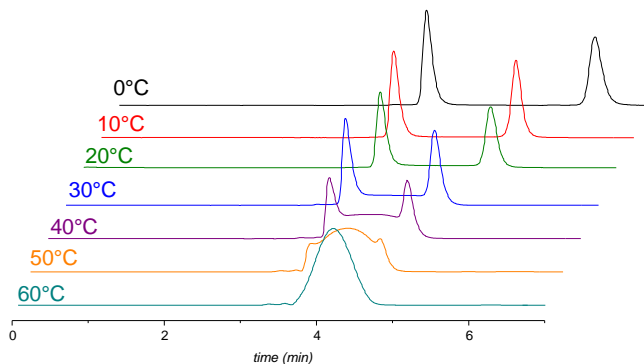


Fig. 2.27 - D-HPLC experiments performed on compound 7. Column: Chiralpak IA; Mobile phase: hexane/dichloromethane/methanol (90/10/1 v/v/v); flow rate: 1 ml/min; Detector: UV 280 nm; T_{col} : variable.

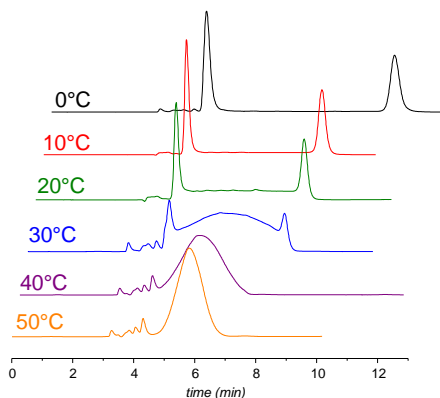


Fig. 2.28 - D-HPLC experiments performed on compound 8. Column: Chiralpak IA; Mobile phase: hexane/dichloromethane/methanol (90/10/1 v/v/v); flow rate: 1 ml/min; Detector: UV 280 nm; T_{col} : variable.

The experimental chromatograms presenting a plateau between the two peaks, indicative of an on-column interconversion, have been simulated with the DHPLC y2k software, to measure the kinetic parameters (fig. 2.29-2.35).

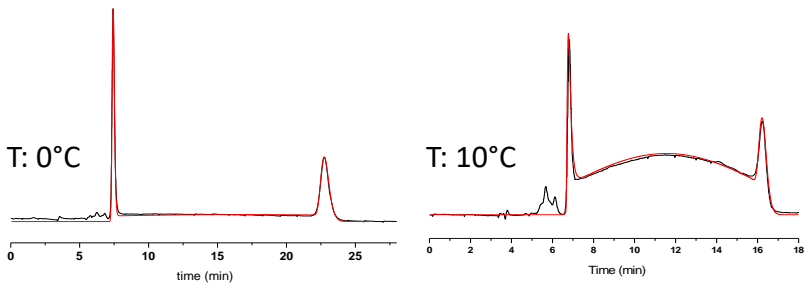


Fig. 2.29 - Simulated (red) and experimental (black) chromatograms of 1.

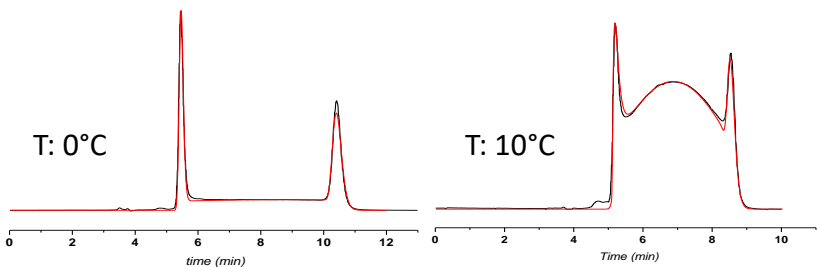


Fig. 2.30 - Simulated (red) and experimental (black) chromatograms of 2.

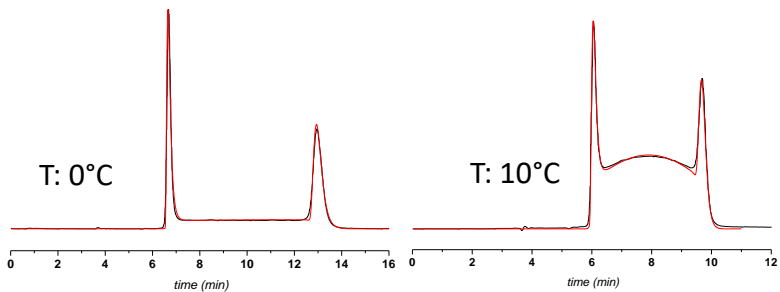


Fig. 2.31 - Simulated (red) and experimental (black) chromatograms of 3.

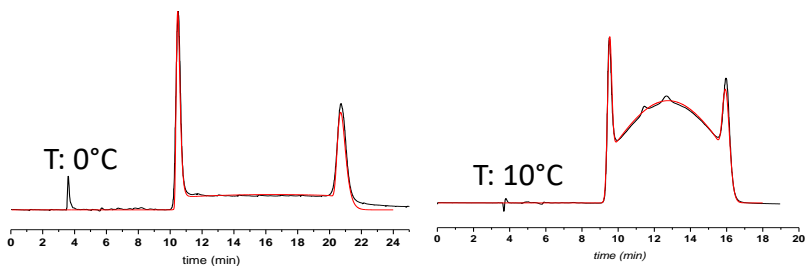


Fig. 2.32 - Simulated (red) and experimental (black) chromatograms of 4.

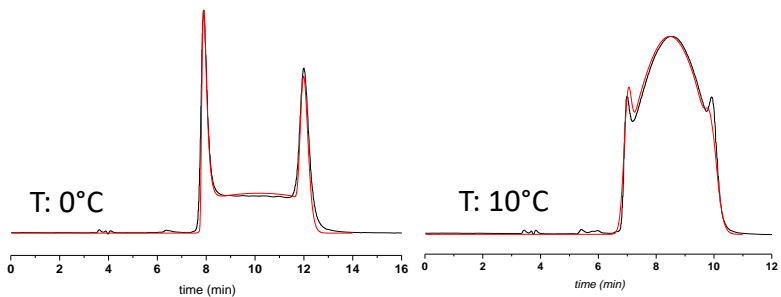


Fig. 2.33 - Simulated (red) and experimental (black) chromatograms of 6.

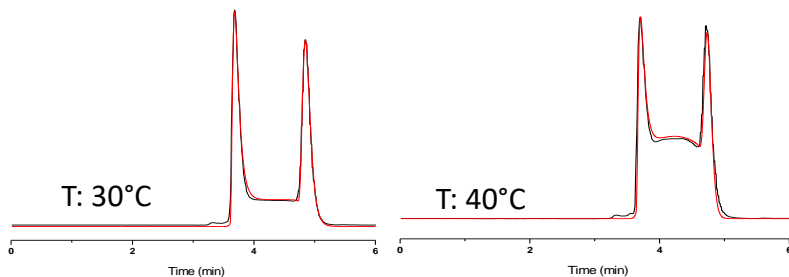


Fig. 2.34 - Simulated (red) and experimental (black) chromatograms of 7.

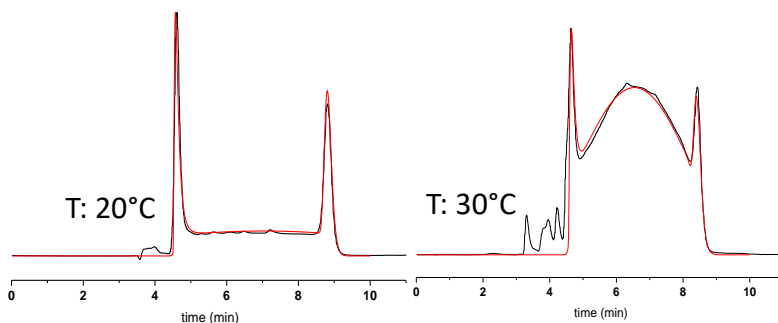


Fig. 2.35 - Simulated (red) and experimental (black) chromatograms of 8.

As reported in table 2.8, for each compound the k_{12} , and k_{21} values are extracted and the corresponding ΔG_{12}^{\ddagger} and ΔG_{21}^{\ddagger} are then calculated. The lowest calculated value of ΔG_{av}^{\ddagger} of enantiomerization is 19,5 kcal/mol for compound **2**, while the highest value was found for compound **7** and is equal to 21,7 kcal/mol. In general, for compound **1** to **6** the activation energy of enantiomerization fluctuate slightly around an

average value of 19,7 kcal/mol. On the other hand, compounds **7** and **8** differ sensibly from the other pseudo-[4]helicenes, having a higher half-life of interconversion within the timescale of minutes.

	T col (°C)	$k_{\text{en } 12}$ (min ⁻¹)	$\Delta G_{\text{en } 12}^\ddagger$ (kcal/mol)	$k_{\text{en } 21}$ (min ⁻¹)	$\Delta G_{\text{en } 21}^\ddagger$ (kcal/mol)	$k_{\text{en av}}$ (min ⁻¹)	$\Delta G_{\text{en av}}^\ddagger$ (kcal/mol)
7	40	0,32	21,62	0,25	21,77	0,28	21,70
8	30	0,47	20,68	0,26	21,03	0,37	20,85
1	10	0,29	19,53	0,12	20,02	0,21	19,78
2	10	0,38	19,39	0,23	19,67	0,31	19,53
3	10	0,25	19,63	0,15	19,90	0,20	19,77
4	10	0,21	19,72	0,13	20,01	0,17	19,87
5	10	0,32	19,51	0,22	19,71	0,26	19,61
6	10	0,26	19,61	0,16	19,89	0,21	19,75

Tab. 2.8 - kinetic rate constants and energetic barriers calculated for the on-column enantiomerization. Column temperatures are intended $\pm 0,1$ °C. Errors in $\Delta G \pm 0,02$ kcal/mol.

The two enantiomers of the more stereochemically stable compounds (**7** and **8**) are separated and furtherly characterized by ECD (fig 2.36-2.37). Few milligrams of

optically pure enantiomers are collected by semipreparative HPLC, scaling up the analytical conditions and keeping the system and the samples refrigerated.

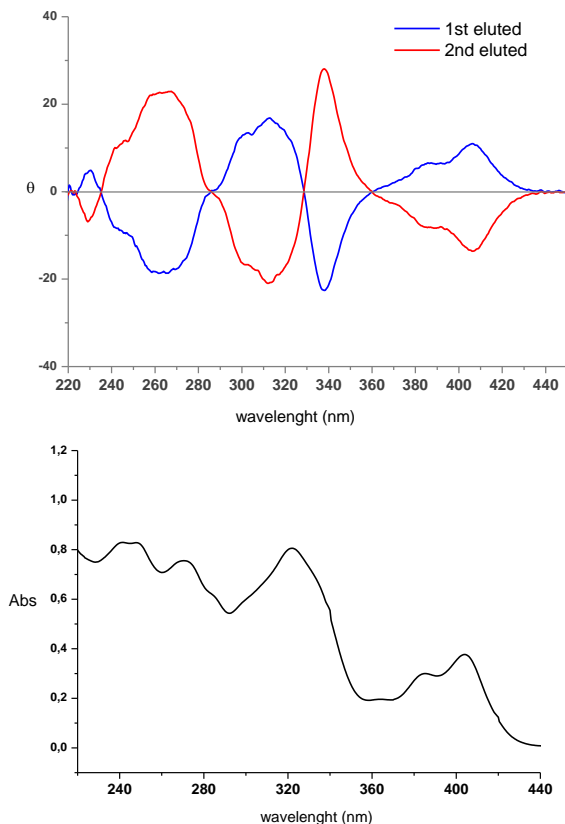


Fig. 2.36 - ECD spectrum (top) and UV-VIS spectrum (bottom) of a solution of **8** ($1,8 \times 10^{-5} \text{M}$) in hexane/dichloromethane 90:10 and a Tcell of 10°C .

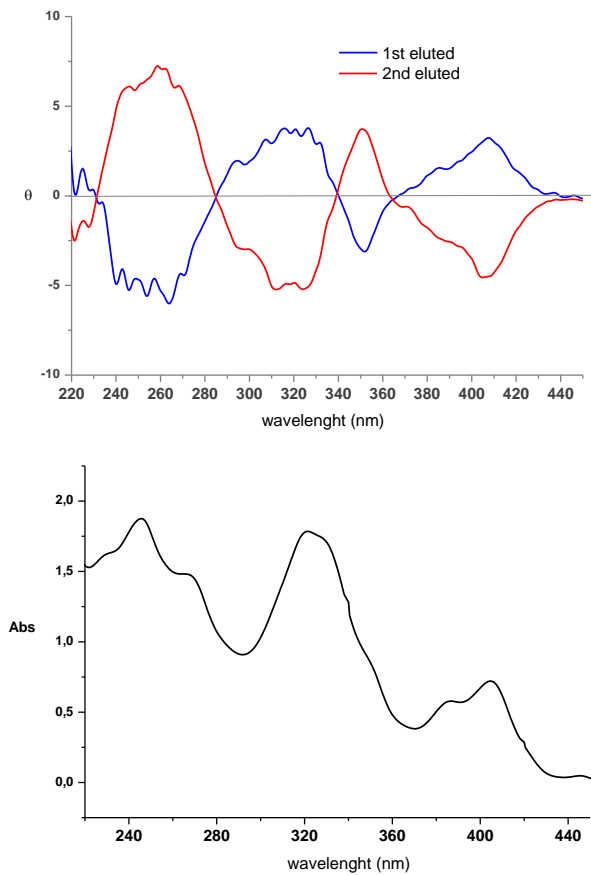


Fig. 2.37 - ECD spectrum (top) and UV-VIS spectrum (bottom) of a solution of **7** ($3,5 \times 10^{-5}\text{M}$) in hexane/dichloromethane 90:10 and a T cell of 10°C .

For both compounds the enantiomeric correlation between the first eluted and the second eluted species is evident by the mirrored ECD spectra. Moreover, strong positive (1st eluted) and negative (2nd eluted) Cotton effects characterise both compounds. Accordingly, the P configuration is then assigned to the first eluted enantiomer by empiric considerations (positive Cotton effect are linked to P helicity) and also confirmed by correspondence between experimental and computed ECD spectra.

2.3.3 Pyreno-Pyrene helicene hybrids

Two Pyreno[a]pyrene-based helicene hybrids (fig 2.38), the synthesis of which is reported [28], have been resolved into enantiomers by CSP-HPLC and the single enantiomers have been used to study the stereochemical stability and to investigate their chiroptical properties.

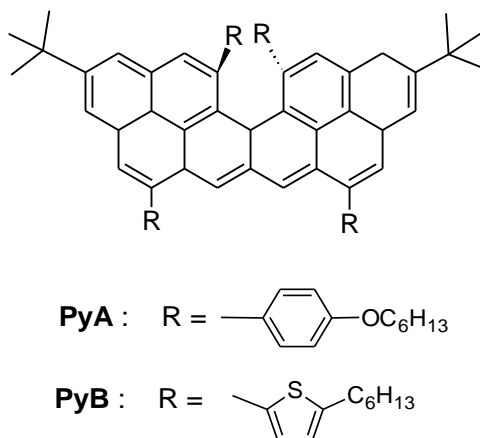


Fig. 2.38 - Structure of the helical derivatives PyA and PyB.

As evidenced by the X-ray of structural analogues of PyA and PyB (fig 2.39), the two substituents in the cove region force the structure to adopt a helical distorted conformation. The helicity makes the compounds chiral and both PyA and PyB are obtained as racemic mixtures.

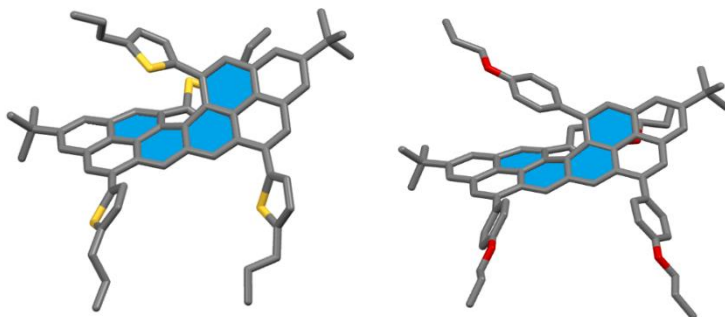


Fig. 2.39 - X-ray structure of a structural analogues of PyA (right) and PyB (left) with shorter sidechains. The [4]helicenes structure incorporated in the Pyreno[a]pyrene is pointed out in light blue.

The chromatographic resolution of the enantiomers (P and M) of both compounds has been successfully achieved. The best analytical conditions have been obtained using a chromatographic column packed with a chiral stationary phase composed by amylose-tris-(3,5-dimethylphenylcarbamate) immobilised on silica gel. For compound PyA elution with hexane and dichloromethane (85/15 v/v) with detection UV-VIS at 254 nm allowed to resolve the racemic mixture in two well separated peaks (figure 2.40 and table 2.9). The two enantiomers of

compound PyB were resolved with a mobile phase composed of hexane and dichloromethane in a slightly different proportion (92/8 v/v) (figure 2.41 and table 2.9).

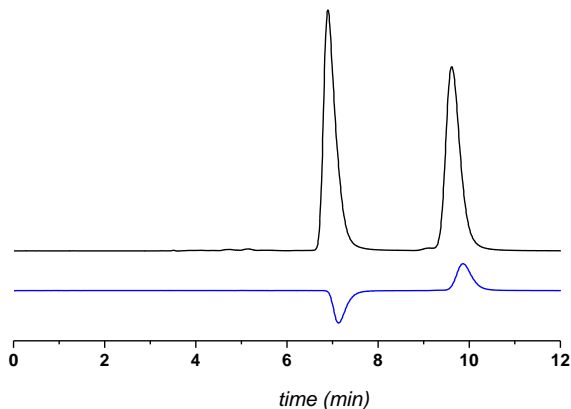


Fig. 2.40 - CSP-HPLC profile of PyA. Column: Chiralpak IA; mobile phase: hexane/dichloromethane/methanol (85/15 v/v); flow rate: 1 ml/min; detector: UV 254 nm (black trace) and CD 280 nm (blue trace); $T_{col} +20^{\circ}C$.

tr1 (min)	tr2 (min)	k'1	k'2	α	A% 1
6,04	9,64	0,71	1,73	2,44	50

Tab. 2.9 - Chromatographic parameters of PyA for the experimental conditions reported in fig 2.40. Capacity factors and selectivity are calculated starting from the retention time and dead time.

A good selectivity factor of 2,44 has been calculated in the experimental conditions. Furthermore, from the CD detection it is evident the enantiomeric relationship between the two species since the two peaks have a 50:50 ratio (A%) and opposite sign at 280 nm.

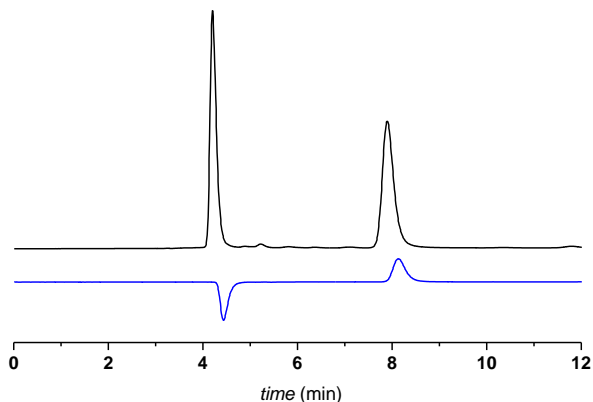


Fig. 2.41 - CSP-HPLC profile of PyB. Column: Chiralpak IA; mobile phase: hexane/dichloromethane/methanol (92/8 v/v); flow rate: 1 ml/min; detector: UV 254 nm (black trace) and CD 280 nm (blue trace); $T_{col} +20^{\circ}\text{C}$.

tr1 (min)	tr2 (min)	k'1	k'2	α	A% 1
4,21	7,89	0,20	1,25	6,25	50

Tab. 2.10 - Chromatographic parameters of PyB for the experimental conditions reported in fig 2.41. Capacity factors and selectivity are calculated starting from the retention time and dead time.

The selectivity of the stationary phase for the enantiomers of compound PyB (tab. 2.10) is even higher than the one calculated for PyA. CD detection shows two peaks with a ratio 50:50 (A%) and opposite sign also for PyB. Scaling up the analytical method to semipreparative level allowed obtaining milligrams of single enantiomers with an e.e. of 99.9% for each one. The ECD spectra of the two enantiomers of the studied helicenes have been registered (fig 2.42). Optically pure samples of PyA and PyB were used to measure the specific optical rotation using monochromatic light filters with different wavelength. The measured values of $[\alpha]_D$ are ± 600 for PyA and ± 507 for PyB, with the first eluted being the (+)enantiomer and the second eluted (-)enantiomer for both compounds. Figure 2.42 shows the optical dispersion registered from the enantiomers of both compounds. The experimental data fit perfectly with the Kramers-Kroenig (K-K) transformed of the CD spectrum (dashed line in fig 2.43).

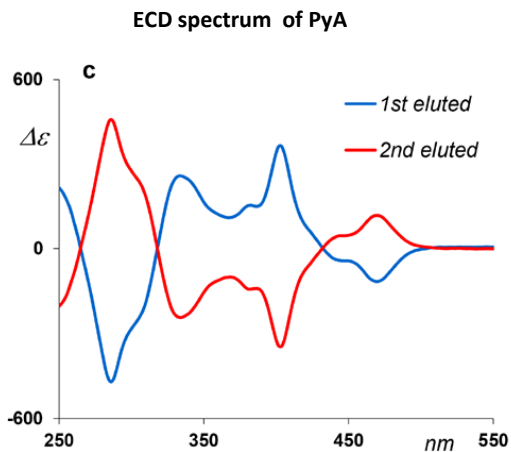


Fig 2.42 - ECD spectra registered between 250 and 600 nm for the first eluted (blue line) and second eluted (red line) of PyA (top) and PyB (bottom) in 10^{-5}M chloroform solution.

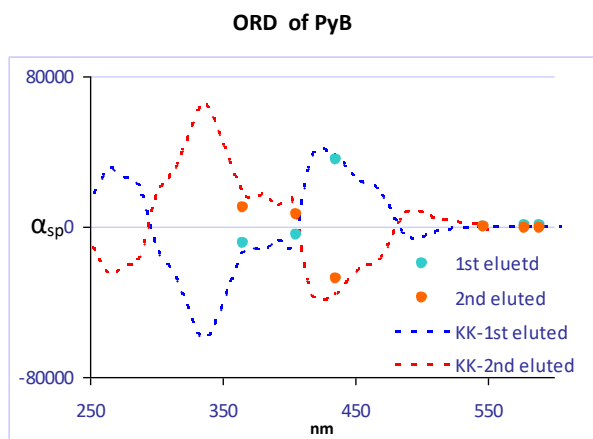
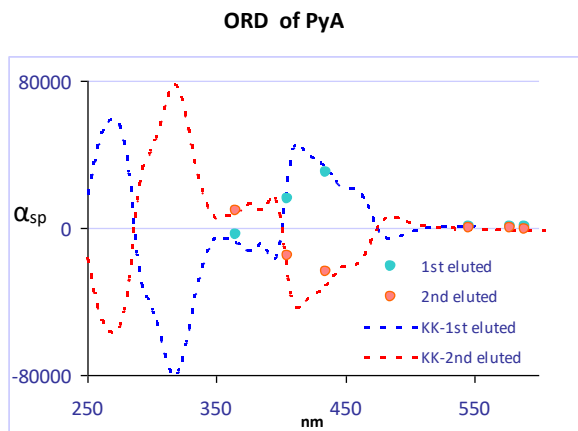


Fig 2.43 - ORD registered for the first eluted (blue line) and second eluted (red line) of PyA (top) and PyB (bottom) in 10^{-5} M dichloromethane solution.

Thermal racemization of the second-eluted enantiomer of PyA in decalin at 150 °C was monitored by CSP-HPLC. The decay of the enantiomeric excess has been measured over time but unfortunately, time of reaction was limited to 30 minutes due to chemical degradation at high temperature. The calculation of the free energy barrier ΔG^\ddagger for the racemization process at lower temperatures was not possible because no sign of racemization was detected during the experiment. Anyway, it can be assumed a ΔG^\ddagger of at least 34 kcal/mol. The same experimental procedures were followed to determine the ΔG^\ddagger of racemization of compound PyB. Thermal racemization of the first eluted enantiomer in decalin at 150°C resulted in a rapid change in color of the solution, indicative of a chemical degradation process. To avoid the limitation given by chemical instability at high temperatures, thermal racemization was performed at lower temperatures. Incubation of the enantiopure sample of PyB at 100°C didn't allow to detect any change in the enantiomeric excess over a 60 min time period. Therefore, a $\Delta G^\ddagger > 30$ kcal/mol can be assumed for racemization of compound PyB.

3. Conclusions

The chiral resolution of the racemic mixtures of a wide range of hetero[n]helicenes and chiral pyreno-pyrenes by CSP-HPLC has been successfully achieved. Polysaccharide-based chiral stationary phases resulted efficient in selectively separate enantiomeric couples of helically distorted PAHs. The rates of interconversion and the energetic barriers of the stereomutation process have been measured with off-column and on-column approaches, depending on the stability of the single enantiomers. Thermal racemization starting from optically pure samples has been monitored over time by HPLC to obtain energetic barriers of racemization up to 33 kcal/mol. Dynamic-HPLC allowed to measure the values of the activation energies of enantiomerization of atropisomeric helicenes. Low temperature d-HPLC was necessary to calculate ΔG^\ddagger of enantiomerization of about 16 kcal/mol for two aza[5]helicenes. For those compounds stable enough to allow the isolation of single enantiomers with a good enantiomeric excess, the chiro-optical properties have been studied, measuring high values of optical rotations.

4.Methods and Materials

4.1 Chemicals and materials

All solvents and reagents were purchased from Sigma Aldrich (St. Louis, MO, USA).

Prof. Menichetti research group (University of Florence) gently provided Aza[n]helicenes.

Pyrene-based and pyreno-pyrene helicenes were gently provided by Prof. W.A. Chalifoux research group (University of Reno, Nevada).

4.2 HPLC measurements

4.2 a Chromatographic apparatus

Analytical chromatography was performed on a HPLC system composed by Jasco (Tokyo, Japan) with a universal Rheodyne 20 μ l injector, Jasco PU 980 pump and Jasco PU 1580 CO₂ pump, a detector Jasco UV 975 and a second detector Jasco UV/CD 995. During dynamic HPLC experiments low temperatures were maintained using a

home-made cooling device. Preparative chromatography was performed with a chromatographic apparatus composed by Waters with a pump Waters Millipore Model 590 and a Waters Millipore Lambda-Max model 481 LC spectrophotometer detector.

4.2.b Chromatographic columns

Chiral resolution of the racemic mixtures by HPLC were performed on a polysaccharide-based chiral stationary phase Chiralpak IA(250 x 4,6 mm L. x I.D., 5 μ m particle size) for the analytical-scale measurements and Chiralpak IA(250 x 10 mm L. x I.D., 5 μ m particle size) for the semipreparative scale, both purchased from Chiral technologies.

4.2 c Simulation of dynamic chromatograms

Simulation of variable temperature experimental chromatograms presenting a dynamic profile were performed by Auto DHPLC y2k (Auto Dynamic HPLC), using the stochastic model. Both chromatographic and kinetic parameters can be automatically optimized by simplex

algorithm until the best agreement between experimental and simulated dynamic chromatograms is obtained.

4.3 Circular dichroism (CD) measurements

ECD spectra of compounds PyA and PyB were recorded on a Jasco 815SE CD spectrometer at room temperature, in a rectangular cell with 10 mm pathlength. Circular dichroism measurements were performed by Prof. Abbate group (University of Brescia).

ECD spectra of compounds 7 and 8 were performed on a Jasco 815 CD spectrometer at 10°C, in a rectangular cell with a 10 mm pathlength.

4.4 Optical Rotation (OR) measurements

All the specific optical rotation measurements were performed at room temperature on a Jasco P 1030 polarimeter, with Na and Hg light sources and filters at different wavelength for studying ORD. A 10 mm cylindrical cuvette was used for the samples.

4.3 UV-VIS spectra measurements

UV-VIS spectra were registered with a Jasco V-550 spectrophotometer, at room temperature and rectangular cell with 10 mm pathlength.

5. References

- [1] Melvin S. Newman and William B. Wheatley, *J. Am. Chem. Soc.*, 1948, 70, 1913-1916.
- [2] F. Bell and D. H. Waring, *J. Chem. Soc.*, 1949, 2689-2693.
- [3] Marc Gingras, *Chem. Soc. Rev.*, 2013, 42, 968-1006.
- [4] Marc Gingras, Guy Felix and Romain Peresutti, *Chem. Soc. Rev.*, 2013, 42, 1007-1050.
- [5] Marc Gingras, *Chem. Soc. Rev.*, 2013, 42, 1051-1095.
- [6] Carsten Schmuck, *Angew. Chem. Int. Ed.* 2003, 42, 2448-2452.
- [7] Michel Rickhaus, Marcel Mayor and Michal Jurička *Chem. Soc. Rev.*, 2016, 45, 1542-1556.
- [8] A. O. McIntosh, J. Monteath Robertson, V. Vand, *J. Chem. Soc.*, 1954, 1661-1668.
- [9] G. Ferguson and J. Monteath Robertson, *Adv. in Phys. Org. Chem.*, 1963, 1, 203-281.
- [10] Yun Shen, and Chuan-Feng Chen, *Chem. Rev.* 2012, 112, 1463–1535.
- [11] Kazuyuki. Mori, Takashi Murase and Makoto Fujita, *Angew. Chem. Int. Ed.* 2015, 54, 6847 –6851.

- [12] Thorben R. Schulte, Julian J. Holstein, and Guido H. Clever, *Angew. Chem. Int. Ed.* 2019, 58, 1 – 6.
- [13] Gourav M. Upadhyay, Harish R. Talele, and Ashutosh V. Bedekar, *J. Org. Chem.*, 2016, 81, 7751–7759
- [14] Wenlong Yang, Giovanna Longhi, Sergio Abbate, Andrea Lucotti, Matteo Tommasini, Claudio Villani, Vincent J. Catalano, Aleksandr O. Lykhin, Sergey A. Varganov, and Wesley A. Chalifoux, *J. Am. Chem. Soc.*, 2017, 139, 13102–13109.
- [15] Yanpeng Zhu, Zeming Xia, Zeying Cai, Ziyong Yuan, Nianqiang Jiang, Tao Li, Yonggen Wang, Xiaoyu Guo, Zhihao Li, Shuang Ma, Dingyong Zhong, Yang Li, and Jiaobing Wang, *J. Am. Chem. Soc.*, 2018, 140, 4222–4226.
- [16] Yunbin Hu, Xiao-Ye Wang, Pi-Xian Peng, Xin-Chang Wang, Xiao-Yu Cao, Xinliang Feng, Klaus Mglgen, and Akimitsu Narita, *Angew. Chem. Int. Ed.*, 2017, 56, 3374 – 3378.
- [17] Yuuta Yanoa, Hideto Ito, Yasutomo Segawa, Kenichiro Itami, *Synlett*, 2016, 27, 2081–2084.
- [18] Yoshito Nakai, Tadashi Mori, and Yoshihisa Inoue, *J. Phys. Chem.*, A 2012, 116, 7372–7385.

- [19] Carlos M. Cruz, Silvia Castro-Fernandez, Ermelinda Maçôas, Juan M. Cuerva, and Araceli G. Campana, *Angew. Chem.*, 2018, 130, 14998–15002.
- [20] Helena Isla, Jeanne Crassous, *C. R. Chimie*, 2016, 19, 39-49.
- [21] Serena Arnaboldi, Silvia Cauteruccio, Sara Grecchi, Tiziana Benincori, Massimo Marcaccio, Alessio Orbelli Biroli, Giovanna Longhi, Emanuela Licandro and Patrizia Romana Mussini, *Chem. Sci.*, 2019, 10, 1539–1548.
- [22] Jan Storch, Květa Kalíková, Eva Tesařová, Vítězslav Maier, Jan Vacek, *J. Chromatogr. A*, 2016, 1476, 130–134.
- [23] Claudio Villani, Benoit Laleu, Pierre Mobian and Jérôme Lacour, *Chirality*, 2007, 19, 601–606.
- [24] Geraldine M. Labrador, Johann Bosson, Zachary S. Breitbach, Yeeun Lim, Eric R. Francotte, Rocchina Sabia, Claudio Villani, Daniel W. Armstrong, Jérôme Lacour, *Chirality*, 2016, 28, 282-289.
- [25] Kais Dhbaibi, Ludovic Favereau, and Jeanne Crassous, *Chem. Rev.* 2019, 119, 8846–8953
- [26] Prince Ravat, Rahel Hinkelmann, David Steinebrunner, Alessandro Prescimone, Ina Bodoky, and Michal Juríček, *Org. Lett.* 2017, 19, 3707–3710.

[27] Caterina Viglianisi, Chiara Biagioli, Martina Lippi, Maria Pedicini, Claudio Villani, Roberta Franzini, and Stefano Menichetti, *Eur. J. Org. Chem.* 2019, 164–167

[28] Radha Bam, Wenlong Yang, Giovanna Longhi, Sergio Abbate, Andrea Lucotti, Matteo Tommasini, Roberta Franzini, Claudio Villani, Vincent J. Catalano, Marilyn M. Olmstead, and Wesley A. Chalifoux, *Org. Lett.*, 2019, 21, 8652-8656.

PART A-2

*Stereodynamics and Optical properties of
axially chiral benzodithiophenes and
Porphyrazine derivatives*

1. Introduction

Conformational chirality derives from the presence of a stereogenic element that differs from the stereogenic centre. In this case the inversion of configuration can take place without breaking a bond, and usually has lower values of energetic barriers. Axial chirality in particular arises from a hindered rotation around a single bond that corresponds to the stereogenic axis. The rotational energy that controls the rate of interconversion between the enantiomers P and M, depends in the first place on steric effects and only on a minor scale on electronic influences. Bond rotation is time-dependent, and half-lives of racemization can vary between seconds and years at different temperatures and in different solvents [1]. Stereoisomers resulting from limited rotation around a single bond were defined as atropoisomers by Khun in 1933 [2]. Classical atropoisomers racemize with a rotational barrier equal or above 22 kcal/mol, and their half-lives allow to isolate them at room temperature [3]. When the rotational energies are lower than 22 kcal/mol the half-lives of interconversion are too short and it is impossible to isolate the single enantiomers, thus in this case the rotation may be

considered as free. Very low temperatures are necessary to isolate this kind of stereoisomers and to have sufficient time to characterize them and to study their stereochemical stability.

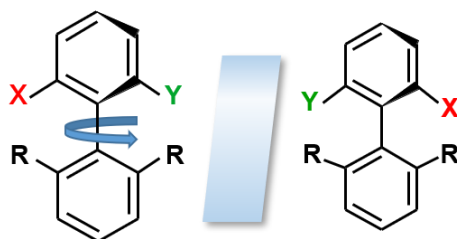


Fig. 1.4 - Mirror images of axially chiral biaryls.

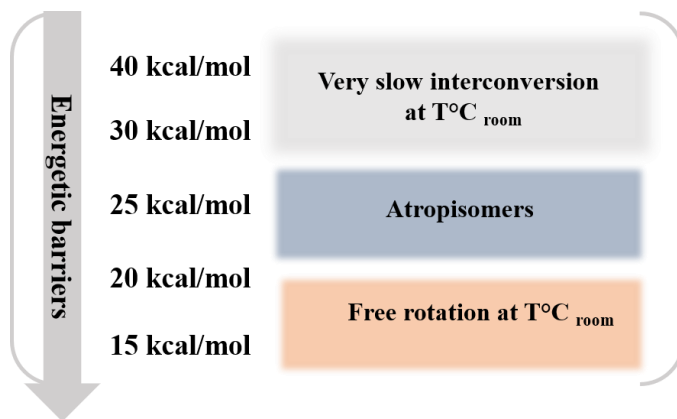


Fig. 1.5 - Torsional barriers of axially chiral compounds.

When the rotational energy is \geq of 29 kcal/mol no interconversion can be observed at room temperature even after very long time. The stereoisomers are stable enough to be isolated and studied. Most of the time, the designing of compounds with locked rotation aims at developing enantioselective synthetic pathways [4] [5]. Biphenyls are a classic example of compounds with axial chirality. The rotational energy of biaryls depends on the presence of substituents in the ortho positions while the addition of a substituent in the *meta*-position produces a so-called buttressing effect. The flexibility of the adjacent *ortho*-substituent is reduced enhancing the steric repulsion around the stereogenic axis. The substituent in the *para* position can alter the rotation just by electronic influence, usually resulting as a less relevant effect.

Atropisomerism generated by axial chirality is an interesting feature that is exploited in many research fields, and it is particularly useful in asymmetric catalysts. Many inherently chiral biaryls are used as axially chiral ligands, as BINAP and BIPHEP. The implications of atropisomerism are considerable also in drug discovery, in biochemistry and in material chemistry. Axial chirality is a major feature of

compounds designed to be used as molecular switches, in sensing applications and in molecular machines. Control of motion of molecular dynamic devices is performed by designing molecules with labile and stable stereogenic elements [6]. The best fitting techniques to study the stereochemical stability of compounds with limited rotation around the stereogenic axis are chromatography and nuclear magnetic resonance. Circular dichroism also is a helpful technique in studying the stable conformations of axially chiral compounds and to assign the absolute configuration, while few studies of chiral light emission are reported for chiral biaryls [7]. Dynamic-NMR and dynamic-HPLC are complementary methodologies that allow to measure low values of ΔG^\ddagger of interconversion [8].

2.Results and Discussion

2.1 Axially chiral dimers of benzodithiophenes

Four chiral derivatives (figure 2.44) of a dimer of benzodithiophenes have been resolved into enantiomers by enantioselective-HPLC.

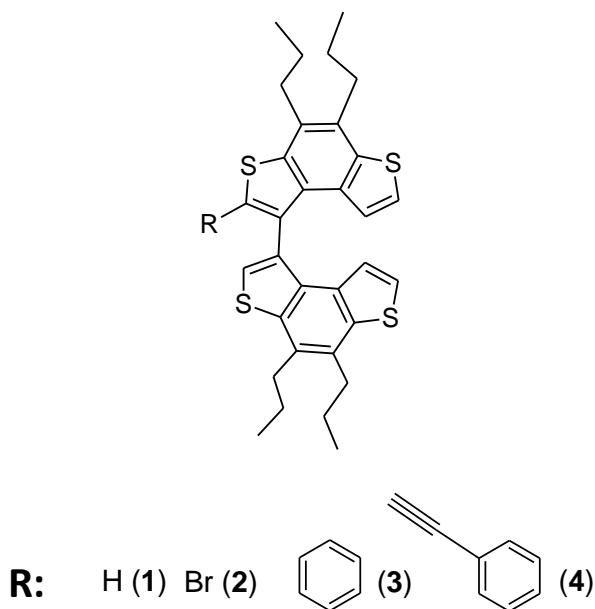


Fig. 2.44 - Structure of the general scaffold and the relative modifications of the four derivatives 1, 2, 3, 4.

All the four derivatives are chiral and the hindered rotation around the single bond that connects the two tricyclic systems generates enantiomers. For compound **1** it is expected a lower rate of interconversion, while the interconversion rate of compounds **2**, **3** and **4** is more affected by the steric hindrance of the substituents in the ortho position. Chiral stationary phases based on cellulose and amylose were effective in selectively resolve the enantiomers of all the four compounds with a mobile phase composed by hexane modified with a percentage of isopropyl alcohol lower than 0.1%. Elution profiles registered at room temperature with the relative experimental conditions are showed in figures 2.45-2.48.

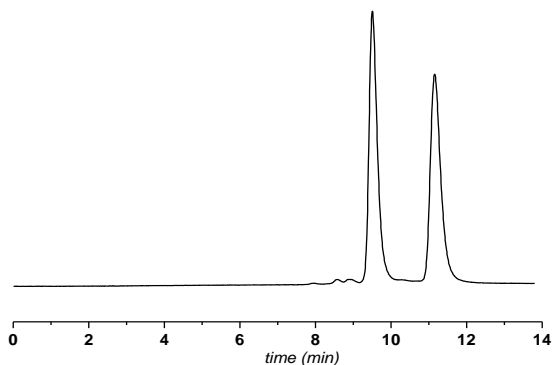


Fig 2.45 - CSP-HPLC profile of **1**. Column: Chiralpak IA 500mm (L); mobile phase: hexane/isopropyl alcohol (100/0,1 v/v); flow rate: 1 ml/min; detector: UV 300 nm. T_{col} 20°C.

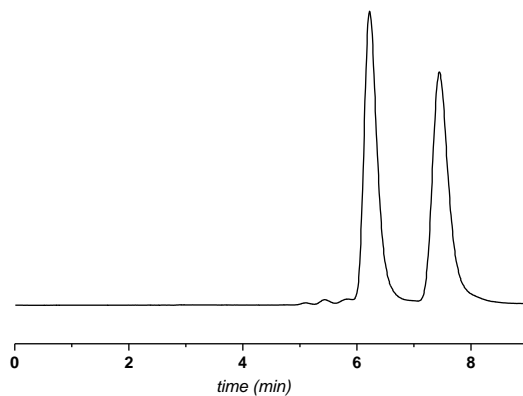


Fig 2.46 - CSP-HPLC profile of 2. Column: Chiralcel OD-H; mobile phase: hexane/isopropyl alcohol (100/0,05 v/v); flow rate: 1 ml/min; detector: UV 300 nm. T_{col} 20°C.

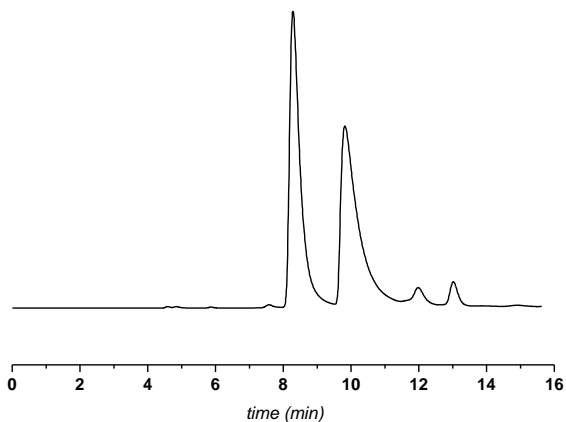


Fig. 2.47 - CSP-HPLC profile of 3. Column: Chiralpak IB; mobile phase: hexane/isopropyl alcohol (100/0,01 v/v); flow rate: 1 ml/min; detector: UV 300 nm. T_{col} 20°C.

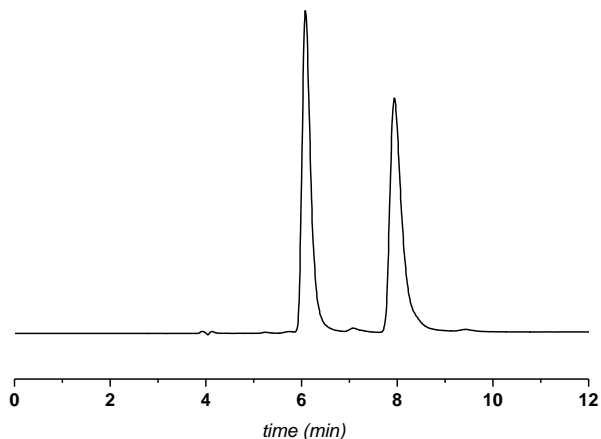


Fig. 2.48 - CSP-HPLC profile of **4**. Column: Chiralpak IB; mobile phase: hexane/isopropyl alcohol (100/0,01 v/v); flow rate: 1 ml/min; detector: UV 300 nm. T_{col} 20°C.

2.1.2 *Stereolabile benzodithiophenes dimer*

Compound **1** has an interconversion barrier lower than the other studied compounds, because it lacks the substituent in the ortho position. Experiments of dynamic HPLC with a chiral stationary phase have been performed to study the stereochemical stability. Starting from the optimized HPLC analytical conditions, the temperature of the column has been increased gradually, observing the progressive coalescence of

the chromatographic peaks. In figure 2.49 are reported the variable temperature HPLC measurements.

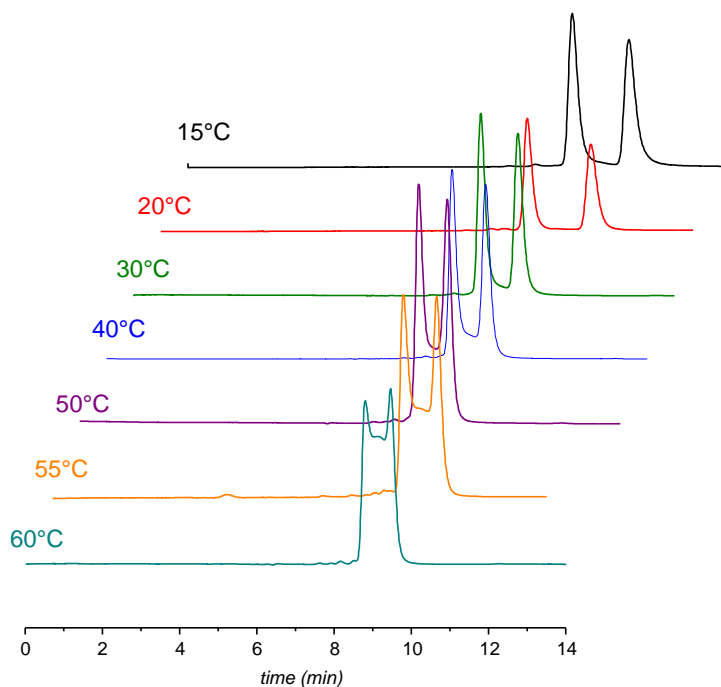


Fig. 2.49 - Dynamic-HPLC elution profiles of compound 1. All temperatures are considered $\pm 0.1^\circ\text{C}$.

A plateau between the peaks is observed starting from a temperature of the column of 40°C . The experimental profiles have been used to calculate the values of the energetic barriers of interconversion. DCWIN y2k software was used

to simulate the experimental chromatograms (fig. 2.50). The dynamic chromatographic profiles obtained at column temperatures of 40°C, 50°C and 55°C were simulated using a stochastic model to obtain the kinetic parameters of the interconversion between M and P stereoisomers (tab. 2.11).

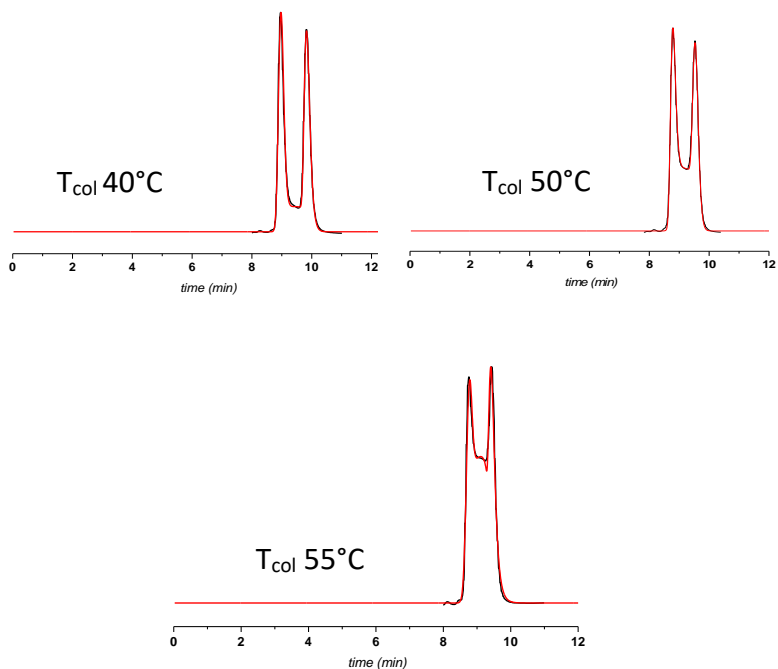


Fig. 2.50 - Simulated (red) and experimental (black) chromatograms of 1.

T col (°C)	k _{en 12} (min ⁻¹)	ΔG [‡] _{en 12} (kcal/mol)	k _{en 21} (min ⁻¹)	ΔG [‡] _{en 21} (kcal/mol)	k _{en av} (min ⁻¹)	ΔG [‡] _{en av} (kcal/mol)
40	0,024	23,23	0,022	23,29	0,024	23,26
50	0,056	23,44	0,052	23,49	0,054	23,47
55	0,095	23,47	0,088	23,52	0,21	23,50

Tab. 2.11 - kinetic rate constants and energetic barrier of the on-column enantiomerization of compound 1. Column temperatures are intended $\pm 0,1$ °C. Errors in $\Delta G \pm 0,02$ kcal/mol.

The activation energy for the rotation around the stereogenic axis is low enough to observe the process at room temperature with a calculated half-life for a single enantiomer of few hours. To confirm the data obtained with dynamic-HPLC, the two enantiomers have been isolated obtaining few milligrams of enantiopure samples. The collected samples have been kept at 0°C to extend their half-lives of racemization. The kinetic of racemization have been studied off-column incubating a solution enriched of the first eluted enantiomer in mobile phase for 90 minutes at 35,5°C ($\pm 0,1$ °C). The decay of the enantiomeric excess (e.e.%) is measured over time by HPLC (fig. 2.51). Plotting the logarithm of e.e. %

against the time, a rate constant of $0,0299 \text{ min}^{-1}$ is calculated for the racemization of **1** (fig. 2.52). ΔG^\ddagger is calculated with the Eyring equation and results $22,75 \text{ kcal/mol}$, in agreement with the value resulting from the on-column experiment. The ECD spectra have been registered for both enantiomers and are reported in figure 2.53.

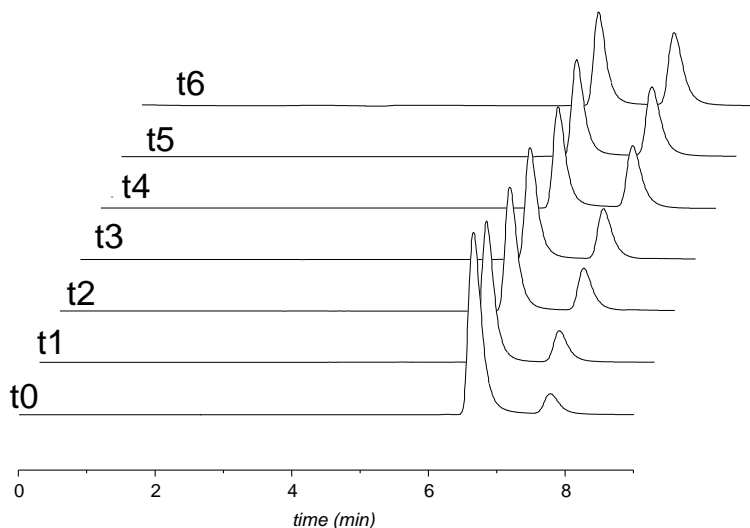


Fig. 2.51 - Thermal racemization of **1** in hexane/isopropyl alcohol (100/0,025 v/v) at $35,5^\circ\text{C}$ starting from a solution enriched in the 1st eluted enantiomer, monitored over time by CSP-HPLC (Chiralpak IB) ($t_0=0 \text{ min}$, $t_1=10 \text{ min}$, $t_2=20 \text{ min}$, $t_3=30 \text{ min}$, $t_4=50 \text{ min}$, $t_5=70 \text{ min}$, $t_6=90 \text{ min}$).

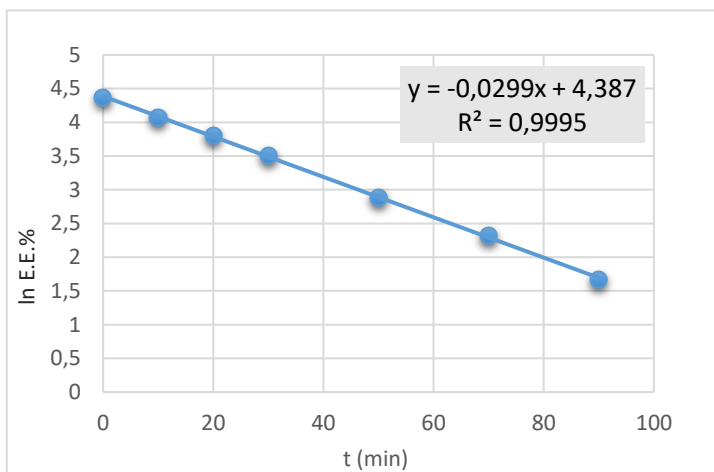


Fig. 2.52 - Decay of the enantiomeric excess over time of an enantioenriched solution of 1 in mobile phase at 35,5 °C.

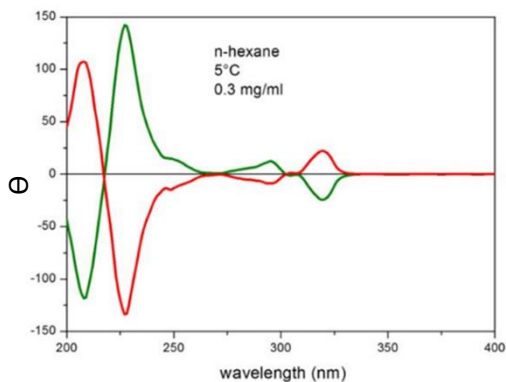


Fig. 2.53 - ECD spectra registered in n-hexane at 5 °C for a solution 0.3mg/ml of the first eluted enantiomer (green) and second eluted (red).

2.1.2 Stereochemically stable benzodithiophenes dimers

Higher rotational barriers than the one calculated for compound **1** are expected for compounds **2**, **3** and **4** given the increased steric hindrance in the ortho position. Single enantiomers with an enantiomeric excess over 95% have been isolated upscaling the analytical method to semipreparative level. To be sure of the stereochemical stability, thermal racemization has been studied for all the compounds. Single enantiomers of **2**, **3** and **4** have been dissolved in decalin and the solution is heated up at 150°C. The reaction has been monitored over time, measuring the decay of the enantiomeric excess by CSP-HPLC. After 30 minutes at 150°C, no change was observed in the e.e.% for any of the sample. Then, the value of the ΔG^\ddagger of racemization is considered to be at least 34 kcal/mol. Consequently, it is assumed that the rotation around the stereogenic axis is too slow to be observed at room temperature and so, the two conformations are considered as locked. The long half-lives of racemization allowed to study the single enantiomers using chiro-optical methods. The specific optical rotation of compounds **2**, **3** and **4** has been registered using chloroform

solutions of the single enantiomers. Values of $[\alpha]_D$ are reported in table 2.12 along with the sign of the optical rotation for the two enantiomers.

compound	1° eluted on Chiralpak IB	2nd eluted on Chiralpak IB	$[\alpha]_D$
2	-	+	69
3	-	+	166
4	-	+	318

Tab. 2.12 - Polarities and values of the specific optical rotation measured from 10^{-3} M chloroform solutions of the enantiomers of compounds 2, 3 and 4. The sign is maintained in all the three molecules while the absolute value is higher for 4.

The ECD spectra registered between 200 and 400 nm (fig 2.54 and 2.55) shows the perfect enantiomeric relationship between the couples of stereoisomers of every compound. From the simulations of different dihedral conformations of the ECD spectra of compound 2, it is assigned the configuration M to the first eluted enantiomer while the second one has the configuration P.

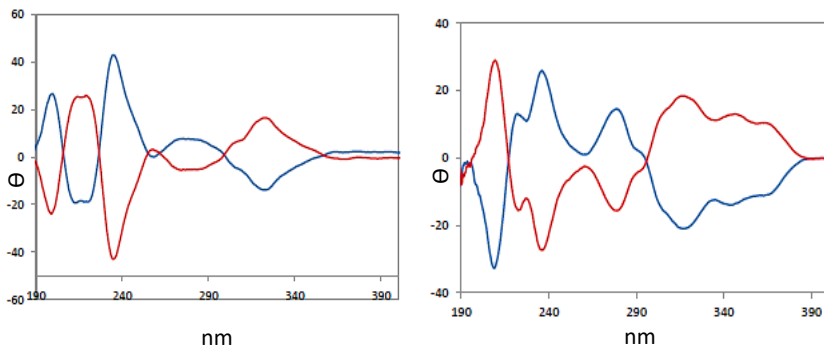


Fig. 2.54 - ECD spectra of n-Hexane solutions ($[C] = 10^{-4}M$) of the first eluted enantiomer (blue trace) and the second eluted enantiomer (red trace) on Chiralpak IB, for compounds 3 (left) and 4 (right).

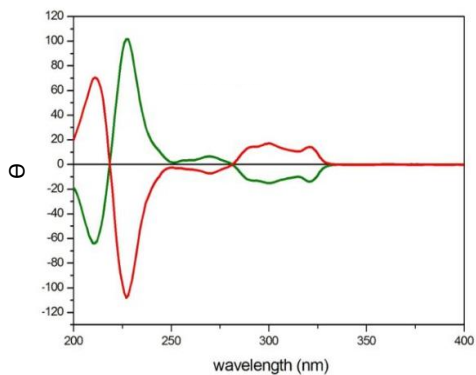


Fig. 2.55- ECD spectra of n-hexane solutions ($[C] = 10^{-3}M$) of the first eluted enantiomer (red trace) and the second eluted enantiomer (green trace) on Chiralcel OD-H, for compound 2.

2.2 Stereochemical Stability and Absolute Configuration of a pyrene-substituted ethylthioporphyrazine

A pyrene-substituted porphyrazine [9] complexed with Pd(II) **PyPz-Pd** (fig 2.56) used as component of nanohybrid materials, displays atropisomerism because of the hindered rotation around the bond connecting the pyrene portion to the macrocycle.

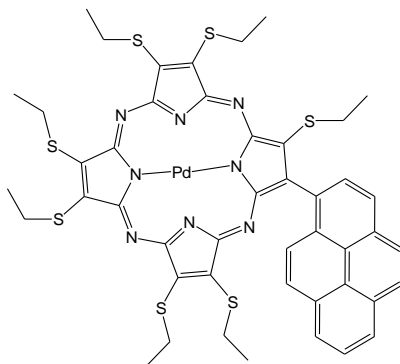


Fig. 2.56 - Structure of the compound PyPz coordinated with Pd.

To study the atropisomerism of the complexed PyPz-Pd and to characterize the single enantiomers, it has been developed

an analytical method by CSP-HPLC to resolve the racemic mixture. The best separation was obtained with a (R,R)-Whelk01 chiral stationary phase and an eluent mixture consisting of hexane/isopropyl alcohol/ dichloromethane (80/10/10 v/v/v). The elution profile (fig 2.57) with a column temperature of 20°C and UV-ECD detection shows two peaks with a plateau in between, symptomatic of an on-column interconversion. The ECD trace registered at 330 nm shows two peaks with the same area but opposite sign.

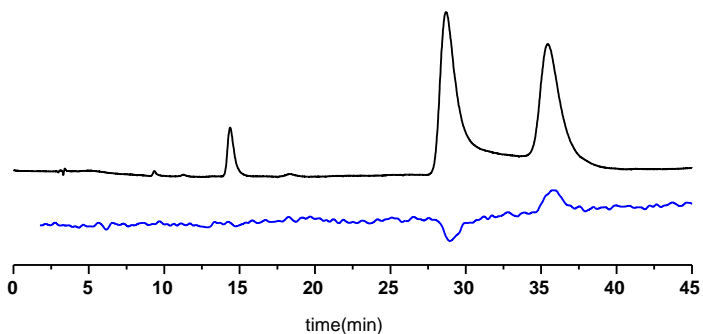


Fig. 2.57 - CSP-HPLC profile of PyPz-Pd. Column: (R,R)Whelk01; mobile phase: hexane/ /dichloromethane/ isopropyl alcohol (80/10/10 v/v/v); flow rate: 1 ml/min; detector: UV 330 nm (black trace) ECD 330 nm (blue trace). T_{col} 20°C.

Decreasing the temperature of the column down to 2°C, the plateau height between the two peaks decreases almost at the baseline indicating that, at this temperature, the interconversion rate is lower (fig.2.58).

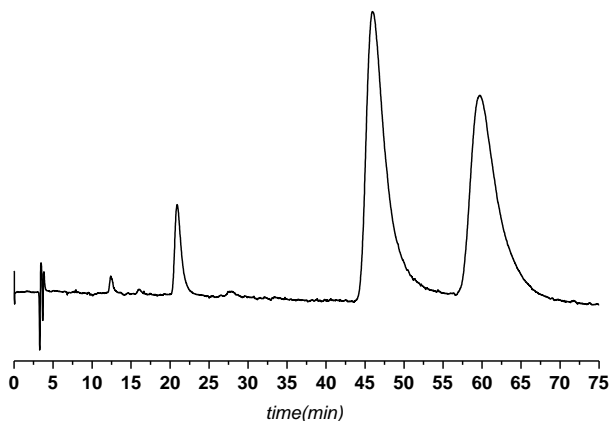


Fig. 2.58 - CSP-HPLC profile of PyPz-Pd. Column: (R,R)Whelk01; mobile phase: hexane/dichloromethane/isopropyl alcohol (80/10/10 v/v/v); flow rate: 1 ml/min; detector: UV 330 nm (black trace); T_{col} 2°C.

tr1 (min)	tr2 (min)	k'1	k'2	α	A% 1
45,9	59,7	13,12	17,37	1,32	50

Tab. 2.13. - Chromatographic parameters of PyPz-Pd for the experimental conditions reported in fig. 2.58. Capacity factors and selectivity are calculated starting from the retention time and dead time.

Compared to the elution profile of the decomplexed PyPz species [9] the presence of the metal increases the retention time of about 15 minutes at room temperature, while the selectivity remains almost the same.

Simulation of the dynamic chromatograms based on the stochastic model gave a value of $k_{app1,2}$ of $0,097 \text{ min}^{-1}$ and a $k_{app2,1}$ of $0,078 \text{ min}^{-1}$ at 20°C from which it is calculated a $\Delta G^\ddagger_{1,2}$ of $22,2 \text{ kcal/mol}$ and a $\Delta G^\ddagger_{2,1}$ of $22,4 \text{ kcal/mol}$ (with an error of $\pm 0,1 \text{ kcal/mol}$). This values are only slightly higher than the one calculated with the same technique for the non-complexed analogue. Therefore, the presence of the palladium in the porphyrazine macrocycle seems to not affect the rotational barrier between the pyrene and the macrocyclic portion. The two enantiomers of PyPz-Pd have been isolated in milligrams quantities, upscaling the analytical method. In order to limit the rapid racemization that could occur at room temperature the chromatographic column and the samples collected have been kept at 2°C . The ECD spectra have been registered for both the enantiopure samples (fig 2.59) dissolved in the mobile phase and maintaining at 10°C the temperature of the cell. At this temperature, the single enantiomers have sufficiently long half-lives to allow for a

complete measurement. The ECD spectrum is very similar to the one registered for the free PyPz in the region 220-400 nm. For the uncomplexed PyPz enantiomers, their absolute configuration is assigned by quantum mechanical calculations of the ECD spectra followed by comparison with those experimentally measured. Consequently, given the high resemblance to the ECD profiles of compound PyPz-Pd it can be assigned the same absolute configuration: the first eluted enantiomer on (R,R)-Whelk01 CSP has configuration P while the second is the M stereoisomer.

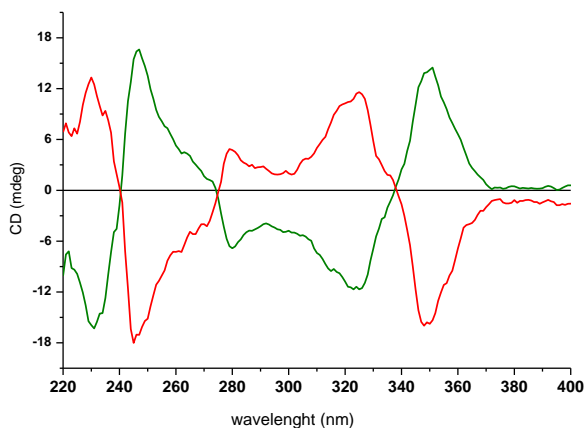


Fig. 2.59 - ECD spectra of the first eluted and second (green) eluted (red) enantiomers of compound PyPz-Pd dissolved in the mobile phase.

Starting from a single enantiomer it has been monitored over time the decay of the ECD at a fixed wavelength of 350 nm and keeping the T_{cell} at 20°C. At this temperature the racemization rate is fast enough to observe a rapid decay of the enantiomeric excess.

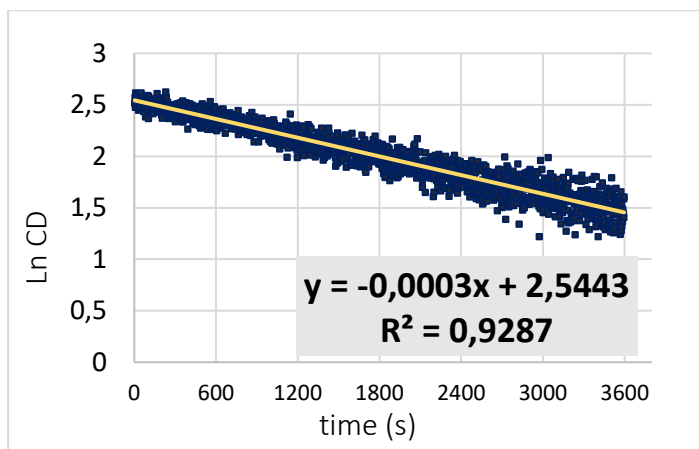


Fig. 2.60 - Variation over time of the \ln of the CD signal at 350 nm starting from a single enantiomer of PyPz-Pd incubated in mobile phase at 20°C monitored by HPLC.

As the signal decreases toward the zero value, the error of the measurements grows, and the variation of the collected points is larger. It is calculated a rotational barrier ΔG^\ddagger 21,9 kcal/mol ($\pm 0,1$ kcal/mol) at 20°C, in accordance with the one obtained

with on-column experiments and with the values calculated for the decomplexed PyPz and with different techniques.

3. Conclusions

The racemic mixtures of four benzodithiophenes dimers have been resolved by normal phase CSP-HPLC in the respective enantiomeric couples. On- column and off-column interconversion rates have been measured for one of the four compounds obtaining similar results with the two techniques. For three of the dimers the energetic barriers of racemization were too high to be measured during the experiments. P and M enantiomers of the stereochemically stable compounds were characterized by chiro-optical method. Time resolved circular dichroism spectroscopy has been used to study the racemization rate of an axially chiral ethyl-thioporphyrzine complexed with Palladium. The activation energy $\Delta G^\ddagger = 22$ kcal/mol, calculated by following the decay of the ECD signal over time, resulted comparable with the value calculated by dynamic-HPLC and typical of an atropoisomer.

4.Methods and Materials

4.1 Chemicals and materials

All solvents and reagents were purchased from Sigma Aldrich (St. Louis, MO, USA).

Axially chiral benzodithiophenes dimers were gently provided by Prof. Licandro group (University of Milano).

Chiral pyrene-substituted ethyl-thioporphyrzine was gently provided by Prof. Belviso group (University of Basilicata).

4.2 HPLC measurements

4.2 a Chromatographic apparatus

Analytical chromatography was performed on a Jasco (Tokyo, Japan) HPLC system with a universal Rheodyne 20 μ l injector, a pump Jasco PU 980 and a second CO₂ pump Jasco PU 1580. Detection is provided by a Jasco UV 975 detector a Jasco UV/CD 995 detector. During dynamic HPLC experiments low temperatures were maintained using a home-made cooling device. Preparative chromatography was

performed with a chromatographic apparatus composed by Waters with a pump Waters Millipore Model 590 and a Waters Millipore Lambda-Max model 481 LC spectrophotometer detector.

4.2.b Chromatographic columns

Chiral resolution of the racemic mixtures by HPLC was performed by polysaccharide-based chiral stationary phases Chiralpak IA(250 x 4,6 mm L. x I.D., 5 μ m particle size), Chiralpak IB (250 x 4,6 mm L. x I.D., 5 μ m particle size), Chiralcel OD-H (250 x 4,6 mm L x I.D. 5 μ m particle size), purchased from Chiral technologies , and a Pirkle type CSP (R,R)-Whelk01 (250 x 4,6 mm L x I.D., 5 μ m particle size) purchased from Regis Technologies Inc.

4.2 c Simulation of dynamic chromatograms

Simulation of variable temperature experimental chromatograms presenting a dynamic profile were performed by Auto DHPLC y2k (Auto Dynamic HPLC), using the stochastic model. Both chromatographic and kinetic parameters can be automatically optimized by simplex

algorithm until the best agreement between experimental and simulated dynamic chromatograms is obtained.

4.3 Circular dichroism (CD) measurements

CD spectra of the benzodithiophenes dimers were recorded on a Jasco 815SE CD spectrometer at room temperature, in a rectangular cell with 10 mm pathlength. Circular dichroism measurements were performed by Prof. Abbate group (University of Brescia)

4.3 Optical Rotation (OR) measurements

Specific optical rotation measurements were performed at room temperature on a Jasco P 1030 polarimeter, with Na and Hg light sources and filters at different wavelength for studying ORD. A 10 mm cylindrical cuvette was used for the samples.

5. References

- [1] Christian Wolf, *Dynamic Stereochemistry of Chiral Compounds: principles and applications*, RSC publishing, Cambridge 2008.
- [2] R. Kuhn, *Stereochemie*, Ed.: K. Freudenberg, Franz Deuticke, Leipzig, 1933, pp. 803 – 824.
- [3] Steven R. LaPlante, Lee D. Fader, Keith R. Fandrick, Daniel R. Fandrick,, Oliver Hucke, Ray Kemper, Stephen P. F. Miller, and Paul J. Edwards, *J. Med. Chem.* 2011, 54, 7005–7022.
- [4] Timothy W. Wallace, *Org. Biomol. Chem.*, 2006, 4, 3197–3210.
- [5] Gerhard Bringmann, Anne J. Price Mortimer, Paul A. Keller, Mary J. Gresser, James Garner, and Matthias Breuning, *Angew. Chem. Int. Ed.*, 2005, 44, 5384 – 5427.
- [6] Jochen R. Brandt, Francesco Salerno and Matthew J. Fuchter, *Nat. Rev. Chem.*, 2017, 1, art. N° 0045.
- [7] Hiroki Tanaka, Yoshihisa Inoue, and Tadashi Mori, *Chem. Photo. Chem.*, 2018, 2, 386 –402.

[8] A. Ciogli, S. Vivek Kumar, M. Mancinelli, A. Mazzanti, S. Perumal, C. Severic and C. Villania, *Org. Biomol. Chem.*, 2016, 14, 11137–11147.

[9] Sandra Belviso, Ernesto Santoro, Francesco Lej, Daniele Casarini, Claudio Villani, Roberta Franzini, and Stefano Superchi, *Eur. J. Org. Chem.*, 2018, 29, 4029–4037.

PART B

*Chiral bioactive tricyclic compounds
with a seven-membered ring: Variable
temperature HPLC and NMR*

1. Introduction

A high percentage of the drugs available on the market, and some of the most prescribed ones, is formulated using a single enantiomer of the active compound. Chiral bioactive compounds exist as couple of enantiomers having frequently very different pharmacological and pharmacokinetic properties. The therapeutical index and the diversity and intensity of the adverse effects differ considerably between a racemic mixture and an optically pure drug [1]. Many examples are reported in literature, but one of the most unfortunate and notable is represented by Thalidomide [2]. Enantioselective design of drugs is complicated by the presence of stereogenic elements different from the stereogenic centre and that generate stereoisomers known as atropisomers [3]. Atropisomerism generates diastereoisomers and enantiomers and it is time and temperature-dependent with half-lives of interconversion usually shorter than 1000 s. When atropisomerism is detected in a new drug, this adds a complication in the designing route. When developing an atropisomeric drug, the same strategies applied in the development of classical stereoisomers should

be considered, keeping in consideration that all atropisomers can potentially be equilibrated depending on temperature. Many examples of drugs developed as single optically pure stereoisomers, if the interconversion rate is considerably low, or as a reproducible interconverting mixture are widely reported [4]. Telenzepine, an antimuscarinic drug used in the treatment of the peptic ulcer disease, has two stable butterfly-like enantiomeric conformations (fig.1.1) that interconvert with an energetic barrier $\Delta G^\ddagger = 35$ kcal/mol and interact with different affinity with the receptor M1[5].

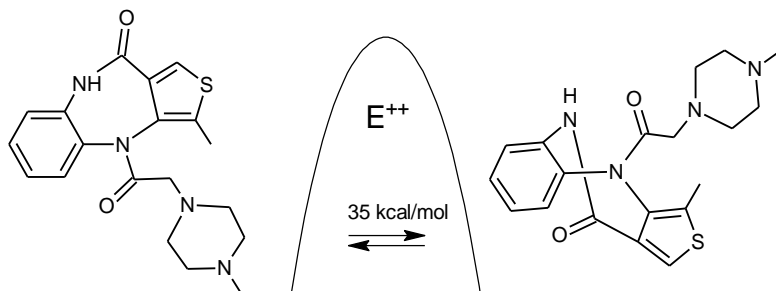


Fig. 1.1- Telenzepine enantiomeric atropisomers.

Numerous drugs with different applications as anxiolytics, antivirals, antiepileptics and antimuscarinic, share a benzodiazepinic or dibenzodiazepinic core, with a 7-membered ring that can flip in two different conformations, one the

mirror image of the other, therefore, existing as couple of enantiomers. Many tricyclic drugs with different biological activities, like carbamazepine and pirenzepine for example, have a butterfly-like structure as confirmed by X-ray analysis [6][7]. Most of the time non-planarity is required for interaction at the active site, and frequently the substrate-receptor affinity is highly influenced by the stereochemistry [8]. Many strategies can be applied to freeze the butterfly-motion [9] and stabilize the atropisomers in order to study the different bioactivities and improve the therapeutic index of drugs. Benzolactams with seven-membered rings are another class of biologically active compounds that exhibit atropisomerism [10]. An example is represented by 1,4-benzodiazepines, the most prescribed drugs for the treatment of sleep disorders and anxiety [11]. The phenomenon of the “ring inversion” allows the interconversion between two boat conformations which are non-superimposable specular images. Diazepam, one of the most prescribed drugs in the world since its commercialization under the brand name of Valium in 1963, exhibit fast interconversion between the two conformational enantiomers, and for the process it has been calculated an energetic barrier of 17.6 kcal/mol (fig 1.2).

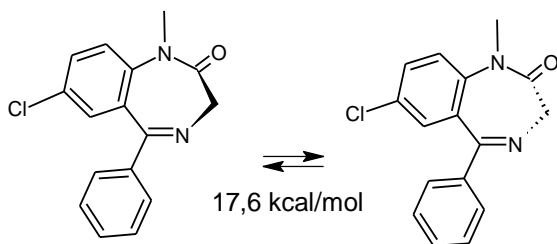


Fig. 1.2 - Non-planar enantiomeric conformers of Diazepam, the methylene group may be above or under the plane of the fused benzene.

Depending on the structural modifications, the energetic barriers of interconversion of benzodiazepines vary in a range between 16 and 22 kcal/mol [12],[13] and the entity of the ΔG^\ddagger of the interconversion process is modulated by steric and electronic effects. For example, substituents at the N1 increase the interconversion barrier [14], therefore, the N1-desmethyl-diazepam has a ΔG^\ddagger of 12.3 kcal/mol. The importance of studying the chirality of the 1,4-benzodiazepine-2-one that interconvert by ring-flip is evidenced by the discovery, by Lee et al. [15] of a certain grade of stereoselectivity in the interaction with the GABA_A bonding site. To study the interconversion process of atropisomeric bioactive compounds, dynamic high-performance liquid chromatography (d-HPLC) with chiral

stationary phase [16] is a well-established technique, and, together with dynamic-NMR, results particularly suitable in measuring low barrier of interconversion. Cryogenic dynamic HPLC [17] operates at temperatures down to -75°C allowing to resolve racemic mixture of fast interconverting stereoisomers.

1.1 Nevirapine

Nevirapine (NVP) is a non-nucleoside inhibitor of the inverse transcriptase used in combination with other drugs for the treatment of HIV. The HAART (highly active anti-retroviral therapy) approach to HIV treatment is the most effective one and Nevirapine (fig. 2.1), as a NNRTI of first generation, is still considered effective in diminishing the mortality and morbidity of the pathology and is still widely and used in therapy in particular in low-resources countries [18][19].

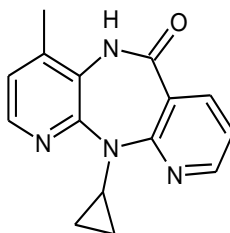


Fig. 1.3 - Nevirapine structure.

Chemically, NVP is a dipyrdo-diazepinone with the nitrogen N4 functionalized with a cyclopropyl group. From the crystallographic data it is evident that the two pyridyl portions are not coplanar. Therefore, the tricyclic system adopts a “butterfly-like” structure and the pyridyl rings can be oriented upwards or downwards with an angle between the two intersecting planes of 121° [20].

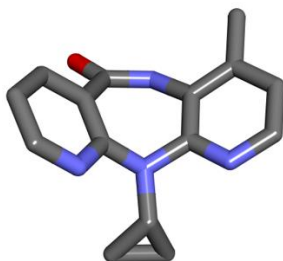


Fig. 1.4 - 3D model of Nevirapine shows butterfly-like structure.

The lack of a plane of symmetry in the NVP structure confers chirality to the molecule. The two enantiomers interconvert by flipping of the diazepinone ring and inversion of the nitrogen atom. By dynamic-NMR and computational studies it has been reported a value of about 17,8 kcal/mol for the ΔG^\ddagger of enantiomerization [21]. NVP is not considered atropisomeric at 25°C, with a half-life of racemization of less than a second.

1.2 Oxcarbazepine

Iminostilbene derivatives are known to be effective on the nervous system and in particular to have anticonvulsant activity. Oxcarbazepine (fig 1.5) is the 10-keto derivative of Carbamazepine [22] and is widely employed in the treatment of epilepsy and trigeminal neuralgia. Oxcarbazepine and its primary metabolite (the monohydrate derivative) are both effective in controlling seizures, probably by acting on the sodium and potassium channels [23].

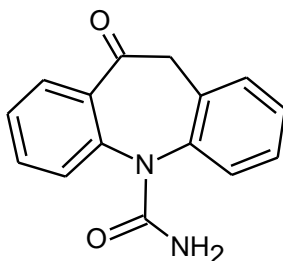


Fig. 1.5 - Oxcarbazepine structure.

The different pharmacokinetic profile [24] compared to Carbamazepine, makes Oxcarbazepine more tolerable, with a sensibly lower incidence of severe adverse reactions. NPV has a butterfly-like structure with C_1 symmetry, generated by the twisted-boat conformation of the seven-membered azepine ring, confirmed by X-ray data, widely reported in literature [25] [26].

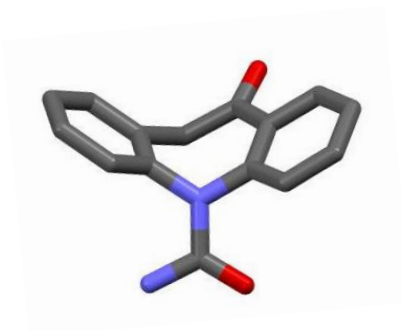


Fig. 1.6 - 3D model of Oxcarbazepine.

1.3 Estazolam

As a classic benzodiazepine drug, Estazolam has anticonvulsant and anxiolytic effects, but its major use is for treating sleep disorders [27]. Structurally, it is a tricyclic benzodiazepine (fig 1.7) and is related to Triazolam, having a triazole ring fused with the diazepinic ring but lacking the methyl group in the triazole. The structure of Estazolam does not have a plane of symmetry and it exist as a mixture of two boat conformation in rapid equilibrium. These conformations are non-superimposable mirror images, but since the interconversion rate is very fast at room temperature the molecule is generally considered as achiral.

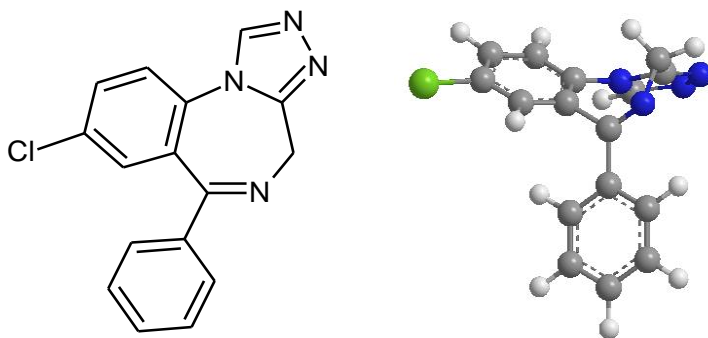


Fig. 1.7- Estazolam structure (left) and 3D molecular model (right).

2. Results and discussion

2.1 Nevirapine

The stereodynamic of the non-nucleoside reverse transcriptase inhibitor Nevirapine has been studied by dynamic-HPLC with chiral stationary phase supported by NMR measurements. The $^1\text{H-NMR}$ spectrum of a solution $4 \cdot 10^{-2}\text{M}$ of Nevirapine in d-Chloroform has been registered and is reported in figure 2.1.

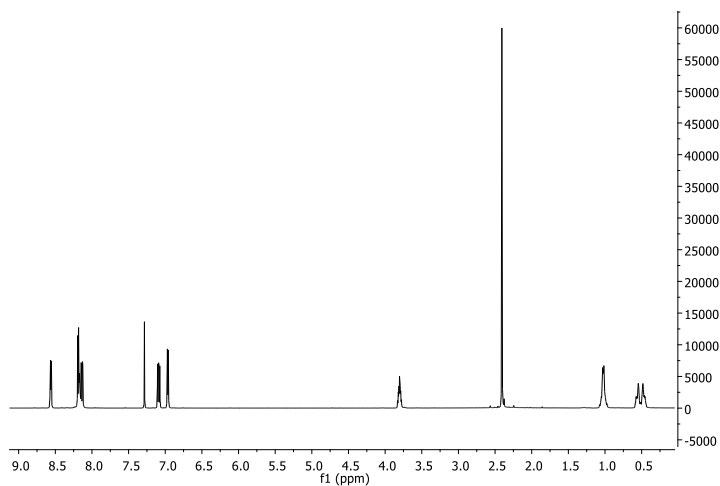


Fig. 2.1 - $^1\text{H-NMR}$ spectrum of Nevirapine in CDCl_3 .

All the signals and in particular the intense signal at 2.41 ppm, corresponding to the three methyl protons, are evidently

split in two signals when a chiral selector is added to the solution. The Pirkle type selector for chiral stationary phases (R,R)-Whelk-O1 (fig 2.2) has been chosen to demonstrate the diastereotopic interactions with the two rapidly interconverting enantiomers of Nevirapine.

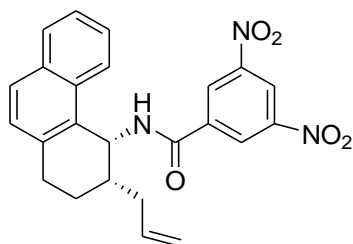


Fig. 2.2 - Structure of the (R,R)-Whelk01 chiral selector.

As evidenced by a comparison of the structure of NVP and (R,R)-Whelk-O1, there are many potential interaction sites that, given the complementary shapes of the two molecules, can lead to relatively stable diastereomeric complexes. Non-covalent interactions as hydrogen bonding, Van Der Waals, π - π and other electrostatic interactions are expected to take place between NVP and the chiral selector, ensuring a good molecular recognition mechanism.

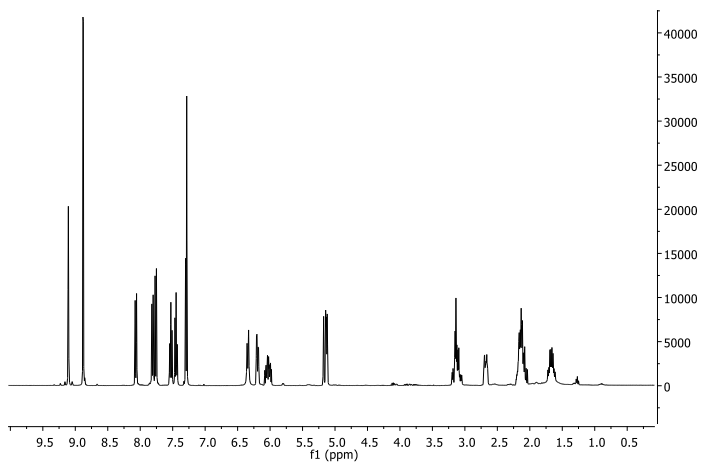


Fig. 2.3- ^1H NMR spectrum of a solution $4 \times 10^{-2}\text{M}$ of (R,R)-Whelk-O1 in CDCl_3 .

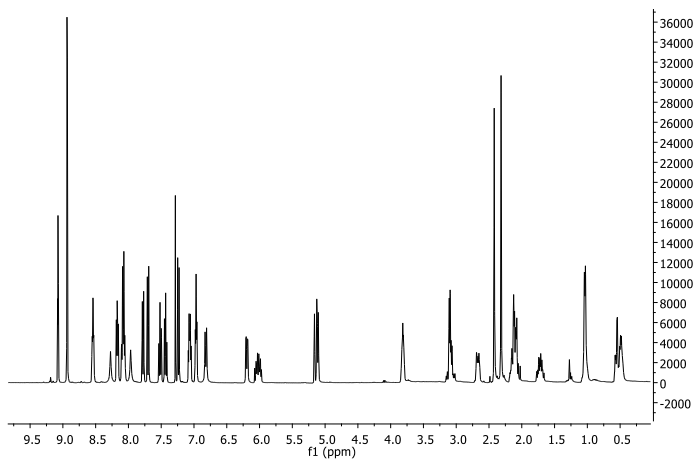


Fig. 2.4 - ^1H -NMR spectrum of a solution of (R,R)-Whelk-O1 selector and Nevirapine (1:1 molar ratio) in CDCl_3 .

In figure 2.4 is reported the ^1H NMR spectrum of a mixture in 1:1 molar ratio of Nevirapine and (R,R)Whelk-O1 in CDCl_3 . In the mixture with (R,R)-Whelk-O1 the signal corresponding to the Nevirapine methyl group is split due to the reversible association with (R,R)-Whelk-O1 selector (see magnified particular in figure 2.5). The two signals have difference of chemical shift ($\Delta\delta$) of 0.1 ppm corresponding to 40 Hz separation and show partial de-racemization as indicated by the integral's ratio of 1:1.13.

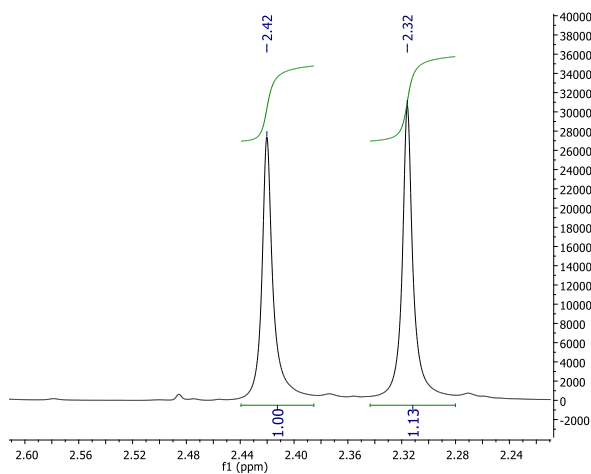


Fig. 2.5 - Magnified particular of the methyl signals of fig 2.4.

The results indicate a good interaction between NVP and the chiral selector, suggesting a potentially high selectivity of a

chiral stationary phase for HPLC based on (R,R)-Whelk-O1. Dynamic-NMR experiments (fig. 2.6) performed increasing the temperature of the probe until +65°C show the coalescence of the signals corresponding to the methyl group. The energetic barrier for the interconversion is calculated as 16,65 kcal/mol from the equation: $\Delta G^\ddagger = 4.58 \cdot T_c \cdot [10.32 + \log (T_c/kc)]$.

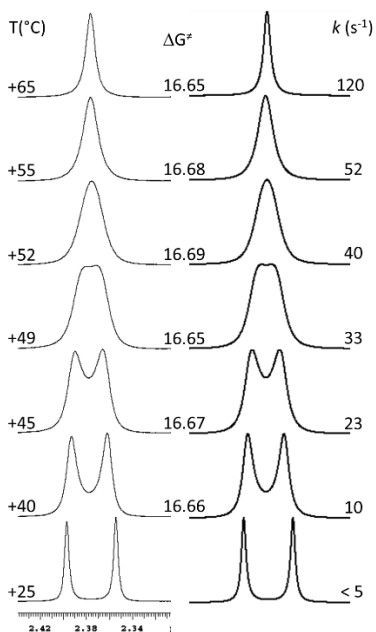


Fig 2.6 - Dynamic-NMR of a solution 1:1 in molar ratio of NVP and chiral selector, experimental (left) and simulated (right).

In the optimized analytical conditions NVP was eluted with a retention time of about 10 minutes on a (R,R)-Whelk-O1 (250x4,6mm Lx I.D.) chiral stationary phase and an eluent composed by hexane and dichloromethane in the same proportions and 2% of methanol. One single broad peak is observed at room temperature (fig. 2.7) while decreasing the temperature of the column down to -50°C the elution profile exhibits two peaks in a 50:50 (Area %) ratio (fig. 2.8).

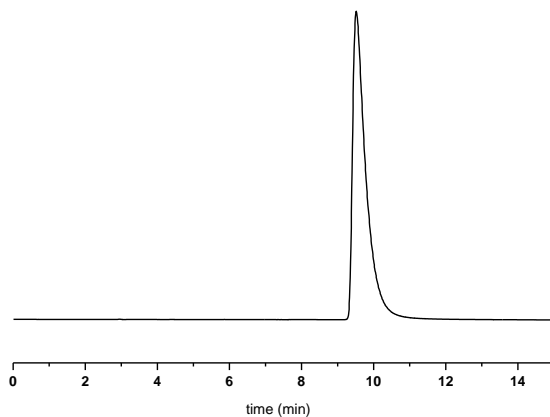


Fig. 2.7 - Elution profile of Nevirapine in NP-HPLC; column: (R,R)-Whelk-O; mobile phase: hexane/dichloromethane 50/50 (v/v) + 2% methanol; flow rate: 1 ml/min; detector: UV 280 nm; T column: 20°C .

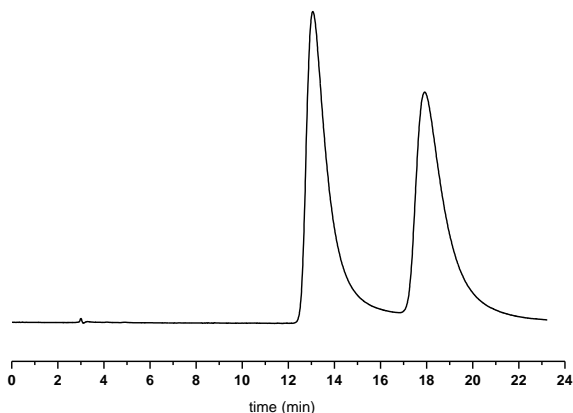


Fig. 2.8 - Elution profile of Nevirapine in NP-HPLC; Column: (R,R)-Whelk-O1; mobile phase: hexane/dichloromethane 50/50 (v/v) + 2% methanol; Flow rate: 1 ml/min; detector: UV 280 nm; T column: -50°C .

tr1 (min)	tr2 (min)	k'1	k'2	α	A% 1
13,07	17,96	3,24	4,83	1,49	50

Tab. 2.1 - Chromatographic parameters for the experimental conditions reported in fig. 2.7. Capacity factors and selectivity are calculated starting from the retention time and dead time.

With a T_{column} of -50°C the peaks corresponding to the two enantiomers of Nevirapine are almost separated at the baseline. To measure the energetic barrier associated with the enantiomerization process, dynamic HPLC experiments at variable temperatures were performed. Gradually decreasing

the temperature of the column (fig. 2.9), the single peak decoalescence is observed, giving two peaks with a plateau in between when the stereomutation is slowed down to a rate comparable to that of the chromatographic process.

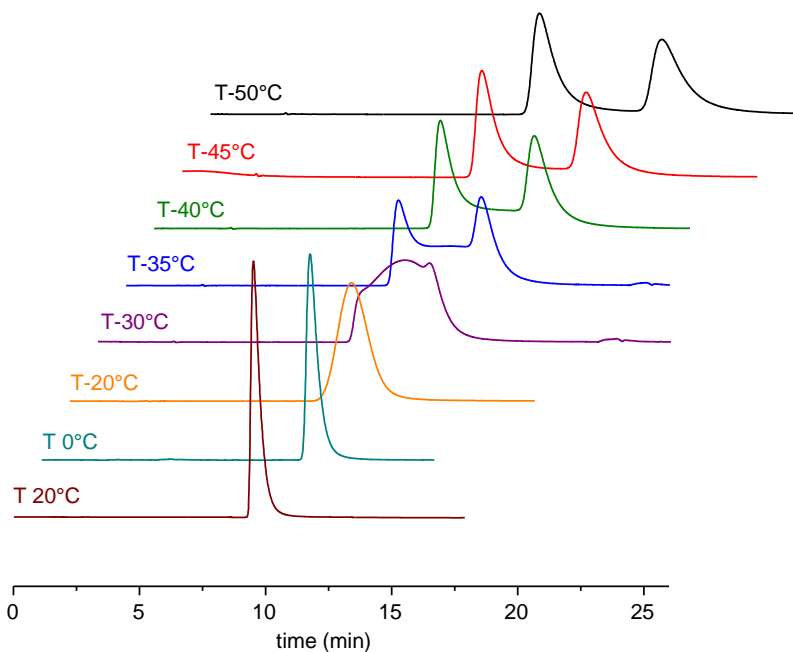


Fig. 2.9 - D-HPLC experiments performed on Nevirapine. Column: (R,R)-Whelk-O1; mobile phase: hexane/dichloromethane 50/50 (v/v) + 2% methanol; Flow rate: 1 ml/min; detector: UV 280 nm; T_{col} : variable as indicated in the figure.

Simulations of the dynamic chromatograms based on the stochastic model, allowed to calculate a kinetic rate constant for the on-column enantiomerization. In figure 2.10 are reported the simulated and the experimental chromatograms. The two profile are not perfectly superimposable because of the high tailing factor caused by the presence of many polar groups in NVP.

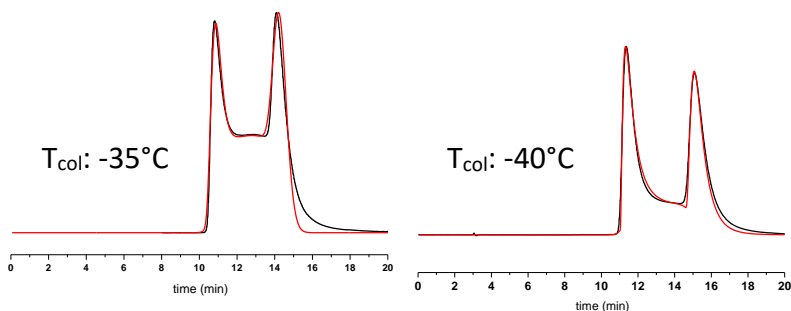


Fig. 2.10 - Simulated (red) and experimental (black) chromatograms of NVP with a T_{col} of -35 and -40 °C

T_{col} (°C)	$k_{en\ 12}$ (min^{-1})	$\Delta G_{en\ 12}^{\ddagger}$ (kcal/mol)	$k_{en\ 21}$ (min^{-1})	$\Delta G_{en\ 21}^{\ddagger}$ (kcal/mol)	$k_{en\ av}$ (min^{-1})	$\Delta G_{en\ av}^{\ddagger}$ (kcal/mol)
-35	0,072	17,01	0,055	17,14	0,063	17,07
-40	0,028	17,08	0,021	17,22	0,024	17,15

Tab. 2.2 - kinetic rate constants and energetic barrier of the on-column enantiomerization of Nevirapine. Column temperatures are intended $\pm 0,1$ °C. Errors in $\Delta G \pm 0,02$ kcal/mol.

Variable temperature HPLC, performed at very low temperatures allowed to resolve NVP in two distinct peaks, confirming the good selectivity that was expected on the Pirkle type CSP (R,R)-Whelk-O1. An enantiomerization barrier of 17,1 kcal/mol is calculated, confirming the fast stereomutation process of Nevirapine.

2.2 Oxcarbazepine

The antiepileptic drug Oxcarbazepine is an iminostilbene derivative that exists as a racemic mixture of fast interconverting enantiomers. Chirality derives from the twisted boat conformation of the azepine ring and the asymmetric substitution pattern.

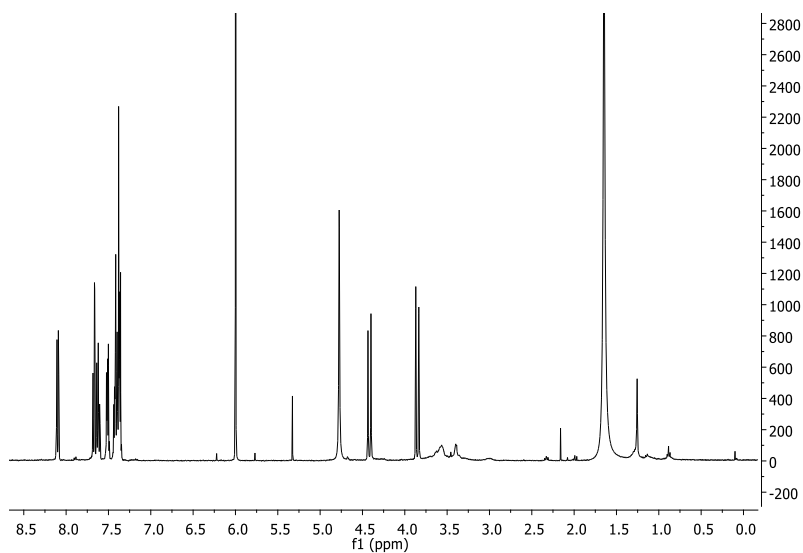


Fig. 2.11 - ^1H -NMR spectrum of Oxcarbazepine in $\text{C}_2\text{D}_2\text{Cl}_4$ (top).

The energetic barrier of interconversion is supposed to be lower than 18 kcal/mol, in agreement with data reported for structural analogues. Dynamic-HPLC with chiral stationary phase was performed in order to resolve the two enantiomers and to study the stereodynamic behaviour.

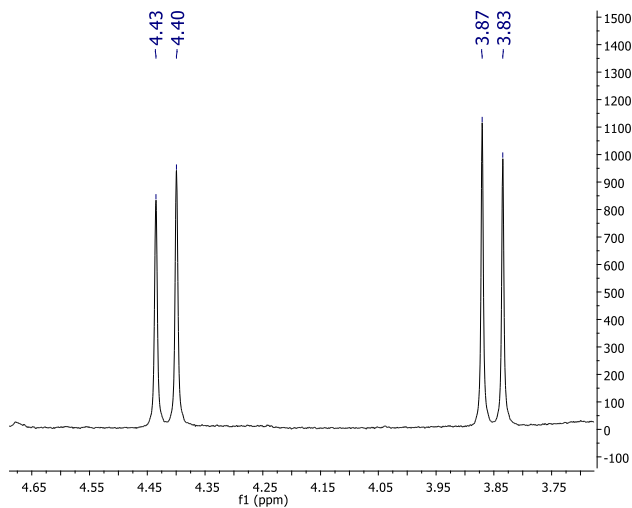


Fig 2.12 - Detail of the double doublet relative to the non-equivalent diastereotopic protons of the methylene group in the seven-membered ring.

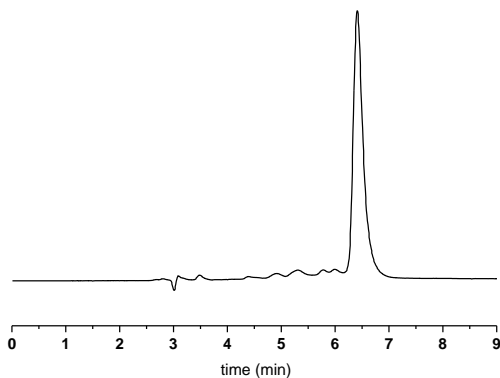


Fig. 2.13 - Elution profile of a sample of Oxcarbazepine extracted from tablets; column: (R,R)-Whelk-O1; mobile phase: hexane/dichloromethane 50/50 (v/v) + 5% methanol; flow rate: 1 ml/min; Detector: UV 290 nm; T column: 25°C

Oxcarbazepine was eluted as a single peak with a retention time of 6,80 minutes in NP-CSP-HPLC, under the experimental conditions reported in figure 2.13. The chiral stationary phase (R,R)-Whelk-O1 is expected to have a good selectivity for the stereoisomers of oxcarbazepine, because of the many possible recognition sites. Fast on-column interconversion translates in the lack of separation, at room temperature, of the peaks corresponding to the single enantiomers. As a matter of fact, when the chromatographic column is cooled down to -50°C (fig 2.14) the peak

decoalescence reveals two separated signals corresponding to the two conformational enantiomers.

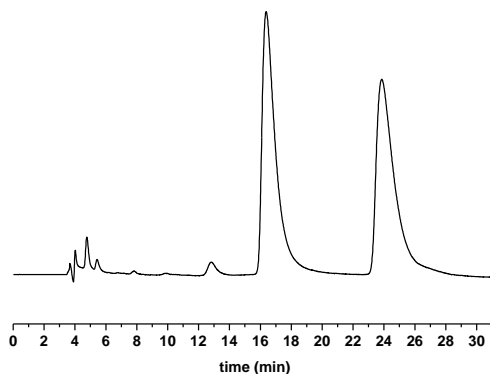


Fig 2.14 - Elution profile of a sample of Oxcarbazepine extracted from tablets; column: (R,R)-Whelk-O1; mobile phase: hexane/dichloromethane 50/50 (v/v) + 5% methanol; flow rate: 1 ml/min; detector: UV 290 nm; T column: -50°C

tr1 (min)	tr2 (min)	k'1	k'2	α	A% 1
16,37	23,82	3,22	5,14	1,60	50

Tab. 2.3 - Chromatographic parameters for the experimental conditions reported in fig 2.11. Capacity factors and selectivity are calculated starting from the retention time and dead time.

Despite the pronounced tailing, the two peaks are well resolved at the baseline. Variable temperature HPLC

experiments (fig 2.15) revealed the gradual decoalescence in relation to the column temperature.

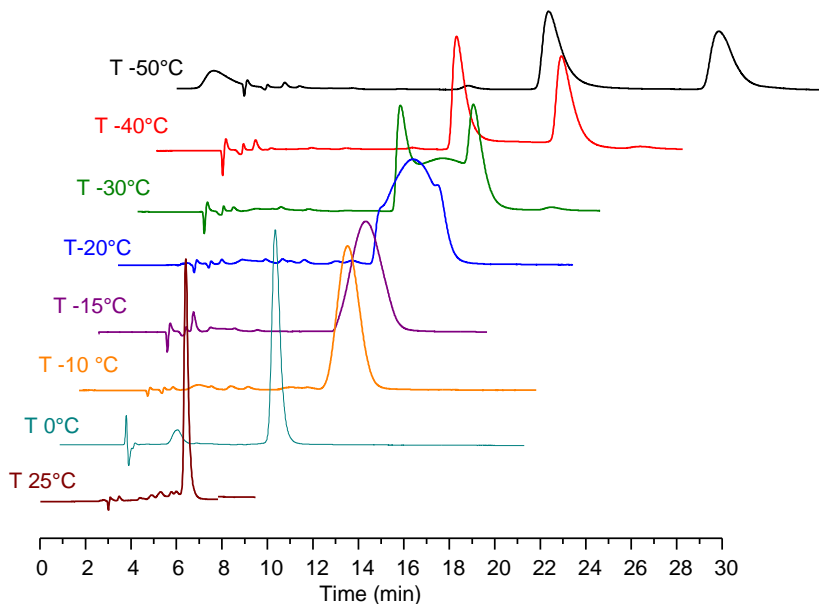


Fig. 2.15 - D-HPLC experiments performed on Oxcarbazepine. Column: (R,R)-Whelk-O1; mobile phase: hexane/dichloromethane 50/50 (v/v) + 5% methanol; flow rate: 1 ml/min; detector: UV 290 nm; T_{col} : variable as indicated in the figure.

When the temperature of the column is maintained at -40°C , -30°C and -20°C , a plateau between the two peaks of the enantiomers indicates an on-column interconversion. These experimental chromatograms have been simulated to

calculate the apparent kinetic rate constant and consequently the energetic barrier of enantiomerization. Simulations have been iterated until a good correspondence with the experimental chromatograms is reached and the best fitting are reported in figure 2.16 along with the free energy of activation in table 2.4.

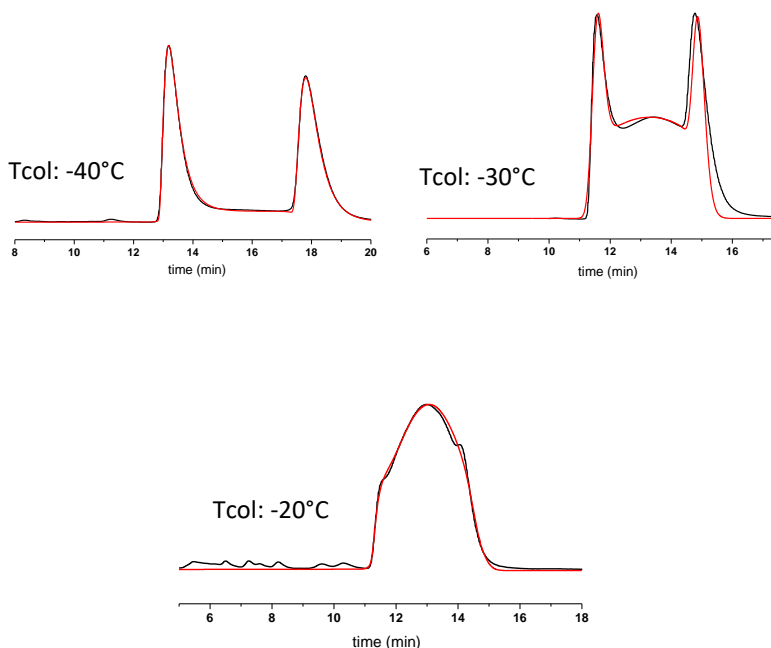


Fig. 2.16 - Simulated (red) and experimental (black) chromatograms of Oxcarbazepine with a T_{col} of -20, -30 and -40 °C

T col (°C)	$k_{\text{en } 12}$ (min ⁻¹)	$\Delta G^{\ddagger}_{\text{en } 12}$ (kcal/mol)	$k_{\text{en } 21}$ (min ⁻¹)	$\Delta G^{\ddagger}_{\text{en } 21}$ (kcal/mol)	$k_{\text{en av}}$ (min ⁻¹)	$\Delta G^{\ddagger}_{\text{en av}}$ (kcal/mol)
-20	0,217	17,55	0,169	17,68	0,063	17,61
-30	0,083	17,30	0,065	17,42	0,074	17,36
-40	0,014	17,39	0,010	17,53	0,012	17,46

Tab. 2.4 - kinetic rate constants and energetic barrier of the on-column enantiomerization of Oxcarbazepine. Column temperatures are intended $\pm 0,1$ °C. Errors in $\Delta G \pm 0,02$ kcal/mol.

Oxcarbazepine cannot be considered atropisomeric, because the enantiomerization barrier is calculated around 17,5kcal/mol. The interconversion between the two stereoisomers takes place with a rate too high to allow the separation of the enantiomers at room temperature, making it impossible to further characterize them. The experimental data obtained by d-HPLC have been furtherly confirmed by dynamic-NMR.

2.3 Estazolam

The two enantiomers of Estazolam, generated by the flipping of the diazepinic ring in two different non-planar boat conformations (fig 2.17), can be separated only at very low temperatures. The energetic barriers of interconversion of 1,4-benzodiazepine-2-ones are generally lower than 20 kcal/mol, making them suitable to be studied with dynamic-NMR (at high temperatures) or dynamic-HPLC with chiral stationary phase (at low temperatures) [28]. The values of ΔG^\ddagger of enantiomerization are affected by the presence of electron-withdrawal group in ortho on the fused phenyl ring and by the presence of substituents on N1.

A fluorine atom in the non-fused phenyl ring lowers the energetic barrier of interconversion, while N1-tert-butyl-1,4-benzodiazepine-2-ones are reported to have higher activation energies [29] and can be considered as atropisomers. Tricyclic benzodiazepines (imidazole or triazole fused in N1 and C2 with the diazepine ring) have usually lower ΔG^\ddagger of enantiomerization than Diazepam (~18 kcal/mol) unless they carry an alkyl substituent in on the five-membered ring in

position C1 [30]. From a structure analysis and based on what previously affirmed, Estazolam must have an energetic barrier of interconversion lower than 17 kcal/mol.

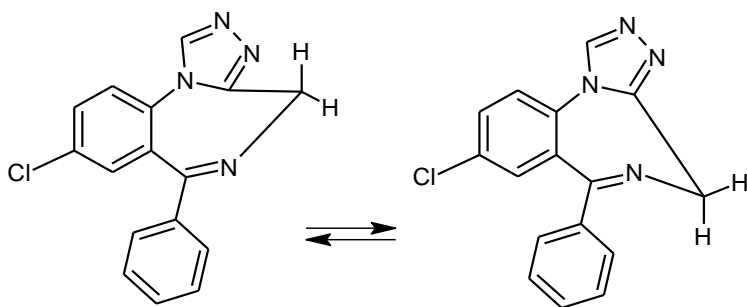


Fig. 2.17 - Ring flipping in Estazolam generates two enantiomeric conformations.

Actually, from dynamic-NMR experiments (fig 2.18) it was calculated a ΔG^\ddagger of enantiomerization of 14,5 kcal/mol, considering the temperatures at which it can be observed the gradual coalescence and decoalescence of the signals related to the two protons Ha and Hb of the methylene in the 1,4-diazepine ring. To further confirm the value obtained with dynamic-NMR, it was performed a dynamic-HPLC experiment at very low temperatures.

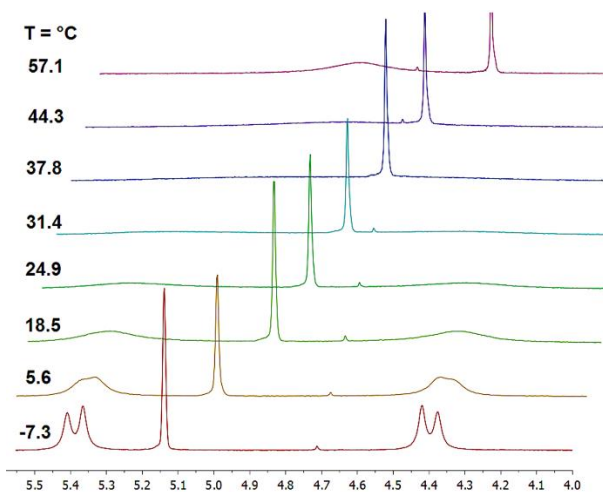


Fig. 2.18 - dynamic-NMR of Estazolam in CD₃OD.

In fact, dealing with very low energetic barriers of enantiomerization requires drastically low temperatures of the chromatographic column and short elution times to take the stereomutation and the chromatographic process on the same time-scale. Nothing less, this is the only condition in which it is possible to observe the classical dynamic elution profile.

Estazolam was then eluted on the chiral stationary phase Chiralpak IA, using a short 5cm x 0,46 cm (L. x I.D.)

chromatographic column with a mobile phase composed by 50% of hexane and 50% of dichloromethane with the addition of 1% of methanol. In these experimental conditions and with no cooling of the chromatographic column, the compound is eluted in five minutes with a k' of 4,39 (figure 2.19).

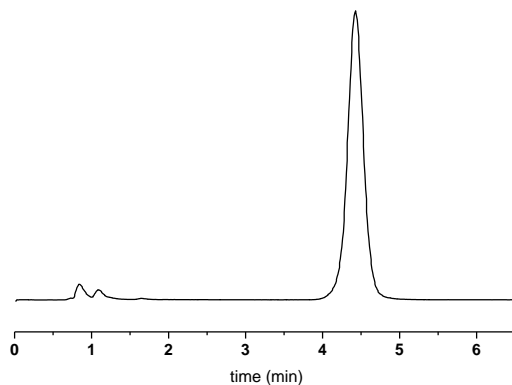


Fig. 2.19 - Elution profile of a sample of Estazolam; column: Chiralpak IA (50 x 4,6 mm L. x I.D., 5 μ m particle size); mobile phase: hexane/dichloromethane 50/50 (v/v) + 1% methanol; flow rate: 1 ml/min; detector: UV 280 nm; T column: 25°C

To contrast the increase in retention due to the low temperature of the chromatographic column, the polar component in the mobile phase has been adjusted to reach

75% of dichloromethane. Cryo-HPLC has been performed decreasing the temperature of the column down to -55°C , -65°C and -70°C (fig 2.20). At -55°C a broad single peak is still present indicating that the interconversion is still faster than the elution process, while a plateau between two chromatographic peaks is detected at -65°C and -70°C .

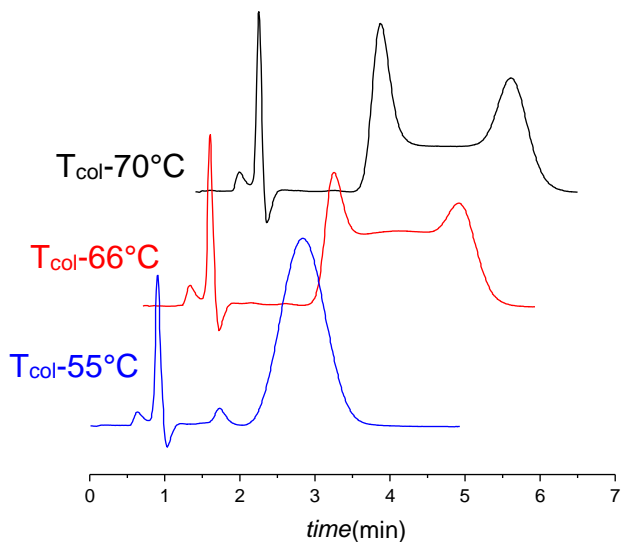


Fig. 2.20 - D-HPLC experiments performed on Estazolam. Column: Chiralpak IA (50 x 4,6 mm L. x I.D., $5\mu\text{m}$ particle size); mobile phase: hexane/dichloromethane 25/75 (v/v) + 1% methanol; Flow rate: 1 ml/min; Detector: UV 280 nm; T_{col} : variable as indicated in the figure.

Although it was reached a temperature of -70°C , the interconversion process was still fast enough to prevent the complete resolution of the peaks. However, it has been possible to calculate the energetic barrier of interconversion by simulation of the experimental chromatograms at -65°C and at -70°C (figure 2.21).

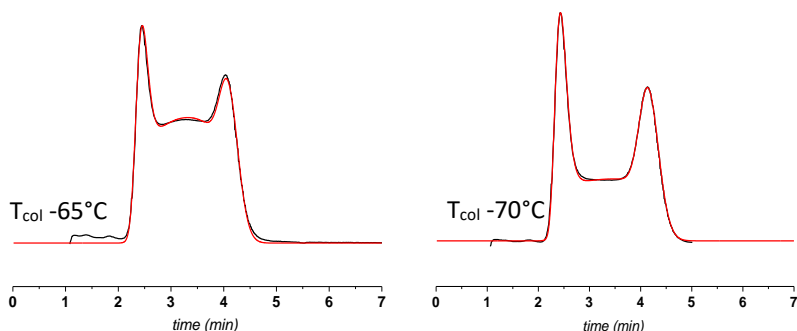


Fig. 2.21 - Simulated (red) and experimental (black) chromatograms of Estazolam with a T_{col} of -65 and -70°C .

Apparent kinetic rate constants and free activation energies of enantiomerization are reported in table 2.5. Results are in line with the value obtained by d-NMR and, as expected, ΔG^{\ddagger} of enantiomerization is ~ 14 kcal/mol confirming the effect of the non-substituted triazole ring on the interconversion rate.

T col (°C)	k_{en 12} (min⁻¹)	ΔG[‡]_{en 12} (kcal/mol)	k_{en 21} (min⁻¹)	ΔG[‡]_{en 21} (kcal/mol)	k_{en av} (min⁻¹)	ΔG[‡]_{en av} (kcal/mol)
-65	0,461	13,98	0,273	14,19	0,367	14,09
-70	0,272	13,92	0,158	14,14	0,074	14,03

Tab. 2.5 - Kinetic rate constants and energetic barriers of the on-column enantiomerization of Estazolam. Column temperatures are intended $\pm 0,1$ °C. Errors in $\Delta G \pm 0,02$ kcal/mol.

3. Conclusions

The stereodynamics of three biologically active tricyclic compounds, Nevirapine, Oxcarbazepine and Estazolam, with three different therapeutical activities have been successfully studied using CSP-HPLC. All the compounds can be considered chiral at temperatures lower than -30°C while at room temperature it is impossible to isolate the single enantiomers. The (R,R)-Whelk-O1 chiral stationary phase has a good selectivity for butterfly-like heterocyclic compounds, as testified by the NMR studies with the chiral selector in solution. The interconversion generated by the conformational change of the seven-membered ring take place with an average ΔG^{\ddagger} value of 14, 17 and 17,5 kcal/mol respectively for Estazolam, Nevirapine and Oxcarbazepine. These values have been measured by dynamic-HPLC, decreasing the temperature of the column down to -70°C and applying the stochastic model for the simulation of the experimental chromatograms. The energetic barriers measured by dynamic-HPLC were found to be positively in agreement with those measured by dynamic-NMR.

4. Methods and Materials

4.1 Chemicals and materials

All solvents and Nevirapine were purchased from Sigma Aldrich (St. Louis, MO, USA).

Oxcarbazepine has been obtained from a tablet containing 300 mg of active compound. The tablet has been triturated and the extraction with CH₃CN resulted in 50 mg of Oxcarbazepine with a chemical purity > 90% measured by ¹HNMR and HPLC.

Estazolam was obtained by extraction from a 2mg tablet. The extraction was performed with CH₂Cl₂ and was followed by filtration on silica gel. The extract was separated from the solvent and re-dissolved in the mobile phase used for the NP-HPLC measurements.

4.2 HPLC measurements

4.2 a Chromatographic apparatus

Analytical chromatography was performed on a Jasco (Tokyo, Japan) HPLC system with a universal Rheodyne 20 μ l injector, a pump Jasco PU 980 and a second CO₂ pump Jasco PU 1580. Detection is provided by a Jasco UV 975 detector a Jasco UV/CD 995 detector. Low temperature dynamic HPLC experiments were performed using a home-made cooling device and dry ice.

4.2.b Chromatographic columns

Chiral resolution of the racemic mixtures by HPLC was performed with polysaccharide-based chiral stationary phases Chiralpak IA(50 x 4,6 mm L. x I.D., 5 μ m particle size) purchased from Daicel Chiral Technologies, and a Pirkle type CSP (R,R)-Whelk01 (250 x 4,6 mm L x I.D., 5 μ m particle size) purchased from Regis Technologies Inc.

4.2 c Simulation of dynamic chromatograms

Simulations of variable temperature experimental chromatograms presenting a dynamic profile were performed by Auto DHPLC y2k (Auto Dynamic HPLC), using the stochastic model. Both chromatographic and kinetic parameters can be automatically optimized by simplex algorithm until the best agreement between experimental and simulated dynamic chromatograms is obtained.

4.3 ¹H-NMR measurements

¹H-NMR spectra were recorded at 400 MHz on a Bruker 400 NMR spectrometer and at 600 MHz (dynamic NMR of Nevirapine) on a Varian Unity-INOVA 600 (Università di Bologna, Prof. Mazzanti research group).

5. References

- [1] Canera H, Gronera E, Levya L, Agranat I, *Drug Discov. Today* 2004, 9, 105-110.
- [2] Smith SW. *Toxicol Sci.* 2009, 110 (1), 4–30.
- [3] Steven R. LaPlante, Lee D. Fader, Keith R. Fandrick, Daniel R. Fandrick, Oliver Hucke, Ray Kemper, Stephen P. F. Miller, and Paul J. *J. of Med. Chem.* 2011, 54 (20), 7005-7022.
- [4] Jonathan Clayden, Wesley J. Moran, Paul J. Edwards, and Steven R. LaPlante, *Angew. Chem. Int. Ed.*, 2009, 48, 6398 – 6401.
- [5] P. Eveleigh, E.C. Hulme, C. Shudt and N.J. M. Birdsall, *Mol. Pharmac.*, 1989, 35, 477-483.
- [6] M. M. J. Lowes, M. R. Caira, A. P. Lötter and J. G. Van der Waat, *J. of Pharm. Sci.*, 1987, 76 (9), 744-752.
- [7] G. Bandoli and M Nicolini, *J. of Crystal. and Spec. Res.*, 1978, 7 (3), 281-293.
- [8] M. Simonyi, *Adv. in Drug Res.*, 1997, 30, 73-106.
- [9] Yuki Kanase, Mai Kuniyoshi, Hidetsugu Tabata, Yuka Takahashi, Susumu Kayama, Shintaro Wakamatsu, Tetsuta

- Oshitari, Hideaki Natsugari, Hideyo Takahashi, *Synthesis*, 2015, 47, 3907–3913.
- [10] Hidetsugu Tabata, Naoya Wada, Yuko Takada, Tetsuta Oshitari, Hideyo Takahashi, and Hideaki Natsugari, *J. Org. Chem.*, 2011, 76, 5123–5131.
- [11] Willy E Haefely, *Eur Arch Psychiatr. Neurol. Sci.*, 1989, 238, 294–301.
- [12] Béla Paizs, Mikló´ S Simonyi, *Chirality*, 2009, 11, 651–658.
- [13] R. Sabia, M. De Martino, A. Cavazzini and C. Villani, *Chirality*, 2015, 28(1), 17-21.
- [14] Norman W. Bela, Perry Rosen, James V. Earley, Charles Cook, and Louis J. Todaro, *J. Am. Chem. Soc.*, 1990, 112 (10), 3969-3978.
- [15] S. Lee, T. Kamide, H. Tabata, H. Takahashi, M. Shiro, H. Natsugari, *Bioorg. Med. Chem.*, 2008, 16, 9516.
- [16] C. Wolf, *Chem. Soc. Rev.*, 2005, 34, 595–608.
- [17] I. D’Acquarica, F. Gasparri, M. Pierini, C. Villani, G. Zappia, *J. Sep. Sci.*, 2006, 29, 1508-16
- [18] Nandi Siegfried, Pieta JU van Deventer, Fazleh Ahmed Mahomed, George W Rutherford, *Cochrane Database Syst Rev.*, 2006, 19 (2).

- [19] Daniel F. Carr, Stephane Bourgeois, Mas Chaponda, Louise Y. Takeshita, Andrew P. Morris, Elena M. Cornejo Castro, Ana Alfirevic, Andrew R. Jones, Daniel J. Rigden, Sam Haldenby, Saye Khoo, David G. Laloo, Robert S. Heyderman, Collet Dandara, Elizabeth Kampira, Joep J. van Oosterhout, Francis Ssali, Paula Munderi, Giuseppe Novelli, Paola Borganiani, Matthew R. Nelson, Arthur Holden, Panos Deloukas, Munir Pirmohamed, *J. of Antimicro. Chemother.*, 2017, 72 (4), 1152–1162.
- [20] Philip W. Mui,¹ Stephen P. Jacober, Karl D. Hargrave, Julian Adams, *J. Med. Chem.* 1992, 35, 201-202.
- [21] Edmund W. D. Burke, Gareth A. Morris, Mark A. Vincent, Ian H. Hillier and Jonathan Clayden, *Org. Biomol. Chem.*, 2012, 10, 716–719.
- [22] M. C. Walker, P. N. Patsalos, *Pharmac. Ther.*, 1995, 67 (3), 351-384.
- [23] TM. J. McLean, M. Schmutz, A. W. Wamil, H.-R. Olpe, C. Portet, and K. F. Feldmann, *Epilepsia*, 1994, 35 (3), S5-S9.
- [24] Gérard Flesch, *Clin. Drug Invest.*, 2004, 24 (4), 185-203.

- [25] A. Hempel, N. Camerman, A. Camerman and D. Mastropaolo, *Acta Cryst.*, 2005, 61, o1313–o1315.
- [26] Katie M. Lutker, Adam J. Matzger, *J. of Pharm. Sci.*, 2010, 99, 794–803.
- [27] Mark W. Pierce, Vincent S. Shu, *The Am. J. of Med.*, 1990, 88 (3A) 6S-11S.
- [28] R. Sabia, A. Ciogli, M. Pierini, F. Gasparri, C. Villani, *J. of Chrom. A*, 2014, 1363, 144-149
- [29] Piero Salvadori, Carlo Bertucci, Giorgio Ascoli, Gloria Uccello-Barretta, Elena Rossi, *Chirality*, 1997, 9, 495–505.
- [30] Norman W. Gilman, Perry Rosen, James V. Earley, Charles M. Cook, John F. Blount, and Louis J. Todaro, *J. Org. Chem.* 1993, 58, 3285-3298.

PART C

*Investigation on the isomerization
cis/trans in conformationally flexible
proline-rich-peptides and small
molecules*

PART C-1

Cis/Trans isomerization by amidic bond rotation in proline-rich small molecules studied by dynamic-HPLC and stochastic model computations

1. Introduction

All the experiments presented in this section have been performed in the research group of Prof. Dr. Oliver Trapp, in the Department of Organic Chemistry of the LMU (Ludwig-Maximilians University) of Munich (Germany).

Carbonyl-Proline bond is a common structural element that can give rise to *trans* and *cis* isomers thanks to rotation around the amidic bond, the number of detectable isomers depends on the number of hindered peptidyl-proline bonds. *Trans/cis* isomerization influences the structure of peptides and proteins and is an important feature in controlling signal transduction, aggregation, enzymatic catalysis and protein folding [1] [2]. The isomerization takes place at room temperature with a half-life of minutes or seconds depending on the aminoacid sequence and on the solvent. Over the years, many studies have focused on studying the kinetics of the process [3] [4]. This pattern is common in catalytically active peptides for which it is well documented the influence of the conformation on the performance of the catalysis and the outcome of the reaction [5] [6]. Recently proline-rich tripeptides have been identified as effective catalysts for

aldol and conjugate addition reactions [7][8][9]. The catalytic mechanism involves an enamine intermediate, and all the catalytically active peptides assume a β -turn conformation. In solution the *trans* isomer is the thermodynamically favoured conformer in equilibrium with the *cis* isomer (fig 1.1).

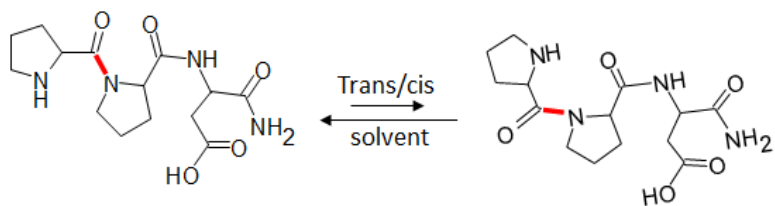


Fig. 1.1 - *trans* (left) and *cis* (right) equilibrium of H-Pro-Pro-Asp-NH₂ peptide.

Among all the tripeptides tested, H-Pro-Pro-Asp-NH₂ is the more efficient and stereoselective, and the best results in term of stereoselectivity are imputable to the *trans* conformers.

Rotation around the tertiary amide bond can affect the three-dimensional structure of the catalyst and has a great impact on the stereoselectivity of the reaction, therefore, it is essential to study mechanism to control the isomerization rate. An interesting example of simultaneous rotation around

more than one amidic bond of proline residues is exhibited by Captopril disulphide. Captopril is an Angiotensin-converting enzyme inhibitor, used in therapy, since its first discovery in 1975, for the treatment of hypertension [10] [11]. As peptidyl-proline bond containing molecule it exists as an equilibrium mixture of two isomers *trans* and *cis*, originated by rotation around the amidic bond [12]. Its principal metabolite is the disulphide dimer, that is formed after oxidation. Captopril disulphide represents a model to study the simultaneous interconversion of three isomers in solution, generated by the presence of two peptidyl-proline bonds [13].

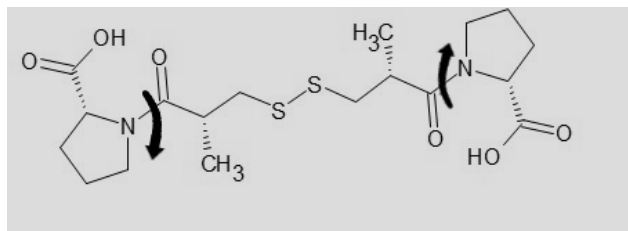


Fig. 1.2 - Captopril Disulphide exists as three isomers *trans-trans*, *cis-trans*, *cis-cis* interconverting by rotation of the amidic bonds of the two proline residues.

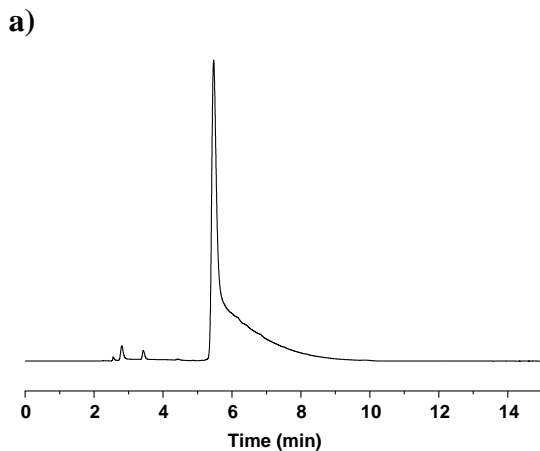
Usually the rotational energy associated to the rotation around the amidic bond is about 20 kcal/mol, thus making it

perfectly suitable to be studied by techniques like variable temperature HPLC or dynamic-NMR. Reverse phase HPLC has been applied in several studies to separate *trans* and *cis* isomers of Proline-containing peptides. The elution order can be predicted by the solvophobic theory considering the greater hydrophobic area of the *cis* isomer compared to *trans* isomer, therefore, the first one would be more retained by a stronger interaction with the hydrocarbon chains of the stationary phase [14]. In dynamic-HPLC experiments, it is possible to slow down or accelerate the interconversion process varying the temperature of the chromatographic column [15]. When the isomerization process takes place within the same time scale of the chromatographic process, a plateau between peaks is observed. Studying this kind of experimental chromatograms with stochastic model or theoretical plate model-based computations it is possible to extract the kinetic parameters. The evaluation of the dynamic chromatograms can be performed using specifically designed softwares. Applying the Eyring equation and using the kinetic rate constant and the K_{eq} of the reaction, the values for the ΔH^\ddagger , ΔS^\ddagger and ΔG^\ddagger associated to the interconversion processes in both directions, can be easily extrapolated.

2. Results and discussion

2.1 H-Pro-pro-Asp-NH₂ a conformational labile peptidic catalyst studied by dynamic chromatography

A sample of H-Pro-Pro-Asp-NH₂•TFA salt has been dissolved in water and analysed by RP-HPLC. A C18 stationary phase has been used with a mobile phase composed by 99% aq. sol. 10mM of phosphate buffer with a pH 6.8 and 1% of acetonitrile as organic modifier. The measurements have been performed at both a column temperature of 25 ° C and 2°C (fig. 2.1).



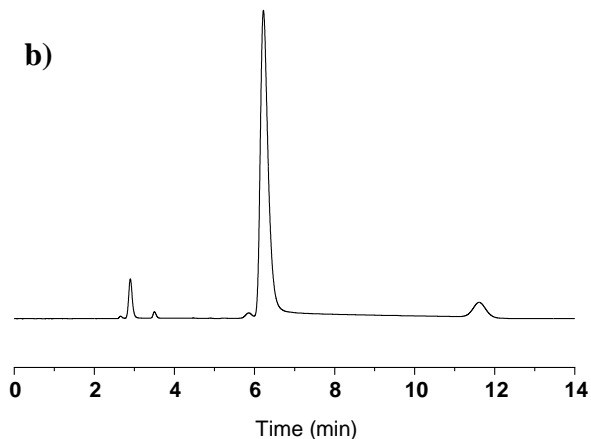


Fig. 2.1 - Experimental chromatograms registered at 220 nm of H-PPA-NH₂ at 25°C (a) and 2°C (b) (column temperatures). Two peaks in a ratio 9:1 can be assigned the *trans* and *cis* isomers.

Even if at room temperature it was possible to observe only one peak with an important tailing, presumably imputable to the isomerization process, at 2°C two peaks with a ratio 9:1 (A:A) are clearly visible. The capacity factors are calculated to be respectively $k'1 = 1.15$; $k'2 = 3.02$ ($T_{col} = 2^{\circ}C$). To check the effect of the ionic strength and pH of the eluent on the chromatographical separation, the eluent was modified using two different phosphate buffer solutions (5mM and 20mM). As showed in fig.2.2, softening the ionic strength of

the eluent results in a larger peak at room temperature. On the contrary, increasing the ionic strength to 20 mM induces a sharpening of the first peak coupled to a higher retention time.

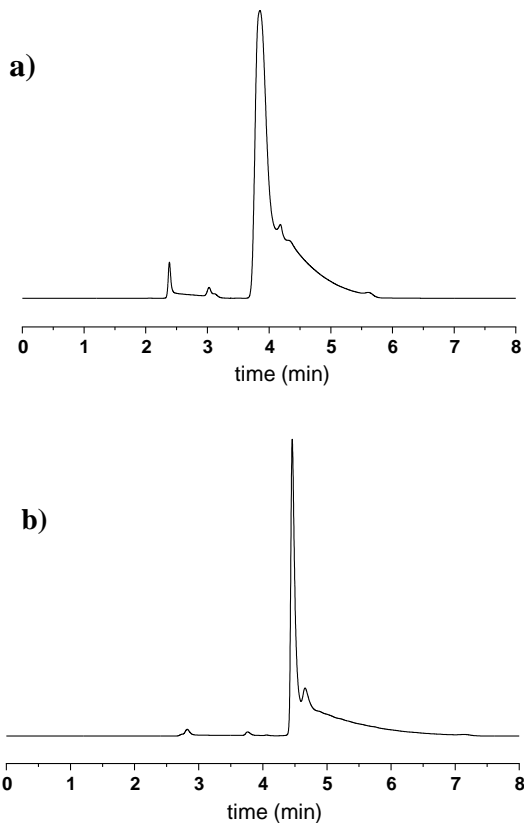


Fig. 2.2 - Experimental chromatograms registered at 220nm of H-PPA-NH₂. a) Phosphate buffer 5mM 97% in the eluent ; b) Phosphate buffer 20mM 98% in the eluent.

As well, small variations of the pH value of the eluent didn't result in a better chromatographic profile. An eluent obtained by mixing solvent A (triethylamine 0.05% + 0.05% trifluoroacetic acid in H₂O) and solvent B: (100% acetonitrile) in a ratio 96:4 (v:v) was used to further investigate the effect of the mobile phase on the separation. Measurements have been performed varying the temperature of the column from 4°C up to 50°C (fig. 2.3). Increasing the column temperature two peaks separated at the baseline are detectable. Decreasing the temperature of the column, the first peak broadens and finally a third peak is detected and a plateau between the first two is visible at 2°C

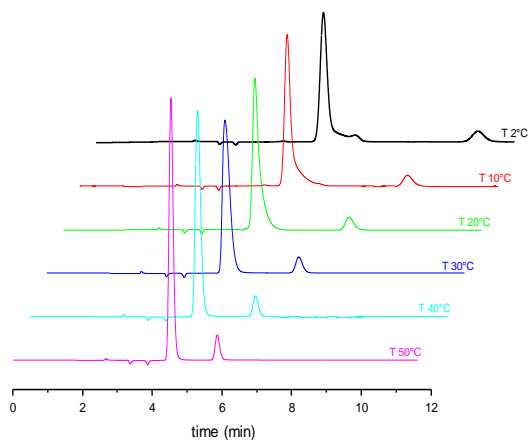


Fig. 2.3 - Variable temperature HPLC measurements of H-PPA-NH₂ with TEA 0.05%/TFA 0.05% aq. solution as solvent A in the eluent.

Analytical conditions have been optimized to identify the nature of the third peak by LC-MS. A suitable buffer for LC-MS experiments is a solution of ammonium acetate. Ammonium acetate 10mM has been used as solvent A in the eluent and Acetonitrile as solvent B, with a ratio A:B = 95:5 (v:v). In these conditions, the chromatographic profile is similar to the one obtained using a phosphate buffer in the eluent (fig. 2.4).

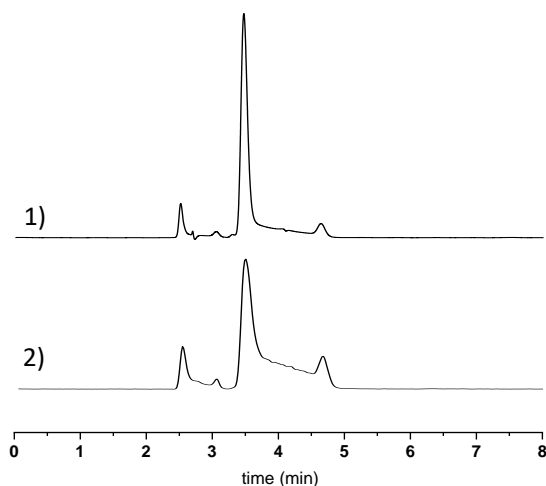
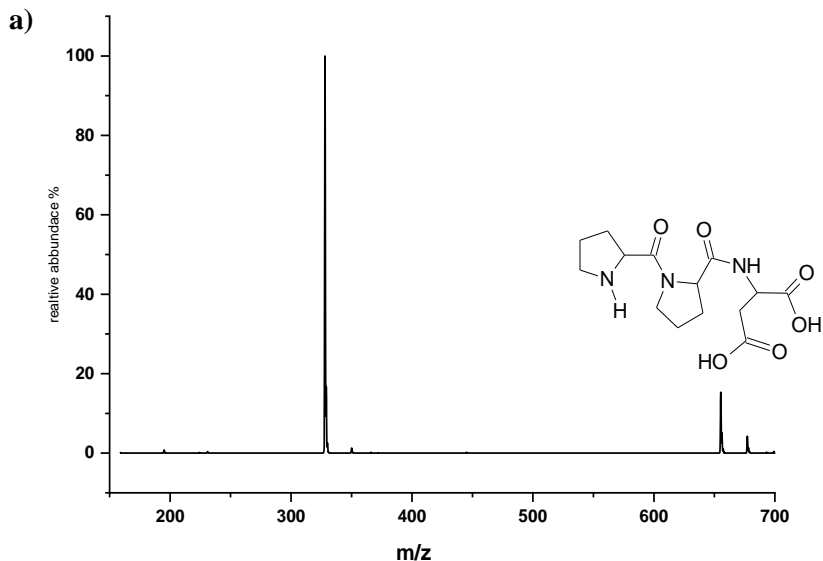


Fig. 2.4 - LC-MS experiments at Tcol 10°C on H-PPA-NH₂: 1) UV trace at 220 nm 2) ESI-MS in positive ion mode

Mass spectra extracted for the first and the second eluted peaks present the same signal patterns, and both have a base

peak with an m/z value equal to the molecular mass of the studied peptide plus one unit. For both the third and the fourth eluted peaks the most abundant ion has an m/z value corresponding to the protonated molecular mass $[M+1]^+$ of H-PPA-NH₂ (fig. 2.5). The first two peaks are identified, based on the m/z values and the chemistry of the compound, as the hydrolysis product H-PPA-OH, that can spontaneously be formed in aqueous solution and it is found to be the only detectable impurity.



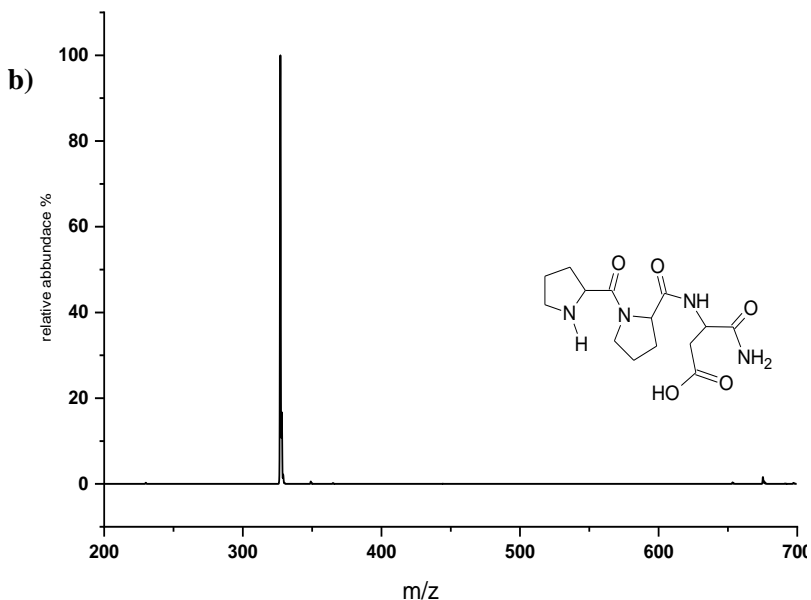


Fig. 2.5 - a) (+)ESI-MS spectrum of the first eluted peak, presumably the free acid H-PPA-OH; signals (m/z): 328.1 (100%), 329.1 (16.77%), 330.1(2.56%). 655.3 (15.31%), 677.3 (4.23%); b) (+)ESI-MS spectrum of the third eluted peak, assigned to the compound with the amidic derivatization H-PPA-NH₂; signals (m/z): 327.1(100%), 328.1 (16.72), 329.1 (2.18%), 675.3 (1.56%).

To avoid the formation of this side product the sample was dissolved in a solution 10mM of ammonium acetate. In this condition the sample results as more stable and it was not possible to observe the formation of any side product even after days in solution. Variable temperature experiments have

been performed in the two best analytical conditions. The temperature of the column ranged from 2°C to 50°C and all the measurements have been replicated three times. A first variable temperature HPLC experiment has been carried out using a mobile phase composed of 99% (v %) phosphate buffer sol. 10mM pH 6.8 and 1% (v %) acetonitrile (fig. 2.6). The sample was dissolved in water and the measurements have been carried out at different column temperatures, thus observing the coalescence and de-coalescence of peaks, with a plateau between the two at intermediate temperatures.

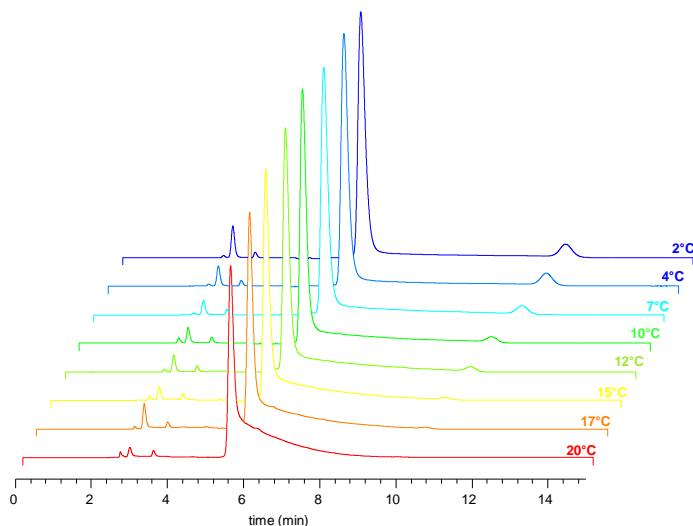


Fig. 2.6 - dynamic HPLC experiment. Sample dissolved in water. Phosphate buffer in the eluent.

A second experiment was carried out with a mobile phase composed by ammonium acetate 10mM solution and acetonitrile in 95:5 ratio (v:v), with the sample dissolved in the buffer solution (fig. 2.7).

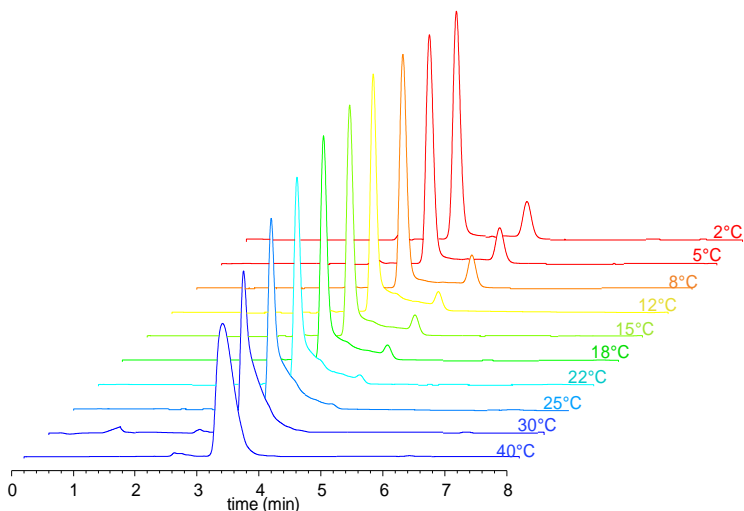


Fig. 2.7 - dynamic HPLC experiment. Sample dissolved in buffer solution. Ammonium acetate buffer in the eluent.

As well, measurements run at different column temperatures in a range between 2°C and 40°C revealed the coalescence of the two peaks corresponding to the *trans* and *cis* isomers into a single broad and asymmetrical peak, while raising the temperature of the column. On the contrary, at 2°C the two peaks are almost baseline separated and the ratio of the areas

corresponds to 85:15, resulting slightly increased compared to the one calculated for the sample dissolved in water. From the experimental chromatograms, obtained by variable temperatures HPLC experiments using ammonium acetate in the mobile phase, the kinetic parameters have been extrapolated using a stochastic-model based computational software. Evaluation of the data was carried out with ChromXwin, a software based on the simulation of the experimental chromatograms starting from the chromatographic parameters and using the stochastic computational model. Chromatographic parameters are calculated by the Origin2018 software using a gaussian dispersion function. Fitting the parameters in the software, after some iteration cycles the kinetic rate constants for both the isomerization processes (*trans* into *cis* and reverse) are obtained. The k_1 value can be used in the Eyring equation as given by the computation, whereas, the k_{-1} must be adjusted using the K_{eq} of the diastereomerization reaction. The kinetic rate constants obtained by the computations have been fitted into the Eyring equation to obtain a linear correspondence (fig. 2.8). The enthalpic contribution to the isomerization process is calculated from the slope of the line,

whereas the entropic contribution factor is derived from the value of the intercept (tab. 1).

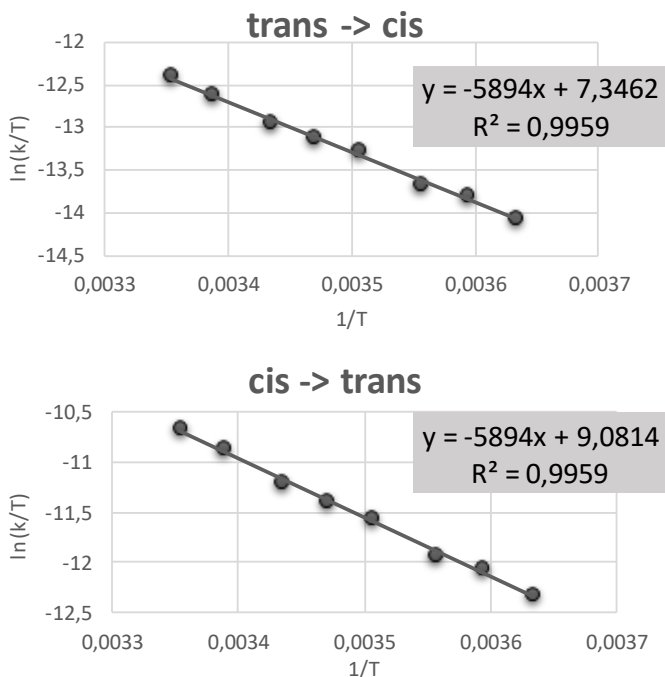


Fig. 2.8 - Eyring correlation between the k values and the temperatures.

ΔH_1^\ddagger (kcal/mol)	ΔH_{-1}^\ddagger (kcal/mol)	ΔS_1^\ddagger (kcal/mol*K)	ΔS_{-1}^\ddagger (kcal/mol*K)
11.66	11.66	-0.032	-0.029

Tab. 2.1 - Enthalpy and Entropy of activation, calculate by Eyring equation. $\Delta H^\ddagger \pm 0.30$ kcal/mol ; $\Delta S^\ddagger \pm 0.0010$ kcal/mol*K

In tab. 2.1 are reported the averaged values of k_1 (min^{-1}) and k_{-1} (min^{-1}) and the corresponding calculated ΔG^\ddagger (kcal/mol).

T°C	k_1 (s^{-1})	k_{-1} (s^{-1})	ΔG_1^\ddagger (kcal/mol)	ΔG_{-1}^\ddagger (kcal/mol)
2	0.00021	0.00121	20.68	19.73
5	0.00028	0.00160	20.76	19.80
8	0.00032	0.00183	20.91	19.94
12	0.00048	0.00274	20.99	20.01
15	0.00057	0.00325	21.12	20.13
18	0.00070	0.00396	21.23	20.23
22	0.00098	0.00558	21.33	20.31
25	0.00123	0.00699	21.42	20.40

Tab 2.2 - kinetic parameters for the two isomerization processes, calculated with the software ChromXwin.

2.2 Captopril disulphide interconversion: a model for an innovative evaluation method of complex dynamic-HPLC profiles.

The disulphide derivative of Captopril has been synthesized following two different routes. In a first attempt, 50 μ l of H_2O_2 10% were added to 1 ml of a solution 1mg/ml of Captopril (figure 2.9). After 24 hours at room temperature the solution was analysed by RP-HPLC, using a C18 column and an eluent composed by Phosphate buffer 10 mM aqueous solution pH 6.8 (A) and acetonitrile (B) in a proportion A:B = 90:10. Three peaks corresponding to the three isomers of the product were detected at 220 nm, out of a complex mixture of other products (fig.2.10).

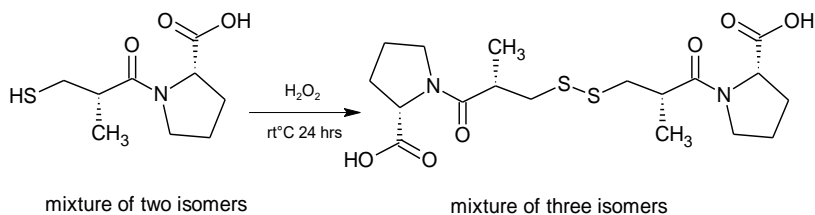


Fig. 2.9 - Synthetic route for the preparation of Captopril disulphide by oxidation with H_2O_2 .

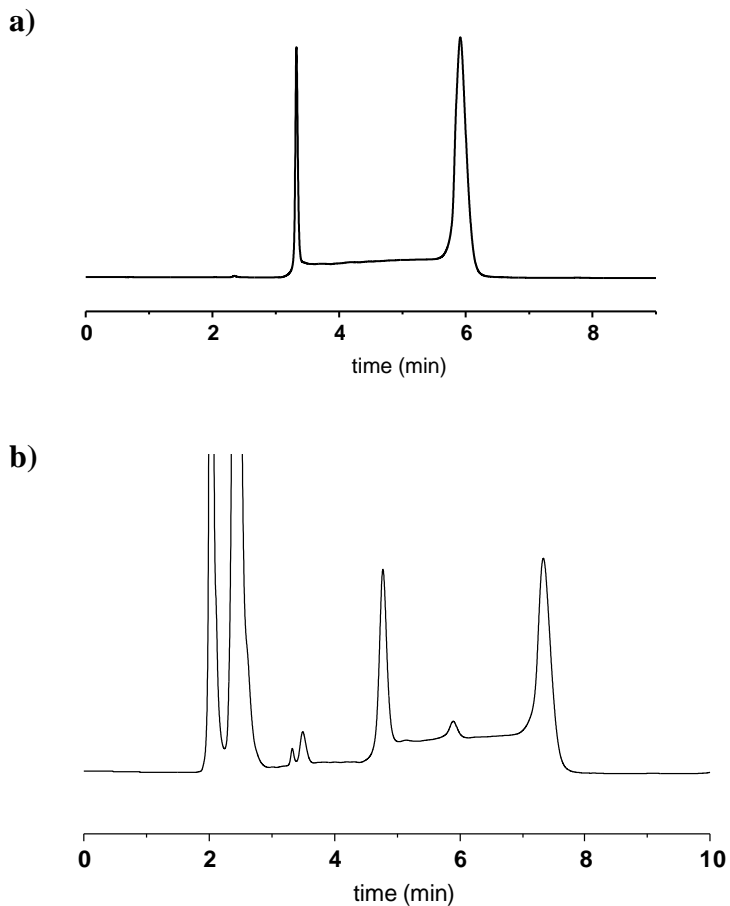


Fig. 2.10- Experimental chromatograms of Captopril 1 mg/ml aq. solution before (a) and after (b) oxidation by H_2O_2 . Column: Ascentis C18, Eluent: 90% A, 10% B; Detection: DAD extracted at 220 nm. Room temperature.

Although the formation of the disulphide is evident by the presence of three new peaks in the elution profile, the starting monomer was still present in the mixture even after 24 hours, furthermore, multiple oxidation products were identified by ESI-MS. In a second attempt Captopril disulphide was obtained following a different oxidation procedure that involves $K_3Fe(CN)_6$ as the oxidizing agent (figure 2.11).. Captopril disulphide was obtained as a white powder and the high chemical purity was checked by RP-HPLC (fig.2.12)

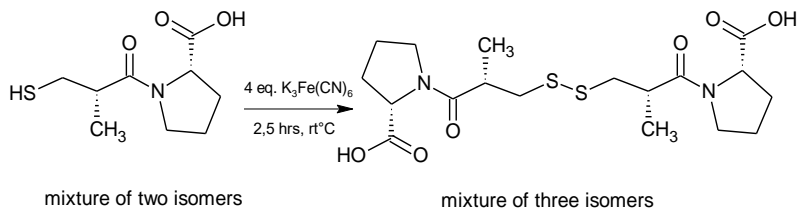


Fig. 2.11 - Synthetic route for the preparation of Captopril disulphide by oxidation with $K_3Fe(CN)_6$.

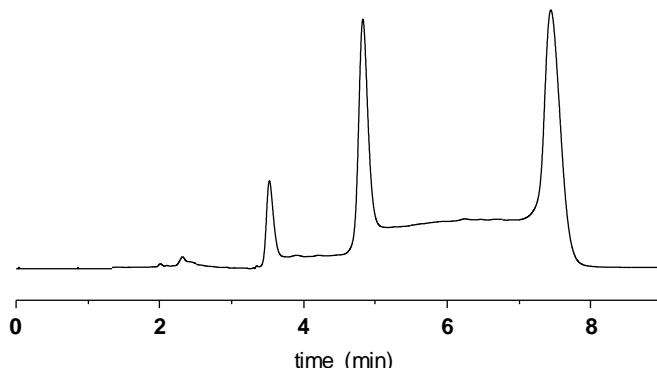


Fig. 2.12 - Experimental chromatogram of Captopril disulphide after oxidation of Captopril with $K_3Fe(CN)_6$. Column: Ascentis C18; mobile phase: 90% A, 10% B; detection: DAD extracted at 220 nm. T column °C 22.

The monomer was completely oxidized into the disulphide dimer that exists as a mixture of three isomers: *trans-trans*, *cis-trans* and *cis-cis*. A solution 1mg/ml of Captopril disulphide in water was analysed by HPLC with an Ascentis C18 column (250 x 4.5 mm, 5µm) and phosphate buffer 10mM pH 6.8 (solvent A) and acetonitrile in the eluent (solvent B). Flow rate was 1.000 ml/min and the UV detection set at 220nm. Varying the temperature of the chromatographic column from 7°C and up to 50 °C it is possible to study the simultaneous interconversion of the three isomeric species, due to rotation around the amidic

bonds of the terminal proline residues. In RP-HPLC the *cis* isomer of this kind of compounds is usually more retained than the *trans* isomer thanks to a greater solvophobic effect, on the other hand the more abundant isomer of Captopril should be the *trans* isomer and consequently the *trans-trans* is expected to be the more abundant for the disulphide derivative. Consequently, the assignment of the configuration to each peak is not immediate and it can be assumed that the second eluted must have intermediate characteristics, thus being the *trans-cis* isomer. Furthermore, the interconversion is more likely to involve the rotation around one amidic bond at a time, thus the process should proceed from a *cis-cis* isomer to give the *trans-cis* and then the *trans-trans* (or the opposite). Baseline separation is achieved at 7°C, and at this temperature the ratio of the areas can be calculated (tab. 2.3 and figure 2.13).

peak	rt (min)	Area%
1	4.17	8.4
2	5.76	39.1
3	9.07	52.5

$K'1$	$K'2$	$k'3$	$\alpha1$	$\alpha2$
0,85	1,56	3,03	1,83	1,94

Tab. 2.3 - Ratio of the areas integrated from the experimental chromatogram measured at $T_{col} = 7^{\circ}\text{C}$ and the calculated k' and α values.

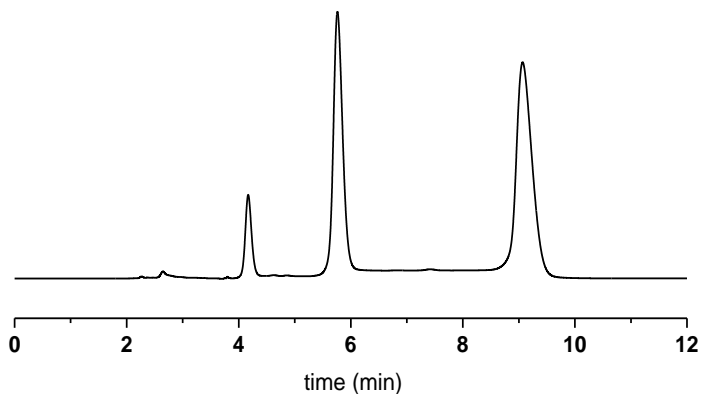


Fig 2.13- HPLC Profile of Captopril disulphide at 7°C .

Measurements were performed at intervals between 2 and 5 degrees, after equilibrating the system for 20 mins (figure 2.14). At column temperatures between 15 and 35°C a plateau between peak 1 and 2 and between peak 2 and 3 is observed. At temperatures above 35°C only one large peak can be identified, indicating a fast interconversion process between the three isomers. All measurements have been replicated three times and the chromatographic parameters,

like width at half peak, area %, relative height, have been calculated with the elaboration software Origin 2018 using the Gaussian dispersion fitting tool.

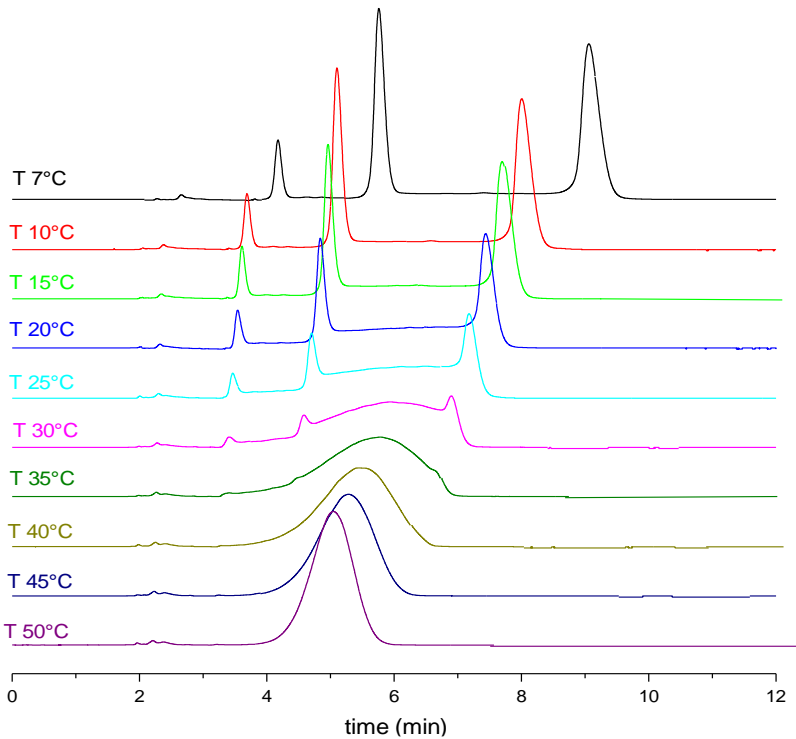
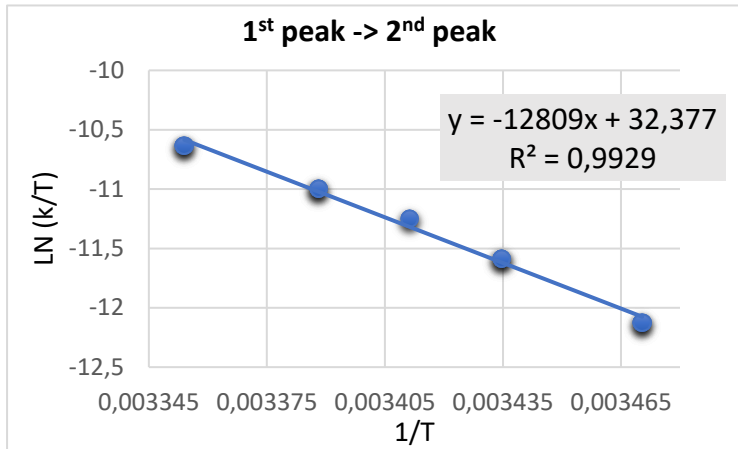


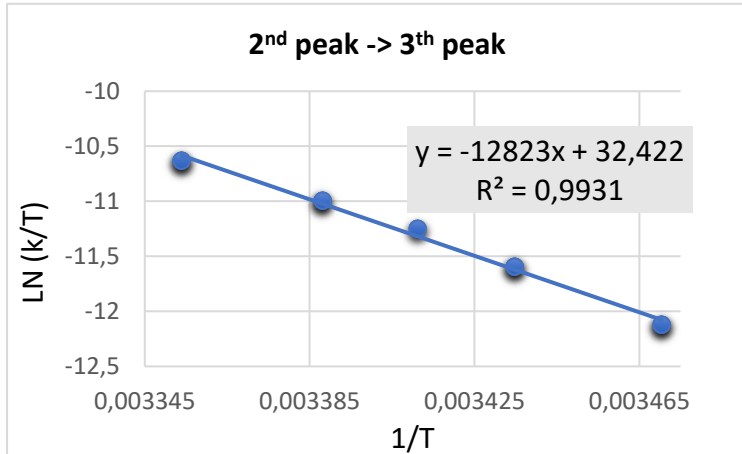
Fig. 2.14 - Variable temperature HPLC experiments on Captopril disulphide.

The experimental data were evaluated in order to extract the kinetic parameters of the two simultaneous interconversion process. An updated version of the software ChromXWin written by Prof. O. Trapp [16] has been used to perform stochastic computations obtaining the kinetic rate constants for the two dynamic processes and extrapolating by the Eyring equation the enthalpic and entropic contributes to the activation energies of the two interconversion (tab. 2.4 a,b,c). The kinetic rate constants for the two interconversions have been calculated in a range of temperatures between 15°C and 25°C. At lower temperatures the interconversion is too slow, and the peaks almost separated at the baseline, while at higher temperatures the partial coalescence of peaks makes it difficult to measure the experimental chromatographic parameters. The two values of the kinetic rate constant for the interconversion processes are almost identical. The simulations of some of the experimental chromatograms generated by the software are also reported below (fig. 2.15).

a)



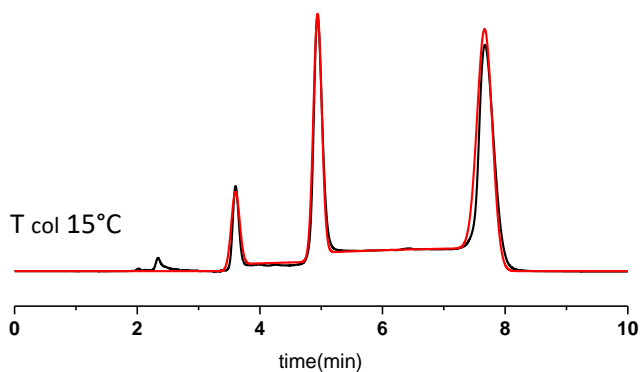
b)



c)

ΔH_1^\ddagger (kcal/mol)	ΔH_2^\ddagger (kcal/mol)	ΔS_1^\ddagger (cal/mol*K)	ΔS_2^\ddagger (cal/mol*K)
25,45	25,48	17,04	17,15

Tab. 2.4 - a) linear correlation between $\ln(k/T)$ and $1/T$ for the interconversion of the first eluted into the second eluted; b) linear correlation between $\ln(k/T)$ and $1/T$ for the interconversion of the second eluted into the third eluted; c) Enthalpy and entropy of activation calculated from the Eyring equation for both the interconversion processes.



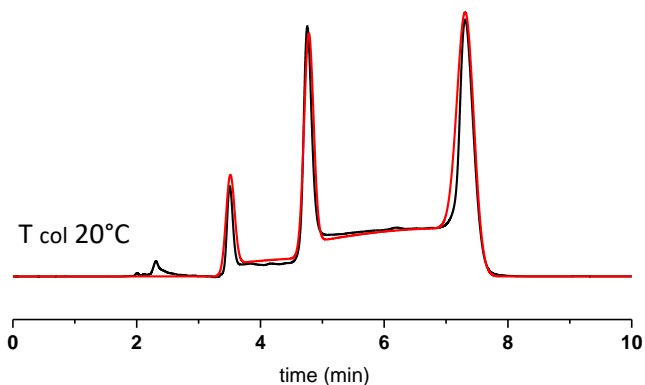


Fig. 2.15 - Experimental (black trace) and simulated (red trace) chromatograms of the disulphide dimer of Captopril registered at a T_{col} of 15°C and 20°C.

Finally, from the activation enthalpy and entropy calculated by the Eyring equation, it is calculated a free energy of activation (ΔG^\ddagger) of 20.4 kcal/mol (85 kJ/mol) at 25°C for both the dynamic interconversions studied.

3. Methods and Materials

All the experiments reported in part C1 have been performed at the Ludwig-Maximilians University (LMU) of Munich (GE) in the research group of Prof. Dr. Trapp (Department of Chemistry).

4.1 Chemicals and materials

H-Pro-Pro-Asp-NH₂ has been purchased as a TFA salt from Buchem. Captopril has been bought from Sigma-Aldrich as a pure chemical. All solvents have been purchased from Sigma-Aldrich and are HPLC grade pure.

Captopril disulphide was obtained dissolving 20 mg of Captopril in 10 ml of H₂O with 4eq of K₃Fe(CN)₆. After stirring for 2.5 hours at room temperature and addition of a base to the solution, the product was extracted with CH₂Cl₂ and then separated from the solvent by evaporation.

4.2 HPLC measurements

4.2 a Chromatographic apparatus

Measurements has been performed using a 1290 Infinity Agilent Technologies UHPLC apparatus.

LC-MS experiments have been performed using a 1200 Series Agilent Technologies HPLC apparatus coupled with 6120 Quadrupole LC-MS Agilent technologies single quadrupole mass detector equipped with an ESI source.

4.2.b Chromatographic columns

Column Ascentis C18 250 mm L. x 4.6 mm I.D. 5µm particle size has been purchased from Sigma Aldrich.

Column Lichrocart C18 250 mm L. x 4.0 mm I.D. 5µm particle size has been purchased from Merck.

4.2 c Evaluation of dynamic chromatograms

Simulations of variable temperature experimental chromatograms presenting a dynamic profile were performed by ChromXWin version 1.5.0.0 written by Prof. Dr. Trapp, using the stochastic model.

4. Conclusions

In conclusion, the optimization of a valid HPLC method to separate the isomers of a tripeptide with catalytic properties has been carried out. The isomerization derived from slow rotation around one of the proline bond has been studied using dynamic HPLC coupled to computational methods, and the value of ΔG_1^\ddagger and ΔG_{-1}^\ddagger have been calculated and found to differ of 1 kcal/mol. A synthetic pathway involving the use of iron salts allowed to obtain pure amounts of Captopril disulphide derivative. The three isomers of the compound have been resolved by reverse-phase HPLC using a C18 column and a mobile phase composed for the 90% of Phosphate buffer 10mM solution (pH6.8) and 10% of Acetonitrile. The process of isomerization between the three species has been studied by dynamic-HPLC, performing measurements at different column temperatures in a range between 7°C and 50°C. The on-column interconversion of the *cis-cis*, *cis-trans*, and *trans-trans* isomers is observed as the plateau height between peaks increases with temperature. Parameters obtained from the experimental chromatograms

have been used to calculate the kinetic rate constants and a ΔG_1^\ddagger of 20,4 kcal/mol.

5. References

- [1] William J. Wedemeyer, Ervin Welker, and Harold A. Scheraga, *Biochemistry*, 2002, 41, 14637-14644.
- [2] Lung-Nan Lin and John F. Brandts, *Biochemistry*, 1983, 22, 553-559.
- [3] Jana Jacobson, Wayne Melander, Gintaras Vaisnys, and Csaba Horváth, *J. Phys. Chem.* 1984, 88, 4536-4542.
- [4] Oliver Trapp, Gabriele Trapp, Volker Schurig, *Electrophoresis*, 2004, 25, 318–323.
- [5] Anthony J. Metrano, Nadia C. Abascal, Brandon Q. Mercado, Eric K. Paulson, Anna E. Hurtley and Scott J. Miller, *J. Am. Chem. Soc.* 2017, 139, 492–516.
- [6] Tobias Schnitzer and Helma Wennemers, *J. Am. Chem. Soc.*, 2017, 139, 15356-15362.
- [7] Jefferson D. Revell and Helma Wennemers, *Tetrahedron*, 2007, 63, 8420–8424.
- [8] Valerio D’Elia, Hans Zwicknagl, and Oliver Reiser, *J. Org. Chem.*, 2008, 73, 3262-3265.

- [9] Jefferson D. Revell, Daniel Gantenbein, Philipp Krattiger and Helma Wennemers, *Biopolymers (Peptide Science)*, 2006, 84, 105–113.
- [10] Ondetti MA, Rubin B, Cushman DW., *Science*, 1977, 196(4288):441-444.
- [11] Cushman DW, Cheung HS, Sabo EF, Ondetti MA., *Am J Cardiol.* 1982, 49(6), 1390-1394.
- [12] Dallas L. Rabenstein and Anvarhuseln A. Isab, *Anal. Chem.*, 1982, 54, 526-529.
- [13] Nishikawa T1, Abe R, Sudo Y, Yamada A, Tahara K., *Anal. Sci.*,2004, 20(10), 1395-1398.
- [14] Wayne R. Melader. Jana Jacobson and Csaba Horvath, *J. of Chromat. A*, 1982, 234(2), 269–276.
- [15] D. E. Henderson, Cs. Horvath, *J. of Chromat.*, 1986, 368, 203-213.
- [16] Oliver Trapp and Volker Schurig, *Comp. and Chem.*, 2001, 25 187–195.

PART C-2

*Anti/Syn isomerization in
polyfunctionalized indole with a stereolabile
centre studied by HPLC and assignment of
the absolute configuration*

1. Introduction

Many demanding goals are at the heart of organic chemistry, and among them the determination of the absolute configuration (AC) is still one of the most challenging. Assignment of the AC of chiral synthetic and natural compounds has been carried out over the years applying different methodologies [1], but the most used approach is based on the measure of the anomalous X-ray scattering[2]. Despite the good reproducibility and reliability of X-Ray crystallography, this method is sometimes limited by the necessity of single pure crystals, which are in many cases difficult to achieve. A great number of examples are also reported in literature about the employment of chiral derivatizing agents and chiral solvating agents in the determination of the enantiomeric excess and absolute configuration by NMR spectroscopy [3]. The recent development of faster and more accurate computational technologies has pushed the research towards methods that profit by the simulation of optical rotation dispersion (ORD) electronic circular dichroism (ECD) and vibrational circular dichroism (VCD) spectra [4] and the subsequent

confrontation with the experimental data to determine the AC. In particular, ECD is highly sensitive and requires only small amount of substance, making it the most widely used chiro-optical technique. Although the many advantages of time dependent (TD-DFT) simulations of the ECD spectra, this method can be applied only if chromophore groups are present in the compound and the computational model for the simulations gets less precise with the increasing of the flexibility of the studied molecule, since it is more difficult to predict the right conformation. In this context, VCD has the advantage to be effective even in the absence of a chromophoric portion and it is applicable to any kind of compound. The progressive improvements in the field of chiral HPLC and in particular the design of enantioselective stationary phases that bloomed in the last decades has made liquid chromatography a precious ally in the determination of absolute configuration [5]. Chiral HPLC in preparative scale allows to obtain optically pure chiral compounds with a good efficiency, a primary requisite to perform X-ray, ECD or VCD measurements. In fact, many examples of the application of HPLC with chiral stationary phase coupled to

chiro-optical techniques in assigning the absolute configuration are reported in literature [6] [7].

2. Results and discussion

Chiral HPLC coupled to circular dichroism measurements has been applied to determine a chemical correlation and the absolute configuration of four stereoisomers of a polyfunctionalized indole derivative featuring a β -ketoester fragment and two stereogenic centres (fig 2.1) [8].

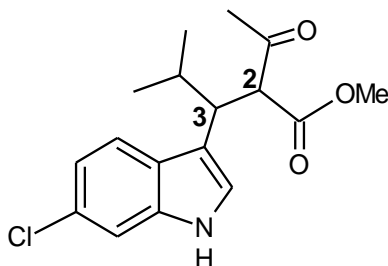


Fig. 2.1 - structure of the polyfunctionalized indole with two chiral centres indicated with 2 and 3.

The studied compound can be synthesized with a reported one-pot methodology [9] that consists of a three-component condensation promoted by $\text{TiCl}_4/\text{Et}_3\text{N}$, involving an aldehyde, an indole and an activated carbonyl compound. A mixture of four stereoisomers results from the reaction (figure

2.2) and the interconversion between the two diastereoisomeric pairs can be easily achieved in base-catalysed conditions [10].

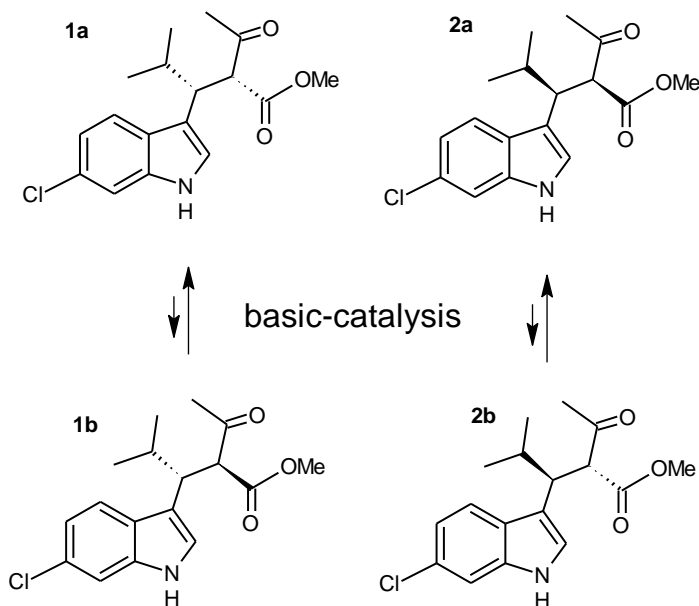


Fig. 2.2 - Enantiomers 1 and 2 of the diastereoisomeric pairs a and b.

Diastereoisomeric couples 1a-1b and 2a-2b interconvert by enolization. The substituents in C2 make the stereocenters relatively labile due to the high acidity of the acetoacetate proton. At the equilibrium the ratio between the two diastereoisomers is 67:33 (a:b) in chloroform at 25°C. The

four stereoisomers have been resolved with chiral HPLC using the amylose-based chiral stationary phase Chiralpak IA and both UV and CD detection (fig 2.3).

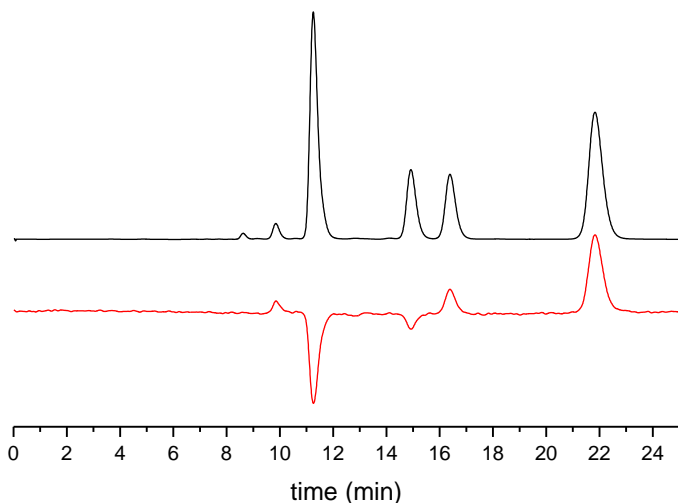


Fig. 2.3 - HPLC separation of compounds 1a, 1b, 2a, 2b. Column: Chiralpak IA; mobile phase: hexane/isopropyl alcohol (93/7 v/v); flow rate: 1 ml/min; T_{col} : 25°C; detector: UV (black trace – top) and CD (red trace – bottom) detection at 280 nm.

The CD detection allows assuming a stereochemical correlation between the eluted peaks: the first eluted and the fourth eluted are enantiomers since they have opposite signs of same intensity. Likewise, the second eluted stereoisomer and the third eluted are in enantiomeric correlation. The most

abundant stereoisomers at the equilibrium must be 1a and 2a, while the second and the third eluted should be 1b and 2b. On the basis of the lability of one of the stereocenters, a chemical correlation between the four stereoisomers can be evaluated. For this purpose, the four single stereoisomers have been isolated scaling up the analytical method to obtain milligrams of the desired compounds. Starting from an optically pure sample of the second eluted (figure 2.4), the diastereomerization reaction was monitored over time by enantioselective-HPLC.

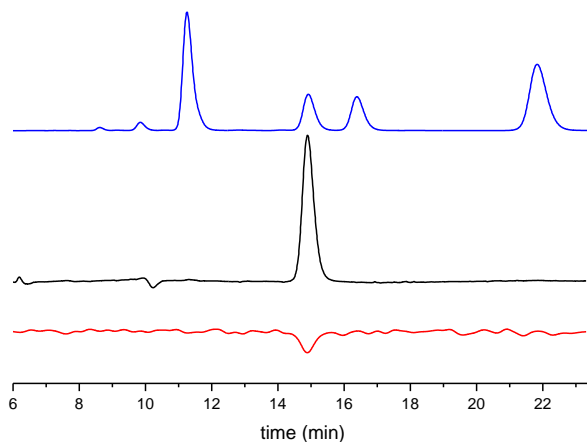


Fig. 2.4 - HPLC profile of the isolated 1b and comparison with the equilibrium mixture (blue trace- top).

A sample of the second eluted enantiomer was dissolved in a solution of Et₃N 0,1M in Chloroform and left to equilibrate at room temperature. The second eluted peak interconverts into the first eluted one and after 18 hours the equilibrium mixture is stable with a K_{eq} of 0,492 (fig 2.5).

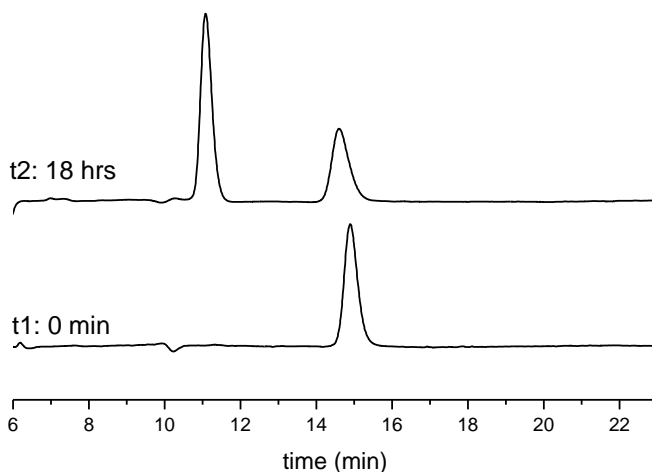


Fig. 2.5 - Starting from a single diastereoisomer (bottom) after 18 hrs at room temperature in a solution of Et₃N 0,1M in chloroform the equilibrium mixture is composed by the second eluted and the first eluted (top).

The first and the second eluted species must differ only for the configuration at the stereocenter in C2 and the same

assumption can be formulated for the third and fourth eluted species. The rate of interconversion has been measured at 43°C, monitoring the process by CSP-HPLC and measuring the integration of the areas at different times (fig 2.6). The analytical method indicated in figure 2.3 was adjusted to have a faster elution and to that end, the polar (isopropyl alcohol) component in the mobile phase was increased up to 10%.

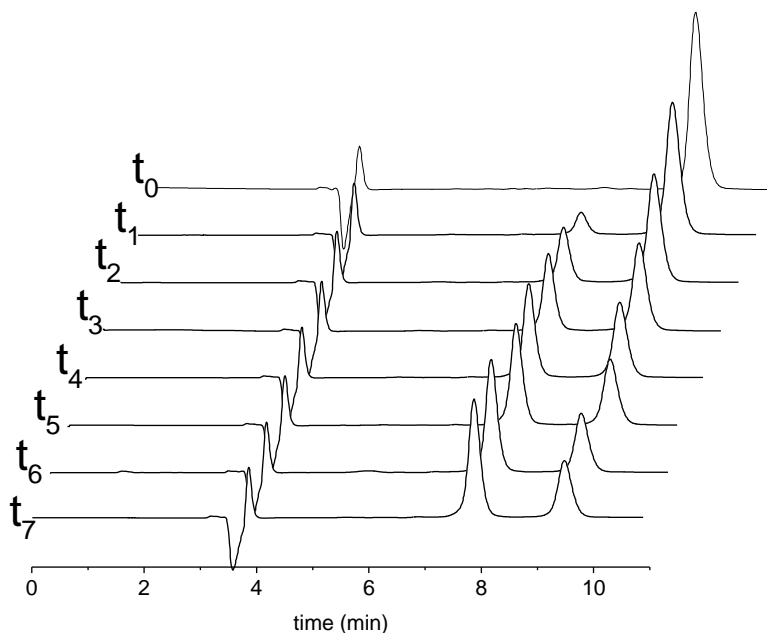


Fig 2.6 - Diastereomerization of the second eluted stereoisomer in ethanol at 43°C monitored over time by CSP-HPLC ($t_0=0$ min, $t_1=15$ min, $t_2=45$ min, $t_3=75$ min, $t_4=105$ min, $t_5=135$ min, $t_6=195$ min, $t_7=255$ min).

The apparent rate constant is obtained by fitting the experimental data into the equation 1, while the direct rate constant is calculated starting from the k_{app} and the K_{eq} based on equation 2.

$$(1) \ln \left[\frac{A_t - A_{eq}}{A_0 - A_{eq}} \right] = -k_{app} t$$

$$(2) k_1 = k_{app} \left[\frac{K_{eq}}{K_{eq} + 1} \right]$$

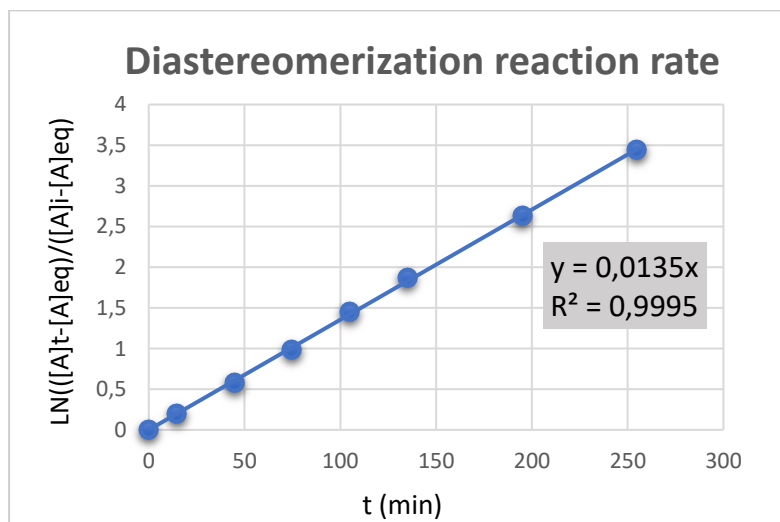


Fig 2.7 - Equilibration starting from the second eluted diastereoisomer in chloroform at 43°C, monitored over time by HPLC.

T (°C)	k ₁ (min ⁻¹)	k ₋₁ (min ⁻¹)	ΔG [‡] ₁ (kcal/mol)	ΔG [‡] ₋₁ (kcal/mol)
43	0,0091	0,0044	24,07	24,52

Tab. 2.1 - Kinetic parameters for the reversible formation of the first eluted starting from the second eluted. ΔG[‡](kcal/mol) values are calculated using the Eyring-Polanyi equation. Errors in ΔG[‡]±0,02 kcal/mol.

The absolute configuration of the first and the third eluted stereoisomers was determined by anomalous dispersion X-ray crystallography facilitated by the presence of the chlorine atom in the structure, and furtherly confirmed by TD-DFT simulations of the electronic circular dichroism spectra, in collaboration with Prof. Mazzanti research group (Università di Bologna). The procedure and the experimental conditions are reported [8] and the 2R,3R absolute configuration was assigned to the first eluted stereoisomer, corresponding to 1a (figure 2.2). The third eluted stereoisomer was found to be 2b fitting with the absolute configuration 2R,3S. Considering the chemical correlations found by base-catalysed diastereomerization and with the help of the circular dichroism detection, being 2b the enantiomer of 1b, this must correspond to the second elute enantiomer that, in fact is at

the same time the diastereoisomer of 1a. So, the absolute configuration of 1b must be 2S,3R. Consequently, an analogous consideration can be applied to assign the absolute configuration of the fourth eluted peak, whose AC is 2S,3S corresponding to the structure of 2a.

3. Conclusions

Chiral HPLC allowed to determine a chemical correlation between four isomers of a polyfunctionalized conformationally flexible indole. The presence of a stereolabile centre, due to the high acidity of the acetoacetate proton allowed to monitor the base-catalysed diastereomerization and to measure an activation energy for the process of 24,56 kcal/mol. The CD detection allowed to recognize the enantiomeric pairs, characterized by a signal of opposite sign and equal intensity. Coupling these results with the data obtained from the anomalous dispersion X-ray crystallography, allowed to determine the absolute configuration for all the four stereoisomers.

4. Methods and Materials

4.1 Chemicals and materials

Compounds 1a, ab, 2a and 2b have been prepared following a reported procedure [9]. All solvents have been purchased from Sigma-Aldrich and are HPLC grade pure.

4.2 HPLC measurements

4.2 a Chromatographic apparatus

Analytical chromatography was performed on a Jasco (Tokyo, Japan) HPLC system with a universal Rheodyne 20 μ l injector, a pump Jasco PU 980 and a second CO₂ pump Jasco PU 1580. Detection is provided by a Jasco UV 975 detector a Jasco UV/CD 995 detector. Preparative chromatography was performed with a chromatographic apparatus composed by Waters with a pump Waters Millipore Model 590 and a Waters Millipore Lambda-Max model 481 LC spectrophotometer detector.

4.2.b Chromatographic columns

Chiral resolution of the racemic mixtures by HPLC was performed with polysaccharide-based chiral stationary phases Chiralpak IA(250 x 4,6 mm L. x I.D., 5 μ m particle size).

5. References

- [1] Marialuisa Menna, Concetta Imperatore, Alfonso Mangoni, Gerardo Della Sala and Orazio Tagliatella-Scafati, *Nat. Prod. Rep.*, 2019, 36, 476-489.
- [2] H. D. Flack and G. Bernardinelli, *Acta Cryst.*, 1999, A55, 908-915.
- [3] Thomas J. Wenzel and James D. Wilcox, *Chirality*, 2003, 15, 256-270.
- [4] Teresa B. Freedman, Xiaolin Cao, Rina K. Dukor, and Laurence A. Nafie, *Chirality*, 2003, 15, 743-758.
- [5] Christian Roussel, Alberto Del Rio, Johanna Pierrot-Sanders, Patrick Piras, Nicolas Vanthuyne, *J. Chromatogr.A*, 2004, 1037, 311-328.
- [6] Chunguang Lv and Zhiqiang Zhou, *J. Sep. Sci.* 2011, 34, 363-370.
- [7] Rosella Ferretti, Simone Carradori, Paolo Guglielmi, Marco Pierinc, Adriano Casulli,e,Roberto Cirilli, *J. of Pharm. and Biomed. An.*, 2017, 140, 38-44.
- [8] Michele Mancinelli, Roberta Franzini, Andrea Renzetti, Emanuela Marotta, Claudio Villani and Andrea Mazzanti, *RSC Adv.*, 2019, 9, 18165-18175.

[9] Andrea Renzetti, Emmanuel Dardennes, Antonella Fontana, Paolo De Maria, Janos Sapi and Stéphane Gérard, *J. Org. Chem.*, 2008, 73, 6824–6827.

[10] Andrea Renzetti, Antonello Di Crescenzo, Feilin Nie, Andrew D. Bond, Stéphane Gérard, Janos Sapi, Antonella Fontana and Claudio Villani, *Chirality*, 2015, 27, 779.

Conclusions and future perspectives

Once again stereochemistry results as a multidisciplinary science, that benefits from collaborations that bring together different knowledges from very different fields.

The synergic effect of HPLC with other spectroscopic techniques as NMR, X-ray, ECD, and ORD in the study of stereodynamics and properties of conformational and configurational isomers has been successfully demonstrated.

The selectivity ensured by polysaccharide-based chiral stationary phase has allowed the separation of enantiomers of helically distorted polyaromatic compounds facilitating the assignment of the absolute configuration by evaluation of the circular dichroism spectra of each enantiomer. CSP-HPLC was employed also to measure the energetic barriers for the configurational inversion, with few exceptions due to the time-scale of the stereomutation process. The exact measuring of free activation energies over 30 kcal/mol has faced many limitations due to solvents boiling point and eventual chemical instability of the studied compounds at high temperatures. Different, but not less limiting, factors

made challenging to measure energetic barrier lower than 20 kcal/mol. Dynamic-HPLC coupled to computer simulations has been successfully used with polysaccharidic and brush-type CSP at very low temperatures to obtain ΔG^\ddagger values of enantiomerization down to 14,0 kcal/mol for therapeutically active compounds that exhibit a lack of symmetry plane. For some of the studied compounds the energetic barriers of isomerization have been furtherly confirmed by variable temperature NMR, a practice that gives even more validity to the two methodologies. Variable temperature chromatography is also successfully applied with achiral stationary phases for the study of diastereomerization processes as those generated by rotation around amidic bond of proline residues, a common feature of small bioactive or catalytically active peptides and proteins. The continuous optimization of computational models and softwares is of great help in the study of stereodynamic processes expanding the number of simultaneous equilibria that can be studied at one time and also improving the precision and reliability of the resulted data. The developing of quantum mechanical computations for the determination of the absolute configuration by confrontation of the experimental data with

the simulation of ECD and VCD spectra can be complementary to X-ray crystallography and HPLC. Each technique fill up the doubts left from the other ones, allowing to have precise results even in the presence of conformationally flexible compounds with few chromophores and numerous stereogenic elements.

List of publications

1. Caterina Viglianisi , Chiara Biagioli , Martina Lippi , Maria Pedicini, Claudio Villani, Roberta Franzini, Stefano Menichetti, “Synthesis of Heterohelicenes by a Catalytic Multi-Component Povarov Reaction” , *Eur. J. Org. Chem*, 2019, 1, 164–167.

2. Radha Bam, Wenlong Yang, Giovanna Longhi, Sergio Abbate, Andrea Lucotti, Matteo Tommasini, Roberta Franzini, Claudio Villani, Vincent J. Catalano, Marilyn M. Olmstead, Wesley A. Chalifoux, “Four-Fold Alkyne Benzannulation: Synthesis, Properties, and Structure of Pyreno[a]pyrene-Based Helicene Hybrids”, *Org. Lett*, 2019, 21, 8652-8656.

3. Sandra Belviso , Ernesto Santoro , Francesco Lelj , Daniele Casarini, Claudio Villani, Roberta Franzini, Stefano Superchi, “Stereochemical Stability and Absolute Configuration of Atropisomeric Alkylthioporphyrazines by Dynamic NMR and HPLC Studies and Computational

Analysis of HPLC-ECD Recorded Spectra”, *Eur. J. Org. Chem.*, 2018, 29, 4029-4037.

4. Michele Mancinelli, Roberta Franzini, Andrea Renzetti, Emanuela Marotta, Claudio Villani, and Andrea Mazzanti, “Determination of the absolute configuration of conformationally flexible molecules by simulation of chiro-optical spectra: a case study”, *RSC Adv.*, 2019, 9, 18165–18175.

Other publications

5. Franzini, R., Ciogli, A., Gasparri, F., Ismail, O.H., Villani, C., “Recent developments in chiral separations by supercritical fluid chromatography”, *Chiral Analysis: Advances in Spectroscopy, Chromatography and Emerging Methods: Second Edition*, 2018, edited by P.L. Polavarapu.

6. Antonio Arcadi, Alessia Ciogli, Giancarlo Fabrizi, Andrea Fochetti, Roberta Franzini, Francesca Ghirga, Antonella Goggiamani and Antonia Iazzetti, “Synthesis of pyrano[2,3-f]chromen-2-ones vs. pyrano[3,2-g]chromen-2-ones through

site controlled gold-catalyzed annulations”, *Org. Biomol. Chem.*, 2019.

Congress Communications

1. Roberta Franzini, “*Study on the stability of conformational isomers of novel “designer benzodiazepines”*: low temperature dynamic-chromatography” presented at the 1st Novel Psychoactive Substances international scientific school, Pula (Italy), 10-13 Oct 2017.

2. Claudio Villani, Roberta Franzini, Alessia Ciogli, Marco Pierini, “*Low Temperature Dynamic Chromatography of Chiral Stereolabile Compounds*” poster presented at 29th International Symposium on Chirality, Tokyo (Japan), 9-12 July 2017.

3. Roberta Franzini, Claudio Villani, “*Isomeria conformazionale investigata mediante HPLC a temperatura variabile: risoluzione e studi di stabilità di stereoisomeri di molecole organiche chirali*” poster presented at Incontri di Scienza delle Separazioni 2018- Roma (Italy), 8-9 Nov. 2018.

4. Roberta Franzini “*Chiral hetero- and carbo-[n]-helicenes: chromatographic resolution and investigation of configurational stability.*” Presented at the International school on organic synthesis A. Corbella (ISOS 2019), Gargnano (Italy), 9-13 June 2019.